

Longitudinal Mode Combustion Instabilities  
in Air Breathing Engines

Thesis by  
James David Sterling

In Partial Fulfillment of the Requirements  
for the Degree of  
Doctor of Philosophy

California Institute of Technology  
Pasadena, California

1987

(Submitted May 15, 1987)



## Acknowledgements

I sincerely thank my advisor, Professor E.E. Zukoski for his support and enthusiasm. Also, the direction provided by Professor F.E. Marble and Professor T. Kubota was appreciated.

Discussions with Dr. Gavin Hendricks and with my other friends at GALCIT were very helpful.

I would like to extend special thanks to my family, the Supper Club, and Ms. Shenda Baker for their moral support during my stay at Caltech.

My graduate studies were made possible by a Daniel and Florence Guggenheim Fellowship in Jet Propulsion, a General Motors Advanced Technologies Fellowship, and the support of the California Institute of Technology. Funding for the research was provided under AFOSR Grant 84-0286.

## Abstract

An investigation of the self-excitation of low frequency (100–600 Hz), longitudinal acoustic modes of a rearward-facing step combustor has been performed. As in combustion instabilities of air breathing propulsion systems, the pressure oscillations are excited by a fluctuating heat release from a flame that is stabilized in a recirculation zone. Flow visualization results and flame radiation intensity data reveal that large vortex structures are responsible for this fluctuating heat release. The vortices are shed at frequencies corresponding to longitudinal acoustic modes of the system or to the first subharmonic of one of the modes.

A series of parametric studies were performed to determine the dependence of the vortex shedding frequency upon the step height, mean flow speed, fuel type, and equivalence ratio. It was discovered that the vortex shedding frequency can shift between modes as a result of changes in the chemical reaction time of the reactants or as a result of changes in the mixing process of the cold reactants with the hot products.

Detailed investigations into the mechanism of sustenance of the oscillations during instability were performed for several operating conditions. The distribution of the combustion associated with vortex shedding was investigated by measuring the radiation intensity from the flame region. These results were used in Rayleigh's Criterion to determine regions of driving and damping of the oscillations.

A one-dimensional linearized acoustic model is used to predict the natural

modes of the system and a fluctuating volumetric source is used to model the oscillatory heat release. First, independent driving is applied to determine the system response to driving at different frequencies. One important result is that the phase difference between the pressure oscillations and the velocity oscillations at the flameholder is very sensitive to the frequency of driving near natural modes of the system.

Finally, a velocity-sensitive volumetric source with a time delay is included as feedback to determine the linear stability characteristics of the system. Various mechanisms leading to nonlinear limit cycle behavior are then discussed and compared to experimental data obtained during transition to instability.

# Table of Contents

Acknowledgments	iii
Abstract	iv
List of Figures	ix
<b>1 Introduction</b>	<b>1</b>
1.1 Definition of Combustion Instability . . . . .	1
1.2 Previous Work . . . . .	3
1.3 Scope of Current Investigation . . . . .	7
<b>2 Experimental Apparatus</b>	<b>9</b>
2.1 The Laboratory Combustor Facility . . . . .	9
2.2 Instrumentation and Flow Visualization . . . . .	13
2.3 Fuels and Chemical Reaction . . . . .	17
2.3.1 Background . . . . .	17
2.3.2 Characteristic Ignition Times in Premixed Flames . . . . .	20
<b>3 Experimental Results</b>	<b>24</b>
3.1 Characteristics of the Combustion Instability . . . . .	24
3.2 Vortex Shedding Frequencies . . . . .	26
3.2.1 Data Reduction Procedure . . . . .	26

3.2.2	Discussion . . . . .	28
3.2.3	Summary . . . . .	31
3.3	Results of Typical Instability Frequencies . . . . .	34
3.3.1	Signals and Spectra: Two Examples . . . . .	34
3.3.2	Mode Shapes . . . . .	36
3.3.3	Cinematography Results with Radiation Intensity Profiles . . . . .	38
3.3.4	The Rayleigh Criterion . . . . .	42
3.3.5	Transition Data: Nonlinear Development . . . . .	47
<b>4</b>	<b>Modeling of Longitudinal Mode Combustion Instabilities</b>	<b>84</b>
4.1	Acoustic Equations with Sources . . . . .	84
4.2	Solution for Quasi-Steady Behavior . . . . .	87
4.2.1	Natural Modes . . . . .	89
4.2.2	Forcing with Mass Source . . . . .	89
4.2.3	Linear Stability Using Velocity-Sensitive Mass Source . . . . .	96
4.3	Solution for Time Development of Normal Modes . . . . .	101
4.4	Nonlinear Development of Combustion Instability . . . . .	104
4.4.1	Path 1: Saturation of Forcing Amplitude . . . . .	105
4.4.2	Path 2: Increases in the Time Delay with Amplitude Growth . . . . .	107
4.4.3	Path 3: Decreases in the Time Delay with Amplitude Growth . . . . .	108
4.4.4	Conclusions . . . . .	109
<b>5</b>	<b>Summary and Conclusions</b>	<b>111</b>
	<b>References</b>	<b>115</b>

A Derivation of Rayleigh's Criterion	122
B Rayleigh's Criterion by Normal Mode Solution	124

## List of Figures

2.1	Combustion Laboratory . . . . .	11
2.2	Laboratory Combustor Design . . . . .	12
2.3	Flameholders . . . . .	13
2.4	Variation of $\tau_{chem}$ with Equivalence Ratio . . . . .	22
2.5	Effect of Equivalence Ratio and Mixture Fraction on $\tau_{ind}$ . . . . .	23
2.6	Laminar Flame Speeds for $CH_4/H_2$ Mixtures . . . . .	23
3.1	Flow Field Classification . . . . .	49
3.2	Map 1: Methane, Single Step . . . . .	50
3.3	Map 2: Methane, Double Step . . . . .	51
3.4	Map 3: 15% Hydrogen–Methane, Single Step . . . . .	52
3.5	Map 4: 15% Hydrogen–Methane, Double Step . . . . .	53
3.6	Map 5: 30% Hydrogen–Methane, Single Step . . . . .	54
3.7	Map 6: 30% Hydrogen–Methane, Double Step . . . . .	55
3.8	Examples of Raw Signals . . . . .	56
3.9	Spectra : Single Step, Methane, $\phi = 1.0$ , $V_{mean} = 60ft/sec$ . . . . .	57
3.10	Spectra : Single Step, 15% $H_2$ – 85% $CH_4$ , $\phi = 0.8$ , $V_{mean} =$ 150ft/sec . . . . .	58
3.11	188 Hz Mode Shape : Methane, $\phi = 1.0$ , $V_{mean} = 60ft/sec$ , $L_{plenum} = 2.82ft$ . . . . .	59

3.12	231 Hz Mode Shape : $15\%H_2 - 85\%CH_4$ , $\phi = 0.86$ , $V_{mean} = 69ft/sec$ , $L_{plenum} = 2.82ft$ . . . . .	60
3.13	457 Hz Mode Shape : Methane, $\phi = 0.79$ , $V_{mean} = 108ft/sec$ , $L_{plenum} = 1.84ft$ . . . . .	61
3.14	535 Hz Mode Shape : Methane, $\phi = 1.0$ , $V_{mean} = 145ft/sec$ , $L_{plenum} = 1.84ft$ . . . . .	62
3.15	188 Hz Shedding Movie: $\phi = 1.0$ , $V_{mean} = 60ft/sec$ , $L_{plenum} = 2.82ft$ . . . . .	63
3.16	Standard Case 188 Hz Shedding : $0^\circ$ Phase Angle . . . . .	64
3.17	Standard Case 188 Hz Shedding : $72^\circ$ Phase Angle . . . . .	65
3.18	Standard Case 188 Hz Shedding : $144^\circ$ Phase Angle . . . . .	66
3.19	Standard Case 188 Hz Shedding : $216^\circ$ Phase Angle . . . . .	67
3.20	Standard Case 188 Hz Shedding : $288^\circ$ Phase Angle . . . . .	68
3.21	188 Hz Shedding : $\phi = 1.0$ , $V_{mean} = 60ft/sec$ , $L_{plenum} = 2.82ft$ . . . . .	69
3.22	188 Hz Shedding : 2nd Half of Cycle . . . . .	70
3.23	535 Hz Shedding : $\phi = 1.0$ , $V_{mean} = 145ft/sec$ , $L_{plenum} = 1.84ft$ . . . . .	71
3.24	535 Hz Shedding : 2nd Half of Cycle . . . . .	72
3.25	Phase Difference Between 188 Hz Components of $p'$ and $i'$ : Standard Case . . . . .	73
3.26	Rayleigh Criterion 188 Hz : Methane, $\phi = 1.0$ , $V_{mean} = 60ft/sec$ , $L_{plenum} = 0.86m$ . . . . .	74
3.27	Rayleigh Criterion 188 Hz : Methane, $\phi = 0.90$ , $V_{mean} = 63ft/sec$ , $L_{plenum} = 2.82ft$ . . . . .	75
3.28	Rayleigh Criterion 231 Hz: $15\%H_2 - 85\%CH_4$ , $\phi = 0.86$ , $V_{mean} = 69ft/sec$ , $L_{plenum} = 2.82ft$ . . . . .	76

3.29	Rayleigh Criterion 457Hz : 15% $H_2$ – 85% $CH_4$ , $\phi = 0.86$ , $V_{mean} = 69\text{ft}/\text{sec}$ , $L_{plenum} = 2.82\text{ft}$ . . . . .	77
3.30	Rayleigh Criterion 267 Hz : Methane, $\phi = 0.93$ , $V_{mean} = 69\text{ft}/\text{sec}$ , $L_{plenum} = 2.82\text{ft}$ . . . . .	78
3.31	Rayleigh Criterion 535 Hz : Methane, $\phi = 0.93$ , $V_{mean} = 69\text{ft}/\text{sec}$ , $L_{plenum} = 2.82\text{ft}$ . . . . .	79
3.32	Rayleigh Criterion 457 Hz : Methane, $\phi = 0.79$ , $V_{mean} = 108\text{ft}/\text{sec}$ , $L_{plenum} = 1.84\text{ft}$ . . . . .	80
3.33	Rayleigh Criterion 535 Hz : Methane, $\phi = 1.0$ , $V_{mean} = 145\text{ft}/\text{sec}$ , $L_{plenum} = 1.84\text{ft}$ . . . . .	81
3.34	Transition: Pressure Signal at Flameholder . . . . .	82
3.35	Transition: Radiation Intensity Signal at 5.0" . . . . .	83
4.1	Quasi-Steady Acoustic Model . . . . .	88
4.2	Pressure Response to Unit Driving . . . . .	92
4.3	Velocity Response to Unit Driving . . . . .	93
4.4	Phase Difference Between $p'$ and $u'$ above Flameholder . . . . .	95
4.5	Interaction Index for Neutral Stability . . . . .	99
4.6	Time Delays for Neutral Stability . . . . .	100
4.7	Stability Characteristics Near 188 Hz Mode . . . . .	102
4.8	Idealized Mechanisms Leading to Limit-Cycle Behavior . . . . .	106

# Chapter 1

## Introduction

### 1.1 Definition of Combustion Instability

When heat is released in an unsteady manner within the boundaries of some vessel, the potential exists for acoustic modes of the system to be excited and for the amplitudes of the pressure fluctuations to grow to large magnitudes. Self-excited pressure oscillations are common in systems in which heat is released as a result of combustion. The occurrence of these oscillations is referred to as a combustion instability.

One of the simplest examples of this phenomenon is that of the Rijke Tube. In this case, a Bunsen burner placed at certain locations within an open pipe will induce pressure oscillations within the pipe. The tone that is produced occurs at one of the natural acoustic modes of the pipe. In some cases, the phenomenon can be controlled to give pulsed combustion which can provide a predictable and efficient heat release. The Schmidt Tube propulsion systems of German V-1 bombs from World War II and many of today's home heating units are examples of pulsed combustors.

In power systems not specifically designed to pulse, however, the occurrence of pressure oscillations is very common and often troublesome. Commercial

power generation stations have large combustors that consequently have very low frequency acoustic modes. Pressure oscillations can produce an unsteady fuel supply rate. This results in an unsteady heat release that can in turn cause the amplitudes of the oscillations to grow to hazardous levels. This type of feedback is thought to be the primary mechanism of self-excitation. In liquid propellant rockets the fuel and oxidizer lines will supply an unsteady flow if subjected to pressure oscillations. Again, combustion instability can result. In solid propellant rockets the response of the heat release rate to pressure waves is not as clear, but some unsteady combustion will occur.

Another type of combustor susceptible to combustion instability is that in which a flame is stabilized in a shear flow. This arises in situations where the flow speed of the reactants of combustion is too high for reaction to occur continuously. Hence, a region of slower flow speeds is created to hold the combustion region within the combustor. In both ramjets and in air-breathing engines with afterburners, this flameholding is accomplished by the use of bluff bodies or abrupt expansions placed in the flow field to create regions of recirculation where the flame is stabilized. In these combustors unsteady combustion can occur as a result of vortex shedding at the separation point that forms the upstream end of the recirculation zone. The vortex shedding is caused by acoustic velocity fluctuations at the flameholder, which provides the feedback for driving to occur. Even in solid and liquid propellant rockets, vortex shedding from baffles or other flow obstacles may contribute to combustion instability.

The pressure variations associated with instability in many propulsion systems can result in structural damage via fatigue of structural components. Combustion instability problems were encountered at both General Electric and Pratt

& Whitney during the development of afterburning turbofan engines. Investigation revealed that low frequency (100-300 Hz) combustion instabilities were associated with the interaction between acoustic oscillations and the stability of flames in the afterburner. A different problem can result within ramjet systems. The inlet shock of the ramjet engine will move as a result of oscillatory pressures encountered during instability. If this shock moves out of the inlet, the engine will unstart and failure will result. In response to these problems, many experimental and theoretical investigations have been performed to identify the mechanism by which the combustion process transfers energy to the acoustic field.

## 1.2 Previous Work

The following discussion provides background and motivation for the present investigation into longitudinal mode combustion instabilities that are self-excited and are characterized by large vortex structures in a turbulent reacting flow.

### Experimental Investigations

Every combustion chamber has acoustic modes that depend on the geometry of the system. Many propulsion systems are cylindrical in shape and consequently have radial, tangential, and longitudinal acoustic modes. Rogers and Marble [1] investigated high-frequency instabilities associated with transverse acoustic modes of an experimental combustion apparatus. The self-excited oscillations in this case were associated with asymmetric vortex shedding from opposite edges of a V-shaped bluff body flameholder. Most high-frequency instabilities of this type can be eliminated by the use of perforated liners that can be tuned to provide damping at the appropriate frequencies. Thus, only low-frequency longitudinal mode combustion instabilities are considered in the

present work.

There have been several recent experimental investigations into instabilities of longitudinal acoustic modes. Rijke tubes exhibit this type of instability. Lawn [2] investigated longitudinal instabilities in a Rijke tube combustor with a diffusion flame, and Mugridge [3] performed a similar study with a premixed flame. Hegde et al. [4] performed experiments to observe longitudinal mode combustion instabilities with a flame stabilized behind an 0.8mm heated nichrome wire at cold flow Reynolds numbers below 10,000. In this investigation, a mechanism of self-excitation was often responsible for pressure oscillations even when acoustic drivers were used to force the acoustics at frequencies other than natural modes. These studies provided information about low-speed laminar combustion instabilities that can be used as a basis for considering instability problems in propulsion systems containing turbulent combustion. Also, the dominance of the self-excitation mechanism was apparent.

Several investigators have observed vortex shedding phenomena during combustion instability. In a review article by Byrne [5], vortex shedding mechanisms of feedback are discussed and compared to experimental results in which vortex shedding was thought to be the important feedback mechanism of instability.

In 1952, Shonerd [6] performed an investigation in which it was determined that large vortical structures were shed from a flame-holding rod at a frequency corresponding to a longitudinal mode of the system. More recently, Ganji and Sawyer [7] observed large scale vortex structures in a rearward-facing step combustor. This finding led Keller et al. [8] and Vaneveld et al. [9] to research longitudinal “chugging” modes, and the effect that the vortical flow field has on

the tendency of a flame in a combustor to flashback. Finally, Smith [10] and Smith and Zukoski [11] observed the flow field during instability in a combustor in which the flame was stabilized behind a rearward-facing step. The shedding of large vortex structures was found to be responsible for the unsteady heat release, which drove the oscillations.

Longitudinal modes of a chamber can actually become excited due to the occurrence of large vortex structures when no combustion is present. The feedback mechanism of these so-called “edgetone resonances” is due to vortex impingement at some downstream location that yields an oscillatory force on the flow (opposite the drag imposed to the impinged wall). The frequency of excitation is therefore velocity-sensitive. Aaron [12] performed an investigation into this phenomenon.

### **Analytical Investigations**

Several investigators have worked on the theory by which various mechanisms generate acoustic energy in combusting systems. Lord Rayleigh [13] explained a mechanism by which energy can be added to an acoustic field due to an oscillatory heat release rate. Modified versions of the “Rayleigh Criterion” are used by most investigators of instability phenomena today. In writing about this criterion, Putnam [14] stated, “In the authors’ experience this explanation has been verified in all cases of combustion-driven oscillations.”

Theoretical work into longitudinal mode instabilities was performed by Crocco and Cheng [15], who developed a linear stability theory for liquid propellant rockets. The use of a pressure-sensitive time lag for the heat release in a combustor led to attempts to construct more complete descriptions for the relationship between the acoustics and heat release rates. Merk [16], Yang [17], Lawn

[2], and Mugridge [3] have constructed models for the heat release rate of a flame using various simplifying assumptions about the flame zone and its response to acoustic waves. Investigations by Yang [17], Westbrook [18], and Ponizy and Wojcicki [19] have used kinetics in a stirred reactor to model the combustion processes during oscillatory combustion at frequencies of longitudinal modes.

Culick [20] has expressed solutions of the acoustic properties during combustion instability in terms of expansions in orthogonal normal modes of a combustor. Using a quite general analytical framework, he has investigated nonlinear gasdynamic effects that give limiting amplitudes for the oscillatory behavior. A different mechanism was proposed by Sterling and Zukoski [21] to explain nonlinear effects; this mechanism will be discussed in this thesis.

Another class of mechanisms of combustion instability involves the generation of acoustic waves by the interaction of entropy gradients with the exit of a combustor. The generation of acoustic energy is discussed by Auerbach [22] for the case of thermal disturbances flowing into a supersonic nozzle. Recent investigations by Abouseif et al. [23] and by Humphrey [24] propose feedback mechanisms of this type for combustion instabilities. The postulated feedback does not involve natural acoustic modes of the combustion system and the mean flow speed is important because entropy fluctuations are convected with the flow. This type of mechanism is not considered in the present work because a linear variation of frequency with velocity is not expected or observed in the experimental facility.

These investigations provide the background and a basis for discussion of many aspects of the general field of combustion instabilities. However, there remain many questions about mechanisms responsible for the types of instabilities

encountered in common propulsion systems. These are self-excited longitudinal mode combustion instabilities of a turbulent combustion process characterized by large scale vortical structures.

### 1.3 Scope of Current Investigation

The objective of the present study is to investigate the mechanism that causes growth and sustenance of pressure oscillations for combustors in which the flame is stabilized by a recirculation zone. More specifically, a detailed understanding of longitudinal mode instabilities associated with premixed combustion is desired. In addition, investigation of instabilities within a high Reynolds number turbulent flow similar to the flow field of common propulsion systems is desired. Previous experimental efforts have not emphasized the mechanism causing the nonlinear evolution of pressure oscillations for these types of flows.

The hypothesis is put forth that the phase difference between the oscillating heat release rate and the oscillating pressure in the combustor determines the stability of the combustion process. Furthermore, it is proposed that a fluid mechanical mixing time and a chemical reaction time are sufficient to describe this phase difference for a particular combustor under given operating conditions. These characteristic times depend on system geometry, fuel type, and equivalence ratio, and they vary with the amplitude of the oscillatory pressure signal. Thus, a nonlinear feedback loop that is closed by the variation of the above time delays and the frequency of oscillation with the amplitude of the signal is postulated. This variation represents a mechanism for the occurrence of finite limiting amplitudes.

In Chapter 2, the experimental research facility is described. The labora-

tory combustion chamber and flow supply system designs are explained. Also, a discussion of the measurement instrumentation, data acquisition and analysis, and flow visualization equipment is included. The types of fuels used and their combustion characteristics are described.

The results of the experiments that were performed are shown in Chapter 3. Results are given for the various vortex shedding frequencies that result upon choices of fuel, equivalence ratio, flameholder geometry, and mean flow speed. The dominant trends in the experimental data are discussed. The results are for steady-state behavior and detailed investigations of these results are presented and discussed for several operating conditions. Results are also shown for the nonlinear evolution of the oscillations.

The theoretical modeling efforts are presented in Chapter 4. First, the governing equations are applied to yield a one-dimensional acoustic wave equation with forcing terms. Then the results of a simple model with independent forcing are shown for quasi-steady oscillatory behavior. Acoustic frequencies and mode shapes for the laboratory apparatus are determined. A velocity-sensitive mass source is then included as a feedback mechanism for the forcing. This constitutes a linear stability theory for the geometry of the laboratory combustor.

Using Culick's general framework for analytical combustion instability theory, a derivation of Rayleigh's Criterion for a simple combustion chamber is included and the dominant trends of linear stability theory are shown.

Finally, the manifestation of these trends in the velocity-sensitive mass source model is discussed. Several models resulting in nonlinear limit cycle behavior are discussed and compared with experimental results to describe the physical transition process as the amplitude of oscillation grows and reaches a finite value.

## Chapter 2

### Experimental Apparatus

#### 2.1 The Laboratory Combustor Facility

To investigate the feedback mechanism for sustenance of pressure oscillations in a dump combustor, Smith [10] designed and constructed a laboratory combustor. This facility with some modifications is used in the present experimental effort. Details of the design and operation of the combustion facility as well as details of the pressure instrumentation, radiation instrumentation, and flow visualization were discussed by Smith.

The facility meets the requirements of the objectives of this study. More specifically, a variety of fuel/air mixtures can be supplied to a combustor in which the flame is stabilized in a recirculation zone. Flow speeds can be produced that give a turbulent, reacting flow similar to those found in propulsion systems. Also, this combustion system has a variety of natural acoustic longitudinal modes as do actual propulsion systems. The use of an exit that is simply open to the environment minimizes the possibility of producing “entropy” modes such as those proposed by Humphrey [24] and Abouseif et al. [23].

Figure 2.1 is a schematic diagram of this system, which consists of a blow-down supply system using dome regulators for the fuel and air lines. This supply

system provides high pressures for the flow through sonic nozzles that have been sized to give a stoichiometric mix for methane and air if the upstream pressures are equal. A three-way valve allows fuel and air lines to be pressurized separately or equally in a “paired mode” of operation. The lines converge into one line and mixing occurs as the gases flow through a length of pipe and a large plenum section. This section converges to an inlet section of constant area in which a flameholder is placed.

The portion of the apparatus that is acoustically important is shown in Figure 2.2. Mixing is enhanced by flow through a porous cone and several wire screens, which are placed in the plenum section. A steel plate, with many small holes in it, can be placed in the plenum chamber along with steel wool upstream of the plate. The steel wool will damp any oscillations in the upstream section so that, effectively, the plenum section is of variable length. The flow then encounters an area reduction and a cross-sectional area change from a circular shape to a 1"x3" rectangular shape.

Ten access ports are spaced at equal distances along the upper wall of the combustor section. One port is provided at the downstream end of the plenum section before the area contraction. The upper, lower, and side walls are cooled by a water jacket, but the side walls can be replaced by Vycore glass walls to allow flow visualization. The two flameholders used in this study are shown in Figure 2.3. The single rearward-facing step has the same blockage as the double step; however, the recirculation zone is twice as large, which is expected to affect fluid residence times and the evolution of vortices shed from the flameholder edge.

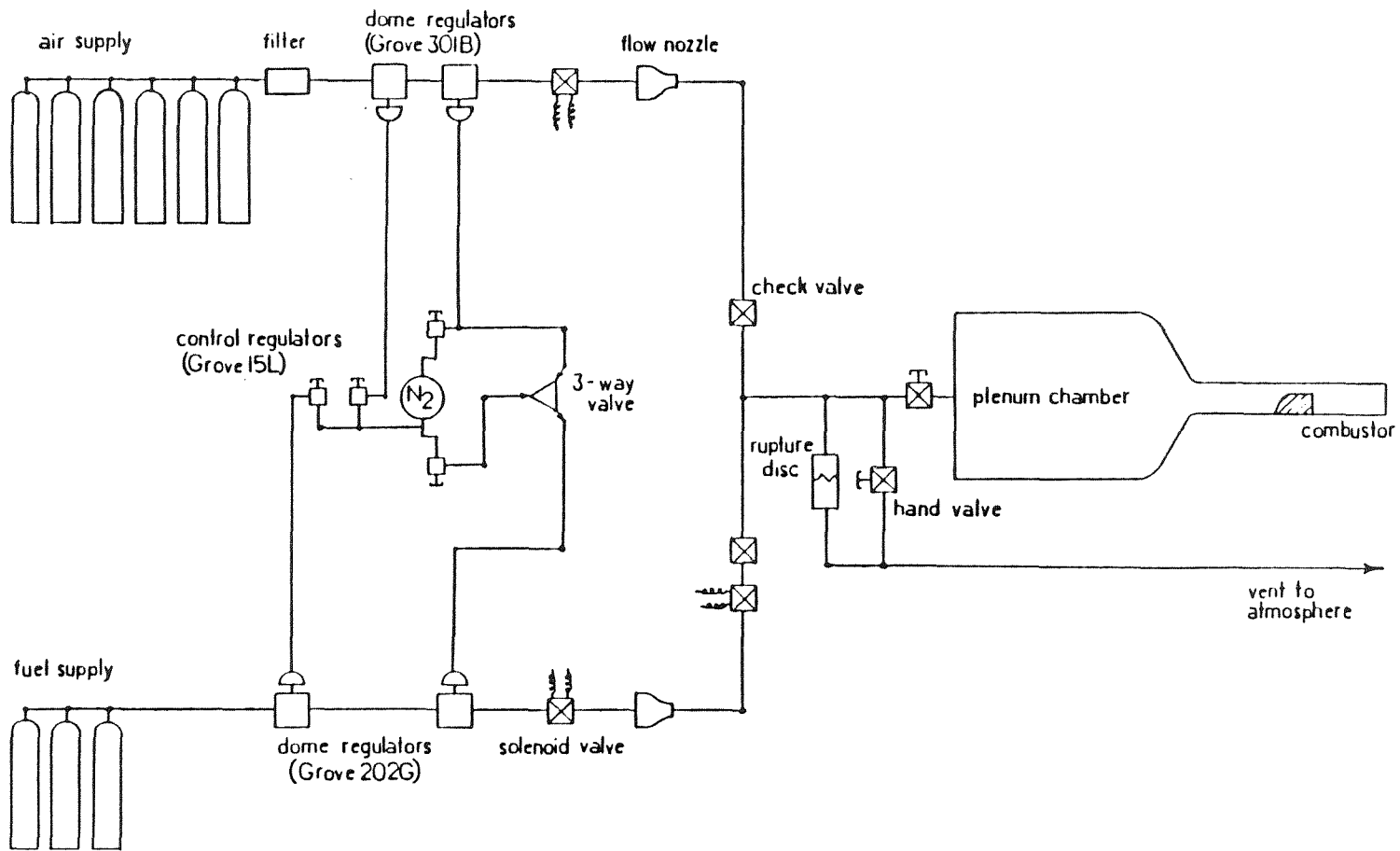


Figure 2.1: Combustion Laboratory

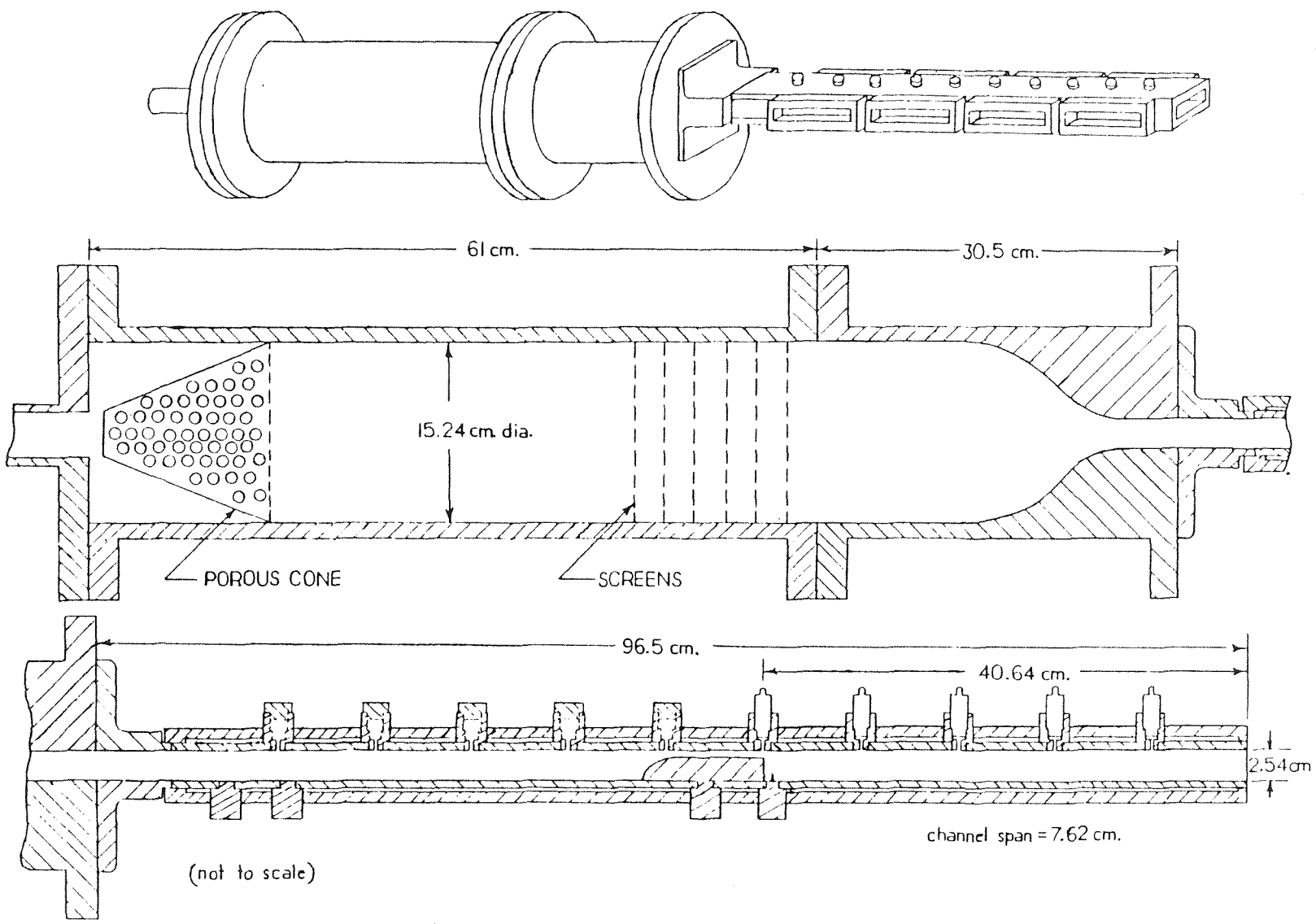
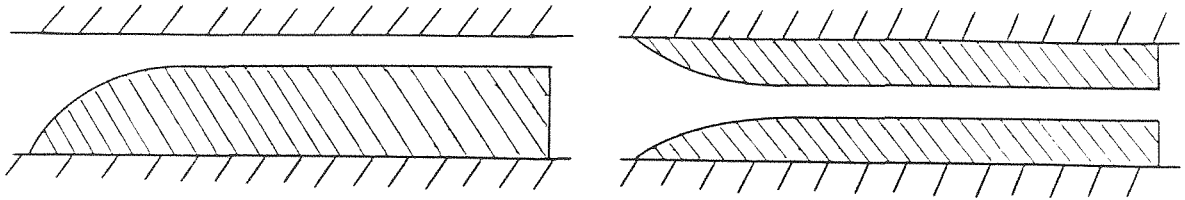


Figure 2.2: Laboratory Combustor Design



Single Step

Double Step

*Figure 2.3: Flameholders*

## 2.2 Instrumentation and Flow Visualization

### Pressure Instrumentation

Oscillatory pressure signals are measured at the access ports mentioned above by PCB model 106b piezoelectric pressure transducers. The transducers are mounted in the water-cooled access ports and are separated from the hot gas by a cavity which is connected to the combustion chamber by small holes. The Helmholtz resonance frequency of the cavity is around 5500 hertz and no correction is needed for the phase and amplitude differences between the measured and the source pressures below around 800 hertz. The cavity protects the transducer from the high combustion temperatures and from rapid pressurization that can be associated with ignition of combustible mixtures.

### Radiation Instrumentation

A photomultiplier tube assembly is used to observe the emitted radiation with broad band spectral coverage. The volume of the flame observed is fixed by

the entire 1" by 3" cross section and a 0.25" length in the axial direction. The assembly is mounted on a traverse mechanism to allow measurement at any point along the combustor where windows are located.

In this study a linear relationship is assumed to exist between the local heat release rate and the broad band radiation emitted by the flame. The physical basis for this correlation is explained by Chomiak [25], who states:

Since the rate of production of excited molecules is proportional to the rate of chemical reaction and the radiation is spontaneous and occurs after a very short relaxation time, it may be assumed that the local intensity of chemiluminescence is proportional to the mass rate of chemical reaction at the point considered, in particular for a homogeneous mixture of constant composition, temperature, and pressure.

Although the mixture composition and temperature of turbulent flames are obviously inhomogeneous, the assumption is still supported by the investigations of Hurle et al. [26], Diederichsen and Gould [27], Huot et al. [28], and by Clark and Bittker [29] for a fixed equivalence ratio. Hurle et al. measured the light emission of CH radicals in an ethylene/air flame as a function of the fuel flow rate and found a linear relationship for a given equivalence ratio. Clark and Bittker also found a linear relationship for propane/air flames, which held for both laminar and turbulent flames. This investigation and one by John and Summerfield [30] both confirmed that mixture composition can change the radiation intensity of a given flame by observing propane/air flames of different equivalence ratios.

For the turbulent, premixed, hydrogen-methane/air flames in this study, the chemiluminescence of radicals is much stronger than the thermal radiation

from the 1"x3" cross-section at near atmospheric pressure. Also, no yellowish luminosity characteristic of carbon particles is observed in flames of this type. Consequently, preliminary tests revealed no significant differences between CH band emission and broad band measurements. Thus, the assumption of linearity between the local heat release rate and the broad band radiation intensity is probably quite accurate for a particular equivalence ratio.

### **Hot-Wire Anemometry**

Flow velocities are measured using a constant temperature hot-wire anemometer with a wire of 5 microns in diameter placed upstream from the edge of the flameholder. Wires and prongs can be repaired using a GALCIT facility. The anemometry circuit was constructed and discussed by Sobota[31].

### **Data Acquisition**

Data are recorded using an HP 3960a four-channel analog tape recorder. The data are analyzed either with an SD360 Spectrum Analyzer or with a Zenith ZW-0248-84 microcomputer using data acquisition and analysis software from RC Electronics. The range of validity for the results of spectrum analysis depends upon the frequency response characteristics of the measurement equipment, the recorder, and the digitization sampling rate. The limitation of the Fast Fourier Transforms used for spectral analysis in this study is due to sampling rates in the digitization of the data. The sampling rate of the Spectrum Analyzer is fixed by the frequency range selected so the resulting spectrum is entirely below the Nyquist frequency. When the data acquisition software is used, sampling rates of 10 KHz or greater are used to give the Nyquist frequency of over 5 KHz. Initial analysis of the data revealed no significant frequencies present over 2400 Hz; therefore, aliasing effects are not expected.

The results of spectrum analysis are easily interpreted only if the data represents a stationary process over the data record analyzed. The processes examined in this thesis are consistently wide-sense stationary. This means that the mean of the signals is a constant, although the strict-sense requirement of statistical invariance under any time shift may not be met. Therefore, to allow interpretation of spectra, ensemble averages of finite-length samples with a Kaiser-Bessel window were obtained for each signal. Most of the data shown in the following chapter represents cases in which the finite-time averages were nearly identical; i.e., the signals represent stationary processes. However, in some cases successive averages were quite different. Due to the apparent non-stationarity of these cases, interpretation is more difficult and specific experiments are considered in the discussion of the results.

### **Flow Visualization**

Flow visualization is performed by using both single frame photography and high-speed cinematography of the shadowgraph images. A spark gap was used as a short duration light source for the purpose of freezing the motion of the fluid flow. Polaroid pictures with excellent resolution can be obtained using the spark that has a duration less than two microseconds. A high-intensity Mercury arclamp is used as the continuous light source for the cinematography. A 16mm Hycam movie camera capable of filming 8000 frames per second is used. The resolution of the flow field is not as sharp as the spark shadowgraphy because the exposure time of one frame is about 50 microseconds. Thus, considerable convection of the fluid can occur during this exposure and some blurring can result.

## 2.3 Fuels and Chemical Reaction

By using mixtures of methane and hydrogen, the effect of the fuel type on the occurrence of combustion instability can be investigated. In this study the fuels used are methane, a mixture of 15.3% hydrogen in methane, and a mixture of 29.8% hydrogen in methane where these are the mass fractions of hydrogen used. The chemical reaction rate depends on the fuel type, the equivalence ratio, and the temperature of the mixture. When a flame is stabilized in a recirculation zone, the flow of the cold mixture encounters the hot products and turbulent mixing occurs. This causes various regions of the mixture to accumulate different temperature histories; hence, different reaction rates will occur. This complex interaction between fluid mechanical mixing and molecular diffusion leading to chemical reaction has been under investigation for quite some time. The following is a discussion of several investigations into the important mechanisms within chemically reacting flow.

### 2.3.1 Background

One element that must be considered in combustion instability phenomena is the variation of the chemical reaction process mentioned above with changes in fuel type and equivalence ratio. Since models of turbulent reaction are built upon an understanding of the governing mechanisms of laminar flames, the following outline is provided as a basis for discussion of the turbulent reacting flow common to propulsion systems and the experimental combustor. Laminar and turbulent reactions are discussed for both premixed and non-premixed flames with the emphasis on the definitions of reaction rate, flame speeds, and the mixing and chemical times required for combustion to occur.

## Laminar Flames

Many investigations into laminar flames have been performed. These include experimental efforts and analytical studies intended to clarify the relative importance of various physical mechanisms. In both premixed and non-premixed flames (diffusion flames), molecular diffusion is ultimately responsible for chemical reaction.

For non-premixed flames, the reaction is limited by the diffusion of reactants to the flame zone. Thus, chemical reaction rates can be considered to be infinite and the flame zone to be infinitesimally thin. These assumptions have been employed by several authors for investigating diffusion flames in various laminar flow fields. Carrier, Fendell, and Marble[32] investigated the effects of strain on a laminar flame sheet. The increase in the mass consumption rate was determined for a given rate of strain and the result has been used by Karagozian[33] and by Hendricks[34] within certain laminar flow fields.

For premixed flames, molecular diffusion of hot products is responsible for heating the reactants to temperatures required for ignition so that effects similar to those in strained diffusion flames may occur. In this case, however, since gradual heating of a combustible mixture occurs, chemical reaction rates must be considered along with molecular diffusion. With these effects considered, reaction in boundary layers, mixing layers, and recirculation zones can be treated analytically for laminar flow fields. Marble and Adamson[35] and Dooley[36] considered these types of problems.

The important effect that chemical kinetics can have in the reaction of a combustible mixture was investigated by Westbrook [18]. He considered a well-stirred reactor that was initialized with hot products mixed with cold reactants to

give some initial temperature and composition. The chemical induction time was determined for various reactant mixture fractions for fixed reactant equivalence ratios. A substantial variation in the induction time was found for changes in either the equivalence ratio or the mixture fraction.

The existence of a laminar flame speed for a premixed flame has been investigated both experimentally and analytically. Asymptotic methods have been used by Bush and Fendell[37] to analyze laminar flame propagation for simple one-step Arrhenius kinetics for different Lewis numbers. Coffee[38] used finite-element methods with multi-reaction kinetics for methane/air mixtures to determine burning velocities, and he compared results of several kinetics models with some experimentally determined flame speeds discussed in Andrews and Bradley[39]. Yu, Law, and Wu[40] experimentally investigated laminar flame speeds of hydrocarbon and hydrogen mixtures with air. If the flame zone thickness is determined, laminar flame speed information may be valuable in defining a baseline chemical ignition delay time for turbulent flames as well.

### **Turbulent Flames**

The above models for combustion have been found to have major shortcomings for turbulent flames. Instabilities of laminar flames lead to rotational flow fields that stretch and distort the flame structure so that some “mixing” occurs that is not due to molecular diffusion. Instabilities of laminar flow also lead to vortical structures and eventually a cascade of fluid mechanical scales. The importance of the ratio of mixing length scales to the laminar flame zone thickness was recognized by Damköhler[41].

To investigate turbulent mixing, efforts in this area generally consider diffusion flames in jets or shear layers. Experimental efforts and simple models

of turbulent reacting flows are discussed by Broadwell and Breidenthal[42] and by Broadwell and Dimotakis[43]. Modeling efforts generally attempt to describe a turbulent flame as a strained laminar diffusion flame, while incorporating a cascade of fluid mechanical scales down to the Kolmogorov scale. To investigate the most elementary effects that turbulence may have on a laminar flame, Karagozian[33] analyzed the effect that a point vortex has on the mass consumption rate of a diffusion flame. Another example is the “ESCIMO” model by Spalding[44] which is based on engulfment of a region of fluid by large vortical structures, stretching of combustion interfaces, coherence of the vortical structures, interdiffusion at the molecular level, and a moving observation at the velocity of the coherent structures.

### **2.3.2 Characteristic Ignition Times in Premixed Flames**

As mentioned in the Introduction, there exists some feedback mechanism between the acoustic field and the fluctuating heat release for combustion instabilities to occur. In this study, the oscillatory heat release is associated with large vortex structures that enhance mixing between premixed reactants and hot products. Thus, it is obvious that the reaction mechanisms discussed above have important implications for this type of combustion instability. The functional relationship between the acoustic velocity fluctuations that cause vortex shedding and the heat release may include effects from the entire hierarchy of mixing scales.

It is often convenient to consider the reaction process of an element of reactant fluid as occurring in two stages that compose the characteristic ignition time. First, mixing of the fluid element with hot products down to the molecular scale must occur. Then, depending on the local mixture fraction, an induction

time will pass before a reaction occurs. In the present study, no assumption about the value of the “first Damköhler number” can be made. Thus, the fluid mechanical and diffusional mixing times may be of the same order of magnitude as the chemical reaction time.

Chemical kinetics controls the chemical reaction time so that this quantity is similar to the reciprocal of either the laminar flame speed, the minimum ignition energy, or the global reaction rate. Experimentally, the relative chemical reaction times of various fuels or equivalence ratios can be investigated by attempting to hold fluid mechanical mixing and diffusion effects constant. Zukoski and Marble [45] performed this type of experiment for a hydrocarbon fuel (molecular weight of about 100) and for mixtures of the same fuel with hydrogen. The method involved the use of flame blow-off studies for a variety of flameholder geometries. The flow velocity and recirculation zone length at the time of blow-off were used to construct a characteristic ignition time for a given fuel and equivalence ratio.

The following results are taken directly from Zukoski’s chapter in the volume by Oates[46], from the paper by Yu, Law, and Wu[40], and from Westbrook’s paper [18]. Figure 2.4 shows the variation of the characteristic ignition time of Zukoski’s heavy hydrocarbon with equivalence ratio. The minimum time shown on this curve is about 0.3 milliseconds, and this changes by almost an order of magnitude for very lean or very rich equivalence ratios. If a laminar flame zone thickness of 0.1 millimeter is assumed, the minimum chemical reaction time from Figure 2.6 would also be near one-quarter of a millisecond for methane. This value can also change by an order of magnitude for very lean or very rich mixtures. Figure 2.5 represents the variation of the chemical induction time with mixture fraction and equivalence ratio, considering only chemical kinetic effects.

In conclusion, the sensitivity of the combustion instabilities in this study to variations of fuel type, mixture ratio, and equivalence ratio suggests that chemical times are important in this study. Therefore, the following chemical reaction times will be used as a basis for discussion of the experimental results.

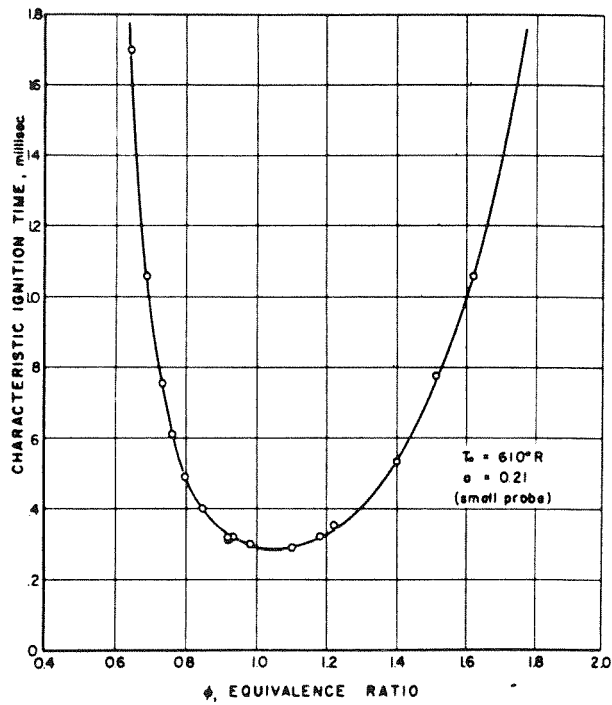


Figure 2.4: Variation of  $\tau_{chem}$  with Equivalence Ratio

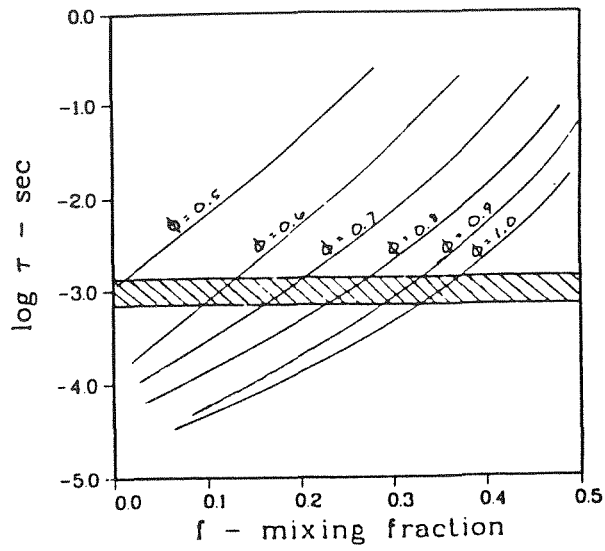


Figure 2.5: Effect of Equivalence Ratio and Mixture Fraction on  $\tau_{ind}$

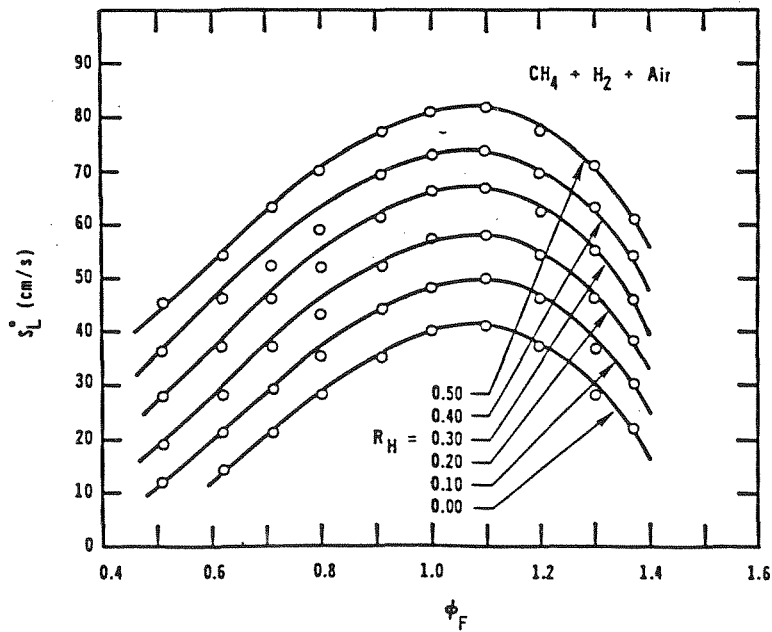


Figure 2.6: Laminar Flame Speeds for  $\text{CH}_4/\text{H}_2$  Mixtures

## Chapter 3

### Experimental Results

This chapter contains the results of experiments that were performed using the laboratory combustor. An explanation of the methods used to obtain the results and a discussion of the results are included in each of the following sections.

#### 3.1 Characteristics of the Combustion Instability

Under certain operating conditions, the oscillatory pressure signal measured at the flameholder grows from low level variations to large fluctuations similar to those in Figure 3.34. This growth is the most basic characteristic of combustion instability.

The difference in the flow field between stable and unstable operation is shown in Figure 3.1. When the pressure oscillations are small, the behavior is called “stable combustion” and a shear layer is observed downstream of the flameholder. This is a reattaching shear layer for both the single rearward-facing step and the double step. For the double step, the jetlike structure of the unburnt gas preferentially reattaches to either one of the sides of the combustor as can be seen in Figure 3.1. Coherent vortex structures associated with free shear layers, are evident in the single step picture.

When the large pressure oscillations are present, the flow field is changed

drastically. Instead of a shear layer, large vortex structures are shed from the flameholder. These vortices are much larger than those in the shear layer and are shed at one of the frequencies present in the oscillatory pressure signal. The velocity fluctuations at the flameholder can become nearly as large as the mean flow, and the shadowgraph pictures reveal that the flow into the combustor almost stops in some cases.

The signals and results of spectrum analysis for the radiation intensity, pressure, and velocity measurements change significantly for different operating conditions. An operating condition is defined by the longitudinal geometry of the system, the geometry of the flameholder, the fuel type, and the equivalence ratio used for a given experiment. A set of example signals is shown in Figure 3.8. There are two reasons that these signals are not necessarily easy to interpret by observing the raw data. For example, consider the signal produced by the superposition of two signals of constant amplitude with a small frequency difference. The resulting signal will show a familiar beating phenomenon. However, if the frequency difference is large, the sum may be difficult to interpret by the eye. The second reason involves the possibility that the amplitudes of different frequency components change with time. In this case, the use of ensemble averages of spectra may result in a repeatable spectrum even though individual spectra show significant differences.

Two general results are mentioned here. First, the amplitudes and frequencies of the measured signals are very sensitive to the operating condition that is chosen. Second, the frequencies of oscillation generally bunch near natural longitudinal acoustic modes of the system. These frequencies are determined in Chapter 4. Because of these results, the simplest classification of a particular

instability involves the identification of the vortex shedding frequency and affiliating the frequency with a longitudinal acoustic mode of the system. The vortex shedding frequency is defined in the following section and always occurs at one of the dominant frequencies present in the pressure spectrum.

## **3.2 Vortex Shedding Frequencies**

### **3.2.1 Data Reduction Procedure**

To determine the possible frequencies at which large pressure oscillations could occur, experiments were performed at various combinations of fuel type, equivalence ratio, and mean flow velocity for both flameholders. For particular operating conditions, the radiation intensity measurements at some axial location were recorded. A Fast Fourier Transform (FFT) was performed on this radiation signal, and ensemble averages were used to obtain repeatable spectra for most operating conditions. An example spectrum of the radiation intensity signal can be seen in Figure 3.9.

During most instabilities, vortex shedding occurred primarily at one frequency, and spectra obtained from various time segments of the data yielded very consistent results. However, in some cases two or more significant peaks were present in the radiation intensity spectrum and the amplitudes of successive spectra would vary. In this case, ensemble averages were used and the largest peak in the averaged spectrum was labelled the “vortex shedding frequency.” If ensemble averages still revealed no repeatable peak in the spectra, which often occurred at high flow speeds, then no shedding frequency was specified. Similarly, if the peaks were below a critical threshold value, which often occurred at very low flow speeds, then no shedding frequency was specified.

The three fuels and two flameholders required a series of six parametric studies to determine vortex shedding frequencies under particular operating conditions. A particular mean flow velocity and equivalence ratio were chosen for a fuel and a flameholder and this choice fixed the operating condition for a vortex shedding frequency to be determined. The mean flow velocity and equivalence ratio were then varied to give a “map” for each fuel/flameholder combination. The resulting vortex shedding frequencies are shown in Figures 3.2–3.7 for a plenum chamber length of 86 centimeters. The mean flow velocity is given for the value over the flameholder.

The vortex shedding frequency was usually very close to a frequency corresponding to a natural longitudinal acoustic mode of the system. The natural modes are discussed in Chapter 4 and under standard operating conditions their corresponding frequencies are: 188, 231, 377, 457, and 535 Hz. To simplify the nomenclature, a vortex shedding frequency is named by the corresponding natural mode frequency during standard operating conditions. Changes in the temperature or mean flow velocity result in shifts of the natural frequencies. Thus, when standard conditions result in a vortex shedding frequency at 188 Hz and changes in conditions result in shedding at 180 Hz, the discussion will still refer to the 188 Hz mode. For this reason, the symbols used in the figures represent the closest natural frequency to the measured vortex shedding frequency. The cross-hatched regions in the figures delimit regions of stable combustion. The other lines roughly divide regions of shedding at different system modes.

At a given mean flow velocity, lean and rich limits of flame stabilization were determined by first obtaining a stable flame and then decreasing or increasing the equivalence ratio until blow-off occurred. A particular operating

condition was fixed by one of two methods. The first method involved obtaining stable combustion at lean conditions and then increasing the equivalence ratio at constant mean flow speed until the operating point was reached. Using the second method, ignition occurred at a fixed equivalence ratio and the mean flow speed was then increased to the operating point desired. With this method, no regions of overlapping symbols representing hysteresis effects could occur.

### 3.2.2 Discussion

Each of the following sections represents one fuel/flameholder combination. The general trends shown for each case are discussed and comparisons made.

#### Map 1

The effect of changes in equivalence ratio are discussed first. The trends present in each figure are similar to those observed in Figure 3.2 for the single step and methane. From this figure, it is observed that at a mean flow velocity between 40 and 120 ft/sec, as the equivalence ratio is increased, the combustion process undergoes transition to instability at the 188 Hz mode. Then, as the equivalence ratio is increased beyond stoichiometric, stable combustion and eventually rich blow-off occur. There exist hysteresis effects so that vortex shedding frequencies depend to some extent on the path of approach to a given operating condition. For example, if there exists shedding at 188 Hz and the equivalence ratio is decreased, stable combustion will first occur at a lower equivalence ratio than the value at transition to 188 Hz instability that occurs when the equivalence ratio is increased during stable combustion. However, as discussed in the previous paragraph, these hysteresis effects are not seen in the figures because of the method of data reduction that was used.

Now consider changes in the mean flow velocity. Near a stoichiometric equivalence ratio, as the mean velocity is increased, the radiation intensity spectra reveal peaks at both the 188 Hz mode and at the 231 Hz mode. Ensemble averages of many spectra result in a spectrum in which the largest peak is repeatable. For this “competition” between the two modes, at mean velocities over 120 ft/sec, the amplitude of the 231 Hz mode is larger than the amplitude of the 188 Hz mode. At even higher flow speeds, both peaks fall below the threshold value.

### **Map 2**

Observing Figure 3.3, if the flameholder is replaced by the double step, the amplitude of the radiation intensity signal at the 231 Hz mode is larger than that of the 188 Hz mode at even very low speeds if the equivalence ratio is near stoichiometric. Also, with this flameholder, the amplitude of both peaks falls below the threshold value at mean flow velocities above 70 ft/sec.

### **Map 3**

When the fuel is changed to include 15% hydrogen, a more complicated map results, as shown in Figure 3.4. At flow speeds less than 75 ft/sec, for equivalence ratios near 0.8, the largest peak is generally near the 231 Hz mode. At higher mean flow velocities a different instability occurs. For this instability there is again a ‘competition’ between two frequency peaks in the spectra. This competition is between the 535 Hz mode and its subharmonic at 267 Hz. Again, as the flow velocity is increased, the spectral peak of the higher frequency becomes dominant. For this map, as the mean flow speed is increased, 267 Hz shedding begins at about 80 ft/sec and the 535 Hz shedding becomes dominant at about 110 ft/sec. The equivalence ratio dependence at 80 ft/sec is nearly symmetrical about an equivalence ratio of 0.8. As the equivalence ratio is increased at this

flow speed, transition from stable combustion to the 188 Hz mode occurs and this is followed by growth and dominance of the 231 Hz mode. As the equivalence ratio approaches 0.8, shedding at 267 Hz begins abruptly.

#### **Map 4**

When the step was replaced by the double step for the same fuel, the results plotted in Figure 3.5 were obtained. For an equivalence ratio of around 0.8, vortex shedding at 267 Hz is observed at flow velocities above 40 ft/sec. Even at higher velocities vortex shedding at the 530 Hz mode does not occur with this flameholder. At lower velocities and at lean or rich equivalence ratios, shedding at the 231 Hz mode is usually dominant.

#### **Map 5**

Finally, for methane mixed with 30% hydrogen, the results become even more complicated as seen in Figures 3.6 and 3.7. A wide range of combustion temperatures occurs for this fuel at different equivalence ratios. Therefore, the natural frequencies shift a significant amount and the modal affiliation becomes more difficult to specify.

For the single step at an equivalence ratio near 0.75, the spectral peak at 265 Hz is dominant but quite small for very low flow speeds. As the speed is increased, shedding at the 188 Hz mode occurs and finally at flow speeds above 75 ft/sec, competition between the 535 Hz mode and its subharmonic begins. The subharmonic shedding is dominant up to a mean flow of about 125 ft/sec, at which point the 535 Hz mode becomes dominant. Again, the results are fairly symmetrical about an equivalence ratio of 0.75 .

#### **Map 6**

For the double step, results are similar except that shedding at the 267 Hz

subharmonic case occurs as a large spectral peak down to mean flow velocities of 30 ft/sec. With this flameholder, the spectra become very noisy at higher velocities and no shedding frequency can be specified. As with the 15% hydrogen fuel, the highest velocity at which a well-defined shedding frequency occurs is around 150 ft/sec.

One last remark about Figures 3.4, 3.6, and 3.7 concerns the shedding at the 460 Hz mode. This shedding is represented by the asterisks in the first two figures and by the upward-pointing arrow in the last figure. For these operating conditions, the lean equivalence ratio results in lower magnitudes of radiation intensity even though flow visualization verifies the presence of large vortex structures in the combustor.

### 3.2.3 Summary

The trends of vortex shedding phenomena discussed in this section are now summarized and some important physical mechanisms are described.

#### Equivalence Ratio Dependence

The dependence of the vortex shedding frequency upon the equivalence ratio reveals a strong dependence upon the chemical reaction process. The chemical reaction times discussed in Chapter 2 are over two milliseconds for very lean and very rich mixtures of methane and air. For the observed combustion instabilities, the combustion associated with the vortex shedding generally occurs within one cycle of the modal frequency. Thus, for higher frequency modes, the combustion feedback must generally occur within a shorter period of time than for the lower frequency modes. As the mixture equivalence ratio approaches stoichiometric, the chemical reaction time reaches a minimum value and therefore the higher

frequency modes would be expected. This is indeed the trend in all of the above figures. Also, the chemical reaction time decreases as the hydrogen fraction in the fuel is increased and therefore the excitation of higher frequency modes is observed.

### **Step Height Dependence**

For a fixed operating condition, use of the double step generally results in the excitation of higher frequency modes of the system. This shift of modes is attributed to smaller fluid mechanical mixing times that occur for the double step. Hendricks [34] investigated this mechanism by using a Flux Corrected Transport method to solve the Euler equations for the two-dimensional flow that resulted as a shock wave was passed over a rearward-facing step. The shock wave was used to produce an increase in the velocity over the step. This velocity was meant to simulate acoustic velocity fluctuations so that the effect on the flow field could be investigated. It was determined that as the fluid surges forward over the step, a large vortex structure is shed which is similar to the structures observed experimentally.

Hendricks found an approximately linear relationship between the magnitude of the upstream velocity fluctuation and the time from vortex shedding to vortex impingement on the lower wall below the step. Since the combustion process is controlled by the mixing of fresh reactants with hot products, the time from vortex shedding to reaction may decrease because of enhanced mixing due to the growth of shed vortices. Therefore, use of the double step is expected to result in a smaller reaction time delay and the excitation of the higher frequency modes.

## Mean Flow Speed Dependence

Increases in the mean flow speed result in the excitation of higher frequency modes. This effect is more difficult to understand because only small changes in the vortex structure are observed with changes in the mean flow speed. Shadow-graph pictures as well as Hendricks' calculations show that as the flow speed is increased, the time from vortex shedding to impingement on the lower wall does not change significantly. However, the location of the impingement point moves downstream with greater flow speeds, even though the general appearance of the vortex does not change. Thus, the fluid mechanical mixing time is not expected to change significantly.

One possible mechanism for the observed trend involves the chemical kinetic effects discussed in Chapter 2. Hendricks' calculations reveal that the amplitude of the fluctuation velocity determines the size of the vortex and that the mean flow velocity determines the location of the impingement on the lower wall of the combustor. Thus, the volume of hot gas trapped upstream of the impingement location combined with the volume of gas in the vortex structure may be representative of the overall mixture fraction of fresh reactants to hot products. This mixture fraction depends on the ratio of the fluctuating velocity to the mean flow velocity. While the mixing is still an important part of the time from shedding to reaction, the chemical time depends on the mixture fraction as shown in Figure 2.5. Thus, as the flow speed is increased, the location of vortex impingement moves downstream for a fixed vortex size. This results in a higher mixture temperature and a shorter chemical ignition delay. This mechanism may be responsible for the excitation of higher frequency modes at greater mean flow velocities.

### 3.3 Results of Typical Instability Frequencies

The instabilities of several operating conditions were investigated in more detail by taking measurements for unstable conditions after the finite limiting amplitude of the oscillation had resulted. The aim was to investigate the mechanism for the sustenance of oscillations by investigating instabilities corresponding to different vortex shedding frequencies.

For future reference, one example was used as the “standard case” and is common to all of the following groups of results. This case consisted of a geometry that was fixed with the single step and the plenum chamber length  $L_{plenum}$  of 2.82 ft. Also, the operating conditions were fixed by using methane at stoichiometric ratio with air and a mean flow velocity at the flameholder  $V_{mean}$  of 60 ft/sec.

#### 3.3.1 Signals and Spectra: Two Examples

Although the frequencies and amplitudes of instability are sensitive to the operating conditions used for a given experiment, results are presented here for two example operating conditions to indicate the general appearance of the raw signals and the resulting spectra measured during combustion instability. The first case represents operation during standard operating conditions. The second operating condition consists of the use of the single step flameholder, the 15% hydrogen mixture at an equivalence ratio near 0.8, and a mean flow speed of 150 ft/sec.

The raw signals of data taken during the example operating conditions are shown in Figure 3.8. For both cases, the top trace is the oscillatory pressure measured at the flameholder, the middle trace is the fluctuating radiation intensity

at 4.7" downstream of the flameholder, and the bottom trace is the velocity 1.25" upstream of the flameholder lip. An FFT was performed on each of the above signals to give the spectra observed in Figures 3.9 and 3.10.

From the spectra for the standard conditions, it is observed that the pressure signal contains large components at both the 188 Hz mode and the 457 Hz mode with smaller peaks around 230 Hz and 420 Hz. The radiation intensity and velocity fluctuations reveal vortex shedding at the 188 Hz mode with smaller peaks near the 231 Hz mode. The velocity fluctuations at the flameholder result in vortex shedding, which affects the combustion. The resulting transfer function between the velocity fluctuations at the flameholder and the radiation intensity at a downstream location is related to the fluid mechanics of the vortex shedding phenomenon and the subsequent combustion process.

For the second case, the spectra in Figure 3.10 reveal that the large pressure oscillations consist of peaks at the 457 Hz mode and at the 535 Hz mode, which yield the beating phenomenon seen in the raw signals. The velocity fluctuations are almost entirely at the 535 Hz mode and the combustion associated with the vortex shedding at this frequency results in a peak in the  $i'$  spectrum. The combustion at 4.7" downstream of the flameholder may be sensitive to the pressure in a nonlinear way so that the radiation intensity signal rises and falls with the beat frequency of the two dominant modes as can be seen in the raw signals. The beat frequency is also evident as a significant peak in the  $i'$  spectrum.

In both cases, pressure oscillations at the 457 Hz mode are present but no significant peaks at this frequency are seen in the  $i'$  spectra. This is discussed in more detail in the section containing the radiation intensity distribution plots. Small peaks at this frequency are generally observed in  $i'$  spectra obtained for

locations closer to the flameholder.

### 3.3.2 Mode Shapes

Oscillatory pressure measurements were recorded at the eleven port locations under several operating conditions using the single rearward-facing step flameholder. The magnitude of the largest peak in the spectrum of each signal was then obtained. These magnitudes were then plotted as a function of axial location. Also, the one-sided cross-spectral density was obtained for the pressure at one location and the pressure at the flameholder. This gave the phase difference of the two signals as a function of frequency. The phase difference for the largest peak in the spectrum was then plotted as a function of axial location. In Figures 3.11–3.14 these results are presented along with the theoretical mode shapes, which are derived by the methods discussed in Chapter 4. The axial location of measurement is plotted on the horizontal axis and the flameholder is located at the origin. The upper plot for each case is the magnitude mode shape for the largest peak in the pressure spectrum, and the experimental value at the flameholder is matched with the theoretical mode shape. The bottom plot is the phase difference with respect to the phase at the flameholder.

The amplitude mode shape for the 188 Hz mode shown in Figure 3.11 reveals a shape that is similar to a standing wave in the plenum chamber. This is close to the resonant mode that would occur if the chamber were considered to have ideal reflection coefficients at both ends. The coupling of this chamber to the rest of the system results in the portion of the mode shape where experimental amplitudes were obtained. The acoustic model predicts quite accurately the shape of the mode and the location of modal nodes.

The phase differences at various locations in the system depend strongly on the reflection coefficients at the ends of the system. Ideal reflection coefficients result in no phase difference between the pressure signals at different locations in the system. However, phase differences are measured experimentally and the greatest phase change occurs across the step for the conditions shown in Figure 3.11. For the acoustic model, independently determined reflection coefficients were used as discussed in Chapter 4. These coefficients can be changed to fit the experimental phase differences more accurately than shown in the figures.

For the 231 Hz shedding shown in Figure 3.12, matching of the model predictions with the experimental value at the flameholder results in an overestimation of the amplitudes upstream of the flameholder lip by nearly a factor of two. However, the mode shapes within each acoustic segment and the location of the nodes are predicted quite accurately by the model. Also, the reflection coefficients again result in an underestimation of the phase differences that are measured.

For the 457 Hz shedding shown in Figure 3.13, a shape very close to a quarter-wave is observed in the combustor section. This is basically the organ-pipe mode of the combustor. Therefore, the flameholder is near a system node for the acoustic pressure fluctuations and near an antinode for the acoustic velocity fluctuations. For this mode, the model underestimates the magnitudes in a portion of the inlet section by nearly a factor of two. However, the mode shapes and the location of the nodes are predicted fairly accurately by the model. The measured phase differences for this mode show excellent agreement with the model predictions. Similarly, the measured modes shape and phase differences for the 535 Hz mode show good agreement with the theory.

Although the amplitude of the pressure oscillation during combustion instability is sensitive to the precise operating condition, a statement can be made that instabilities of higher frequency modes generally have higher amplitudes of the pressure oscillations. If two different operating conditions result in vortex shedding of the same frequency, the amplitude of the associated pressure oscillations may vary by a factor of two. However, the general trend of higher amplitudes at higher frequencies can be observed in the example conditions chosen for the above mode shapes. For example, the 535 Hz mode shape has a peak amplitude about four times the peak amplitude of the 188 Hz mode shape.

### 3.3.3 Cinematography Results with Radiation Intensity Profiles

Shadowgraph movies were taken by Smith [10] for two example operating conditions during combustion instability. The single step and methane were used for both conditions but the plenum chamber length and mean flow speed were different. A sequence of frames from the film of the instability under standard operating conditions is shown in Figure 3.15. The oscillating pressure and velocity were measured at the flameholder. The component of these signals at the vortex shedding frequency of 188 Hz is plotted beside the film sequence.

From this figure, it is observed that the flow velocity at the flameholder results in the shedding of a large vortex during each cycle of oscillation. The pressure and velocity components at the vortex shedding frequency are measured to be  $183^\circ$  out of phase for these conditions. For other modes, the phase difference is different, so no generalization can be made about this result. However, this is a very important quantity in the dynamics of instability and will be discussed in detail in Chapter 4.

An investigation of the distribution of the heat release rate was performed for the two example conditions using the radiation intensity data in the following manner. The magnitudes of both the mean and the oscillatory components of the radiation intensity signals at 0.5" increments along the combustion chamber were obtained. The largest peak in the radiation intensity spectrum and its first harmonic were then added to the mean value to reconstruct the radiation intensity distribution at various times during one cycle of the primary frequency.

This radiation intensity distribution was plotted beneath shadowgraph pictures of the same scale in Figures 3.16–3.20. These represent five equally separated movie frames during one cycle of oscillation for the standard operating conditions. These figures allow comparison of the distribution of the heat release rate to the derivative of the density gradient that is responsible for the shadow effect seen in the pictures. Because of the assumption of linearity between the radiation intensity and the heat release rate as discussed in Chapter 2, the following discussion includes interchangeable use of these terms.

The resulting figures reveal that the radiation intensity in the first half of the combustion chamber continues to rise after the initial combustion front of the vortex has passed. In Figure 3.16 a vortex is in the early formation process and the associated combustion is very low, whereas the combustion associated with the previous vortex is responsible for high levels of radiation throughout most of the observed section. The residual combustion along the upper wall of the combustor is significant and results in a large mean level of combustion that declines at the downstream end of the first window, i.e., beyond 5.0 inches.

In Figure 3.17, it is seen that as the vortex rolls up, the level of radiation intensity actually drops but above-average reaction continues from 3.5 to 5.5

inches because of the previous vortex. Even as the vortex passes 2.0 inches in Figure 3.18, the level of radiation is below average and downstream combustion from the previous vortex has ceased.

In Figure 3.19, as the vortex moves to the middle of the chamber and is affected by the lower wall, the radiation intensity is still near the mean value. As the vortex impinges on the lower wall, the flow of the fresh reactants is concentrated along the lower wall. Finally, in Figure 3.20, as the gas associated with the vortex nears the end of the window section, the upstream combustion level has risen to above-average levels. This flow field results in the occurrence of the largest fluctuating radiation intensity near the end of the window.

Five sequential plots of the radiation intensity distribution were superimposed and data points were replaced by cubic-spline fits through the points. These curves were then plotted under the corresponding frames of the movie in Figures 3.21–3.24. The two figures for each operating condition represent the first and second halves of the period of the vortex shedding frequency, respectively. There were no data points between 5.5 and 7.5 inches downstream of the step because no window was located in that region. Therefore, the cubic-spline may underestimate the magnitude of the peak as the vortex moves into that region.

For the 188 Hz shedding in Figures 3.21 and 3.22, the vortex motion can be tracked by observing the peak in the radiation intensity that moves downstream. The magnitude grows and decays during the period of oscillation. The peak occurs around 5.0 inches at a time about three-quarters of a cycle after the vortex was shed. By plotting the location of the peak at different times in the cycle, a vortex speed can be determined and was calculated to be nearly half the mean flow speed for this case.

For the second operating condition shown in Figures 3.23 and 3.24, the vortex shedding frequency corresponds to the 535 Hz mode. As in the previous case, the largest fluctuating values are around 5.0 inches. In the first four inches of the combustor, the combustion remaining from the previous vortex is still significant even as the new vortex approaches. This results in radiation intensity values that are almost constant at locations between 1.0 and 3.0 inches. Indeed, radiation intensity spectra from those locations reveal peaks that are quite small; and surprisingly, the peak at around 457 Hz is the largest. This frequency is not observed in the figures because only the shedding frequency and its harmonic were used to reconstruct the radiation intensity distribution.

Both the vortex shedding and the largest fluctuating radiation intensities in most of the chamber occur at the 535 Hz mode. However, it appears that there is a region of combustion where contributions from the previous vortex and the newly formed vortex are nearly equal. This is a region of nearly constant combustion, which may be sensitive to pressure oscillations. Thus, fluctuating combustion may occur as a result of both velocity-sensitive vortex shedding and pressure-sensitive combustion in a region that is approximated by a well-stirred reactor. The pressure spectra for this case show large peaks at both 535 Hz and at 457 Hz, and the excitation mechanism of the latter is not clear from flow visualization and may be related to a pressure-sensitive combustion response.

The sequences shown above support the idea that the fluid mechanical mixing time and the chemical induction time may be of the same order of magnitude. Near the flameholder, the passing of the vortex occurs without much mixing taking place, and the reaction moves into the fresh reactants towards the upper wall as the vortex moves downstream. As the vortex impinges on the lower wall,

vigorous mixing occurs, and the peak in the radiation intensity at downstream locations occurs only shortly after a peak is reached at locations near the flameholder. This results in an apparent combustion front that travels much faster than the vortex and even faster than the mean flow speed over the flameholder.

### 3.3.4 The Rayleigh Criterion

#### Introduction

Investigations into combustion instability phenomena generally include some reference to the mechanism of energy transfer from the combusting gases into the acoustic field. Lord Rayleigh[13] stated the commonly cited criterion, which follows.

If heat be given to the air at the moment of greatest condensation, or be taken from it at the moment of greatest rarefaction, the vibration is encouraged. On the other hand, if heat be given at the moment of greatest rarefaction, or abstracted at the moment of greatest condensation, the vibration is discouraged.

A mathematical statement of this criterion is derived in Appendix A and can be written,

$$\Delta E = \frac{\gamma - 1}{\gamma \bar{p}} \int dV \int_t^{t+\tau} p' q' dt, \quad (3.1)$$

where  $\Delta E$  in this equation is the energy added to the acoustic field as a result of the coupling between the oscillatory pressure  $p'$  and the oscillatory heat release rate  $q'$  during time  $\tau$ . This is one type of source for energy addition to small disturbances. Chu[47] discussed other sources, which include coupling between oscillations of pressure with mass sources, entropy with heat release rate, and velocity with body forces. Using a formulation based upon expansion of the

oscillatory pressure in normal acoustic modes of the system, Culick[48] derived an expression similar to Equation 3.1 for the criterion.

Now, if we are interested in the energy addition to frequency  $f_o$ , at one particular location  $x_o$ , where reaction is taking place, then the above equation becomes,

$$\Delta E_{f_o, x_o} = \frac{\gamma - 1}{\gamma \bar{p}} \oint p'_{f_o, x_o} q'_{f_o, x_o} dt. \quad (3.2)$$

The one-sided cross-spectral density for  $p'$  and  $q'$  is written,

$$G_{p'q'}(f) = |G_{p',q'}(f)| \exp \{-i \theta_{p',q'}(f)\}, \quad (3.3)$$

where the magnitude indicates to what extent a component exists at frequency  $f$  in both signals and  $\theta_{p',q'}(f)$  is the phase difference between the components of the two signals at frequency  $f$ . Now, if the fluctuating radiation intensity is linearly related to the heat release rate, then the acoustic energy added at frequency  $f_o$  can be plotted as a function of the location in the combustor by using these CSD results in Equation 3.2 to get

$$\Delta E_{f_o, x_o} = C_1 |G_{p',i'}| \cos(\theta_{p',i'}), \quad (3.4)$$

where  $C_1$  is a constant and  $p'$  and  $i'$  are the spectral components of the oscillatory pressure and radiation intensity signals at frequency  $f_o$  measured at axial location  $x_o$ .

Radiation intensity data at 0.5" increments along the combustor and oscillatory pressure data at the flameholder were taken for various example operating conditions using the single step. Oscillatory pressure signals at each 0.5" location were obtained by using the results of the mode shape previously discussed.

## Experimental Results

Figure 3.25 represents the phase difference between the two signals at different axial locations during combustion instability with standard operating conditions. These phases were used to determine the Rayleigh Criterion for the standard case, which is presented in Figure 3.26. The square symbols represent  $\Delta E_{x,f_o}$  and the circles represent  $|i'_{x,f_o}|$ . Since changes in fuel and equivalence ratio affect the radiation intensity level and the proportionality constant between the radiation intensity and the heat release rate, magnitudes for different figures cannot be compared. The dashed line represents the region between windows where no radiation intensity data could be obtained.

Figures 3.26–3.33 are plots of  $\Delta E_{x,f_o}$  and  $|i'_{x,f_o}|$  during combustion instability, which resulted from a number of operating conditions. Figures 3.29 and 3.31 represent cases in which  $f_o$  was very nearly twice the vortex shedding frequency, whereas the others represent the acoustic energy added at the vortex shedding frequency.

## Discussion

### Combustion Wave Velocity

As discussed in the previous section, as a large vortex structure associated with combustion instability is convected downstream, the combustion levels at upstream locations continue to rise. The peak combustion at upstream locations occurs only shortly before combustion associated with the core of the vortex structure. Thus, a combustion wave appears to travel down the combustor at a higher velocity than the vortex structure. By measuring the phase difference between the radiation intensity and the pressure at different axial locations, this velocity can be determined. The slope of the line in Figure 3.25 reveals that for

standard operating conditions this velocity is about twice the mean flow speed over the flameholder and is nearly a constant for the entire combustor.

As the vortex moves into the second half of the combustor, the vortex structure becomes increasingly mixed with hot products and the combustion follows the structure core more closely than in upstream sections, where combustion increases long after the vortex passes. However, the velocity of the vortex increases because of the expansion of gases in the upstream section. Hence, counteracting effects produce a velocity of the combustion wave that is nearly constant. Using this velocity and the amplitude of the radiation intensity as a function of axial location, the following Rayleigh Criteria were determined for various operating conditions.

#### Rayleigh Criteria

For standard operating conditions, Figure 3.26 reveals that  $p'$  and  $q'$  have components at the vortex shedding frequency of 188 Hz that are in phase between the flameholder and 4.0 inches. In this region the coupling of these oscillations adds energy to the acoustic field. However, between 4.0 and 10.0 inches, the signals are out of phase and energy is extracted from the acoustic field. The peak in the fluctuating radiation intensity signal occurs around five inches downstream of the step. At this location,  $q'$  lags  $p'$  by about one-quarter of a cycle and therefore the peak is bisected by a line that divides regions of driving from regions of damping of the acoustic field. These regions are of nearly equal area, the expected result when no growth or decay of amplitudes is observed. A lower equivalence ratio was used to obtain the results shown in Figure 3.27. The results are indistinguishable within the accuracy of the measured values.

In Figure 3.28 the shape of the curve is similar to the standard case. In this

case, the component of the  $i'$  signal at the first harmonic of the vortex shedding frequency feeds energy into the 457 Hz mode. Although the  $i'$  peak is much smaller for the harmonic, the pressure oscillations are much larger for the 457 Hz mode. The regions in which energy is added to this mode due by the first harmonic of the vortex shedding frequency are shown in Figure 3.29 to be nearly the same as in the previous figures.

Under particular operating conditions with the short plenum section, vortex shedding is observed at around 230 Hz even though no natural mode exists near that frequency. For the long plenum chamber, the shedding near 230 Hz may be associated with both the 231 Hz natural mode and the subharmonic of the 457 Hz mode. However, for conditions resulting in the data presented in Figure 3.4, shedding near 267 Hz can be associated only with the subharmonic of the 535 Hz mode.

In Figures 3.30 and 3.31 the Rayleigh Criteria for shedding at around 267 Hz are shown for both the shedding frequency and the first harmonic of the shedding frequency at the 535 Hz mode. For the 267 Hz case, the region in which the  $i'$  magnitude is near a peak is in a region where the pressure oscillations lead the heat release by more than one-quarter of a cycle so that a negative value for  $\Delta E_{x,f_n}$  is seen. However, the component of  $i'$  at 535 Hz is in phase with the pressure oscillations at that frequency and driving occurs in the regions of positive  $\Delta E_{x,f_n}$  in Figure 3.31.

The curves shown in Figures 3.32 and 3.33 are for the short plenum chamber, the single step flameholder and methane. The flow speeds are fairly high and a lean equivalence ratio is used in the second case. Vortex shedding in the first figure occurs at 535 Hz, whereas the change in chemistry for the second case

results in 457 Hz shedding. For the first case, driving of the instability occurs near the region of the largest fluctuating radiation intensity. For the 457 Hz shedding, the results are similar except that the peak driving occurs closer to the flameholder. Also, at the upstream end of the second window, the driving is positive, whereas in the previous case slight damping is measured.

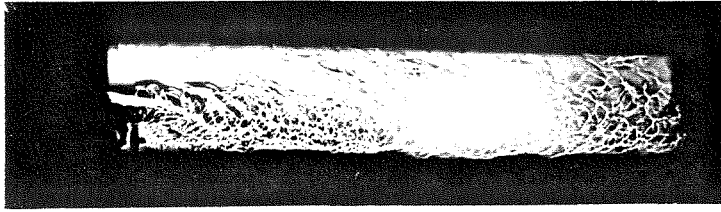
In conclusion, pressure oscillations at the vortex shedding frequency and often at the harmonic of the shedding frequency can be attributed to fluctuating heat release rates that are in phase with the pressure signal. The potential for energy addition as a result of this coupling is very large. During instability, the driving by this mechanism must equal the damping in the system. This damping is primarily due to the same coupling mechanism with signals having opposite phase. Also, non-ideal reflection of acoustic waves at the exits and viscous losses in the boundary layers contribute to damping of the acoustic field. The distribution of the heat release rate throughout the combustion chamber is important in the determination of the mechanism of sustenance for a particular instability frequency.

### **3.3.5 Transition Data: Nonlinear Development**

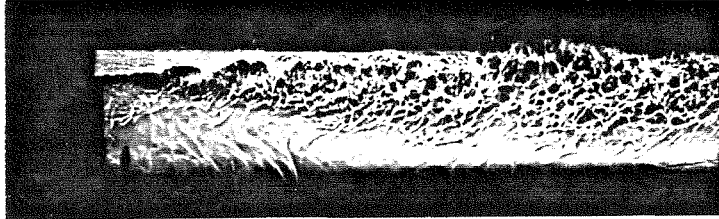
The results presented thus far were obtained to characterize the flow conditions during instability and to gain a better understanding of the mechanism by which an instability is maintained. The following results document the evolution of the combustion process from stable combustion to the oscillatory conditions previously presented. Several different physical mechanisms that could result in limit cycle behavior are presented in Chapter 4. The results presented here are used to describe the evolution process during standard operating conditions.

As an example of the type of signal obtained during transition to instability, the oscillatory pressure signal at the flameholder and the radiation intensity signal at the location specified were plotted during transition from stable to oscillatory combustion. Figures 3.34 and 3.35 are traces of these signals for standard operating conditions. The spectra shown previously reveal that the pressure signal is not as clean as the radiation intensity signal that shows the evolution of the vortex shedding phenomenon. The growth is seen to occur over only a few cycles of oscillation and a finite limiting amplitude is reached.

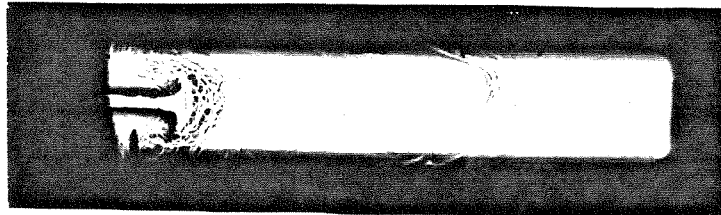
The radiation intensity signal was measured 5.0" downstream of the flameholder. During stable combustion, a significant mean value of radiation intensity is observed because of the reaction within the shear layer. However, as transition to instability occurs, the mean value is seen to decrease as the fluctuating component increases because of the passage of the large vortex structures.



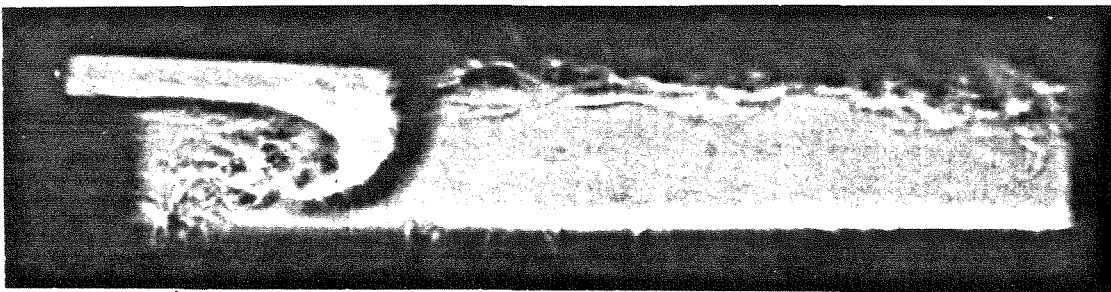
Double Step: Stable Combustion



Single Step: Stable Combustion



Double Step: Combustion Instability



Single Step: Combustion Instability

*Figure 3.1:* Flow Field Classification

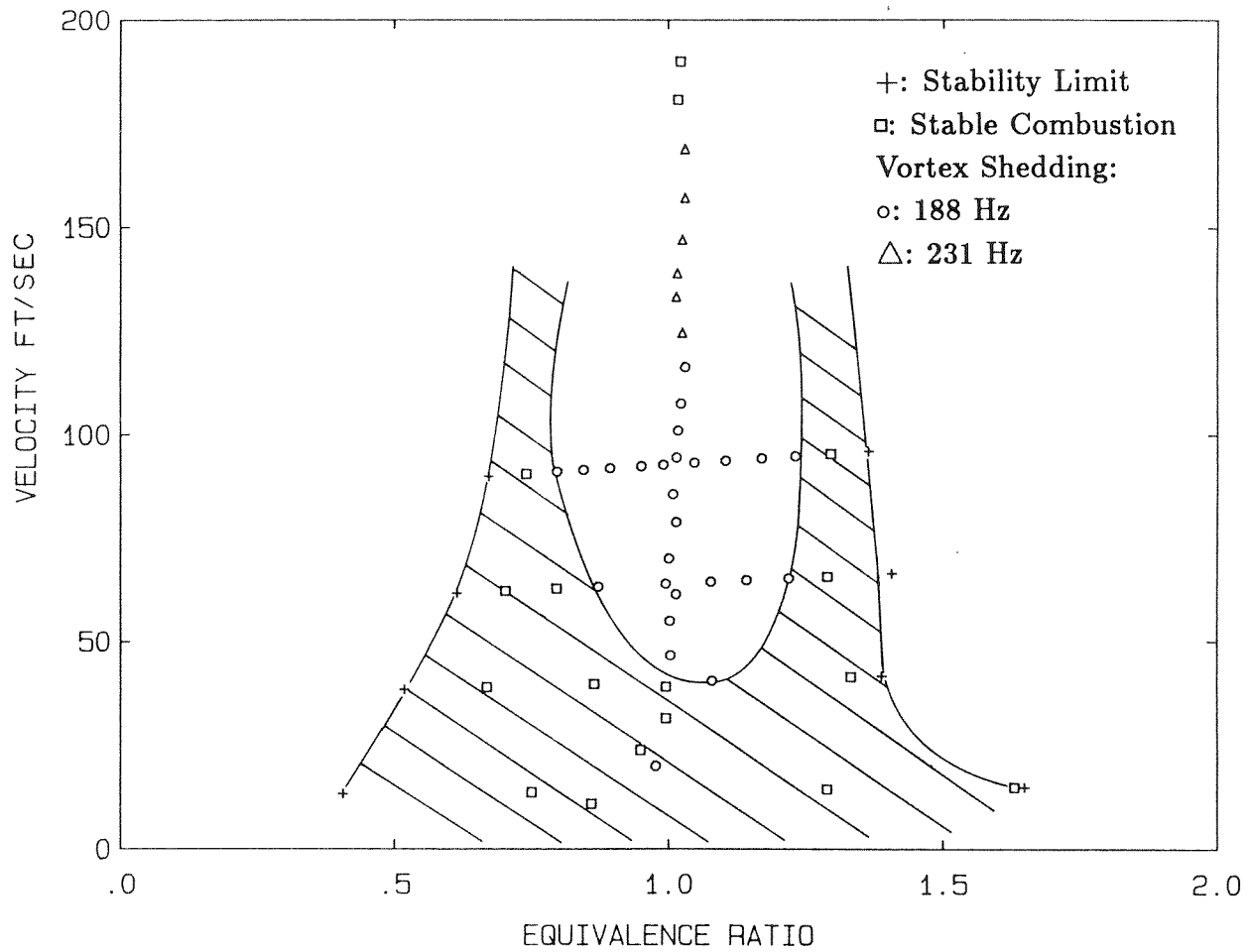


Figure 3.2: Map 1: Methane, Single Step

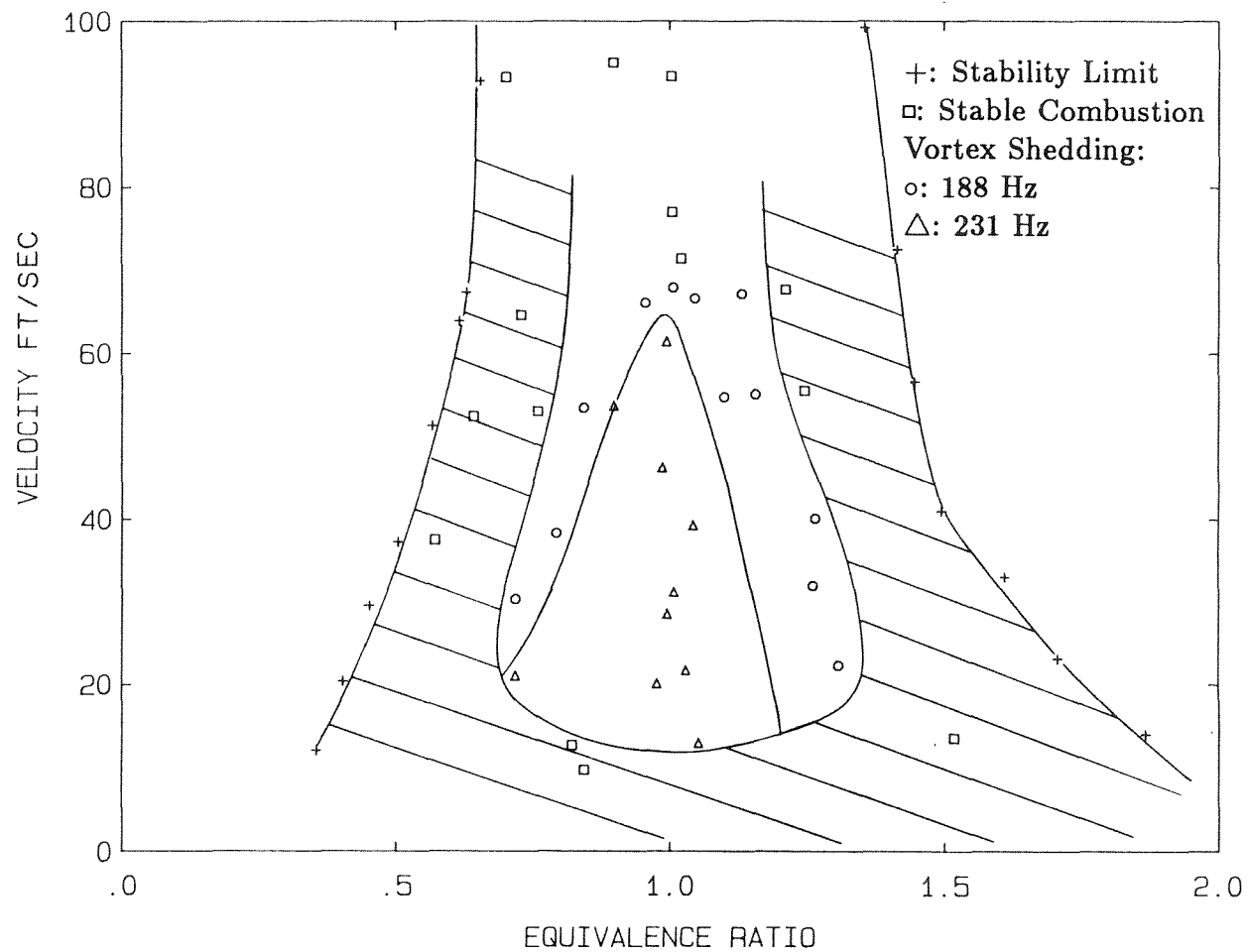


Figure 3.3: Map 2: Methane, Double Step

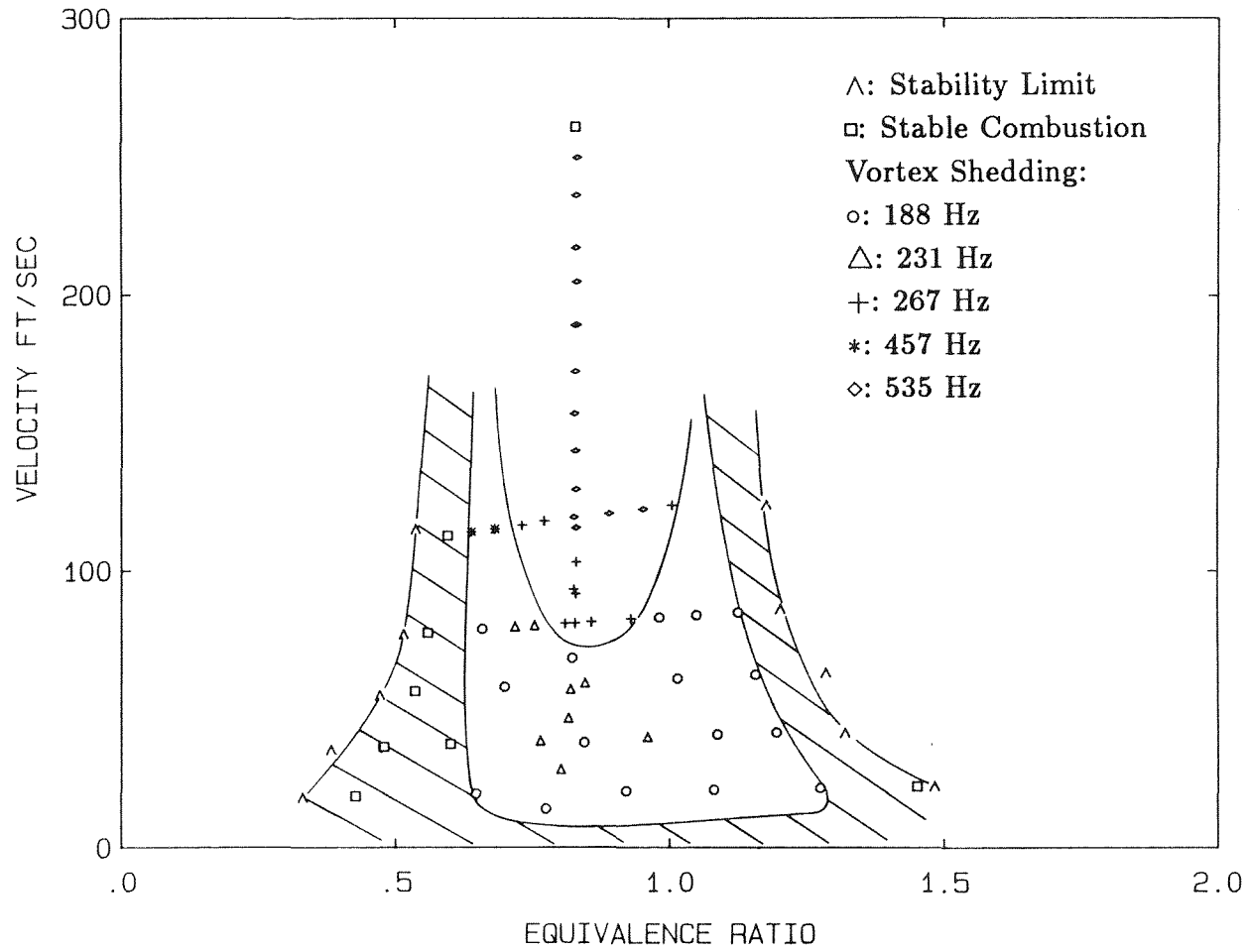


Figure 3.4: Map 3: 15% Hydrogen-Methane, Single Step

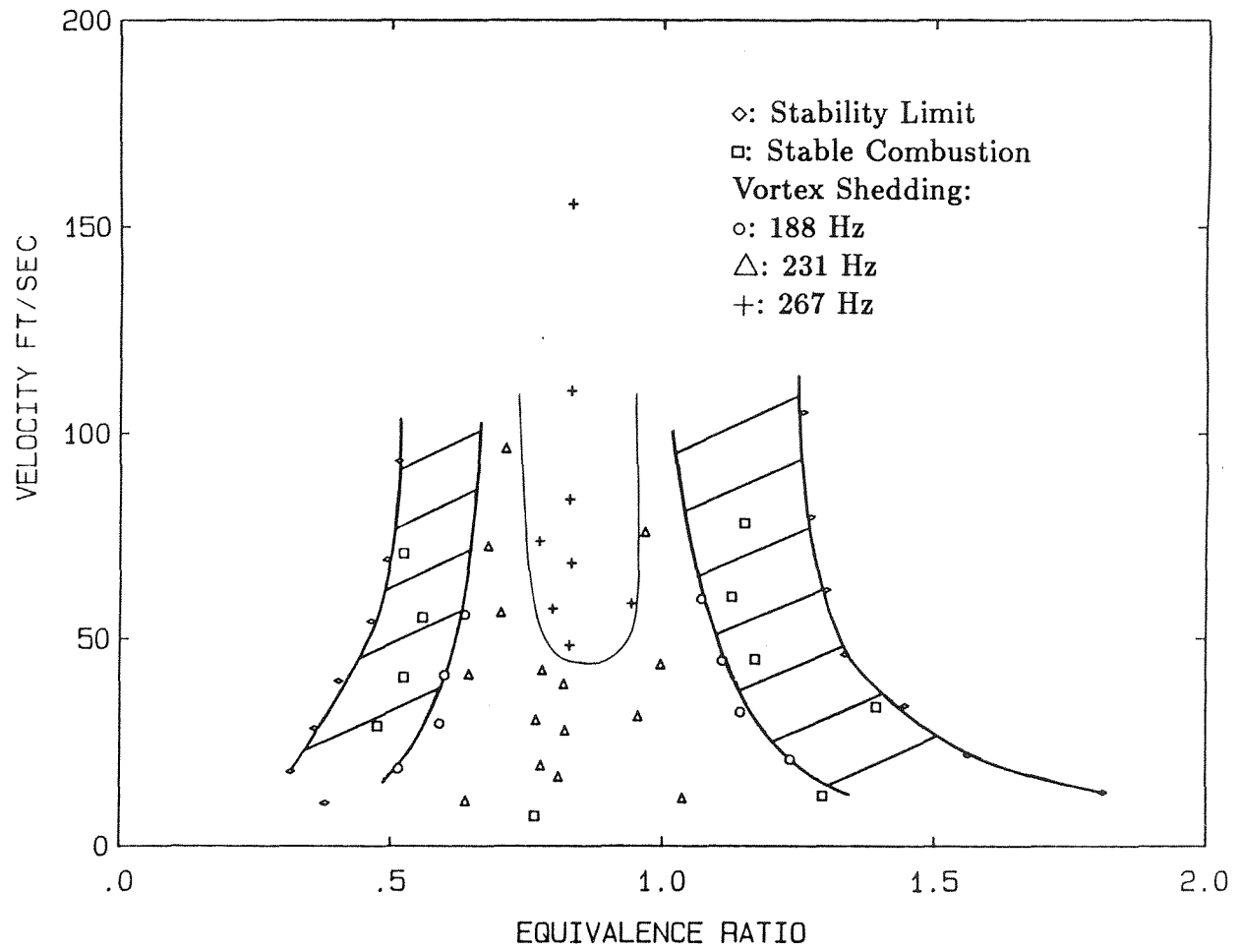


Figure 3.5: Map 4: 15% Hydrogen-Methane, Double Step

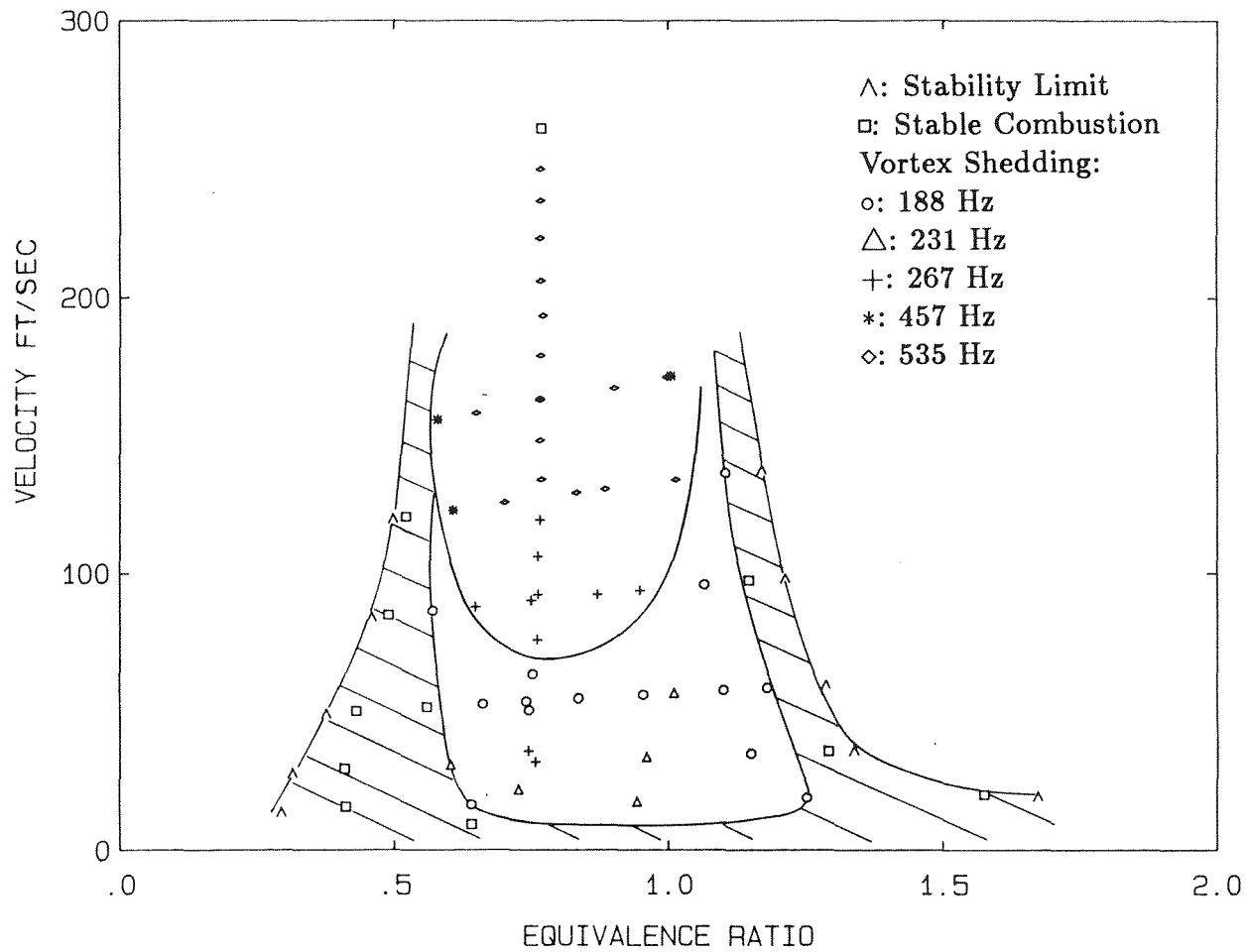


Figure 3.6: Map 5: 30% Hydrogen-Methane, Single Step

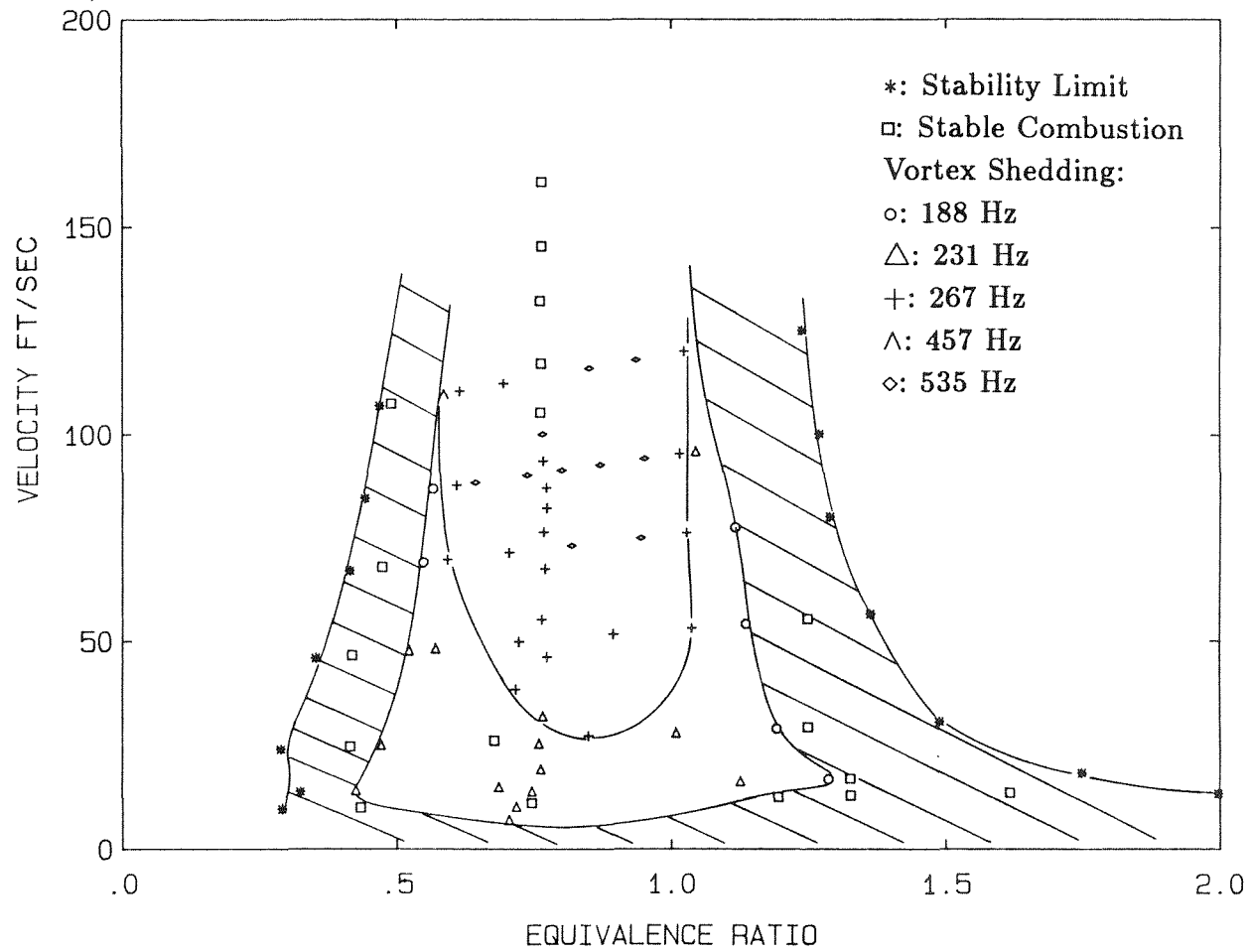
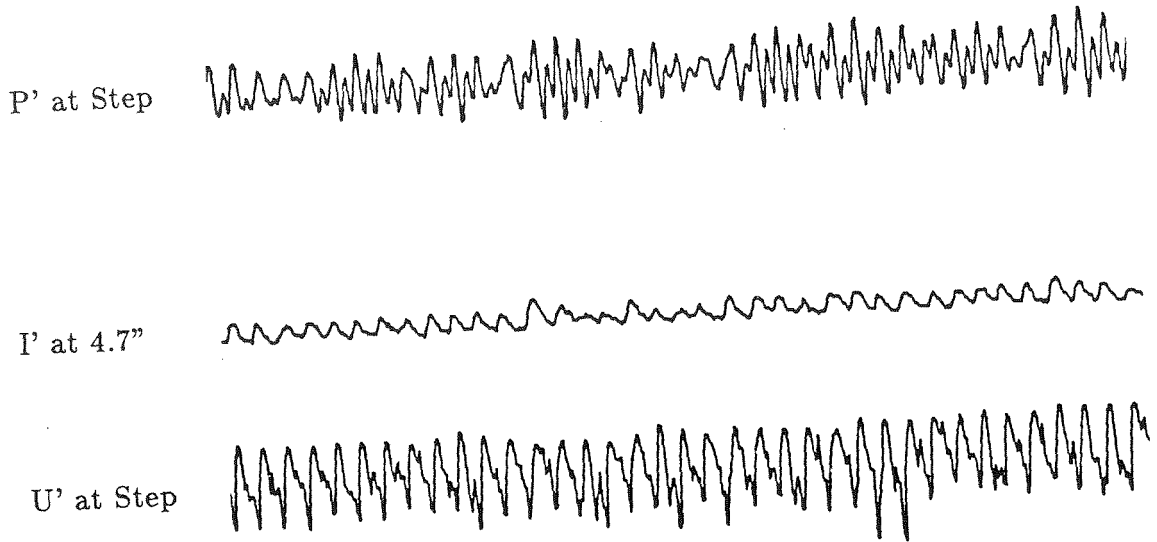
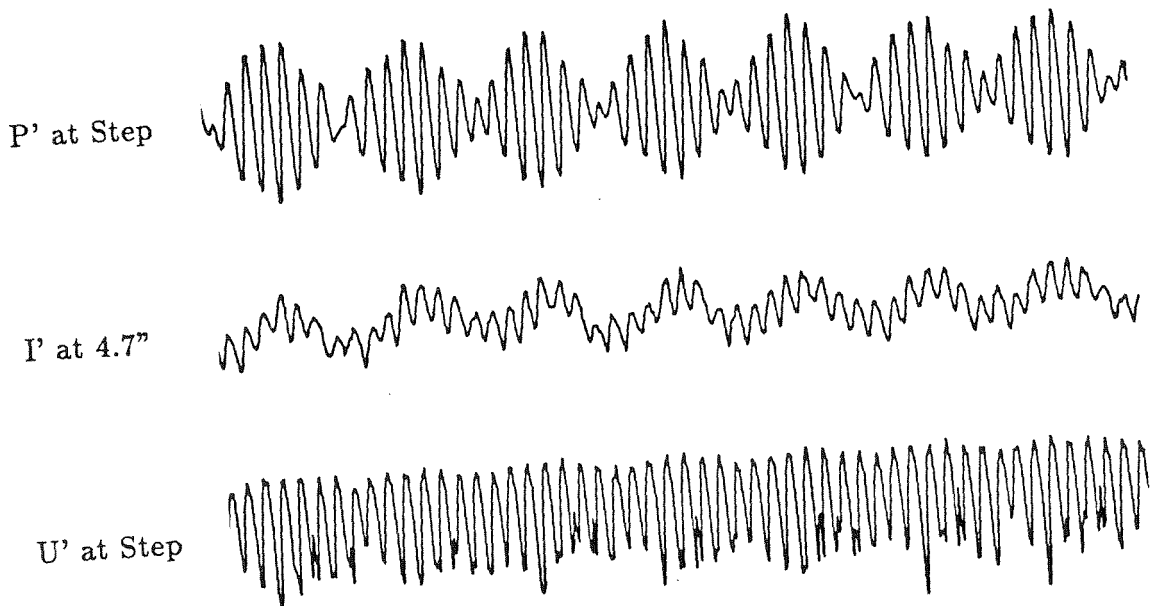


Figure 3.7: Map 6: 30% Hydrogen-Methane, Double Step



188 Hz Instability



535 Hz Instability

Figure 3.8: Examples of Raw Signals

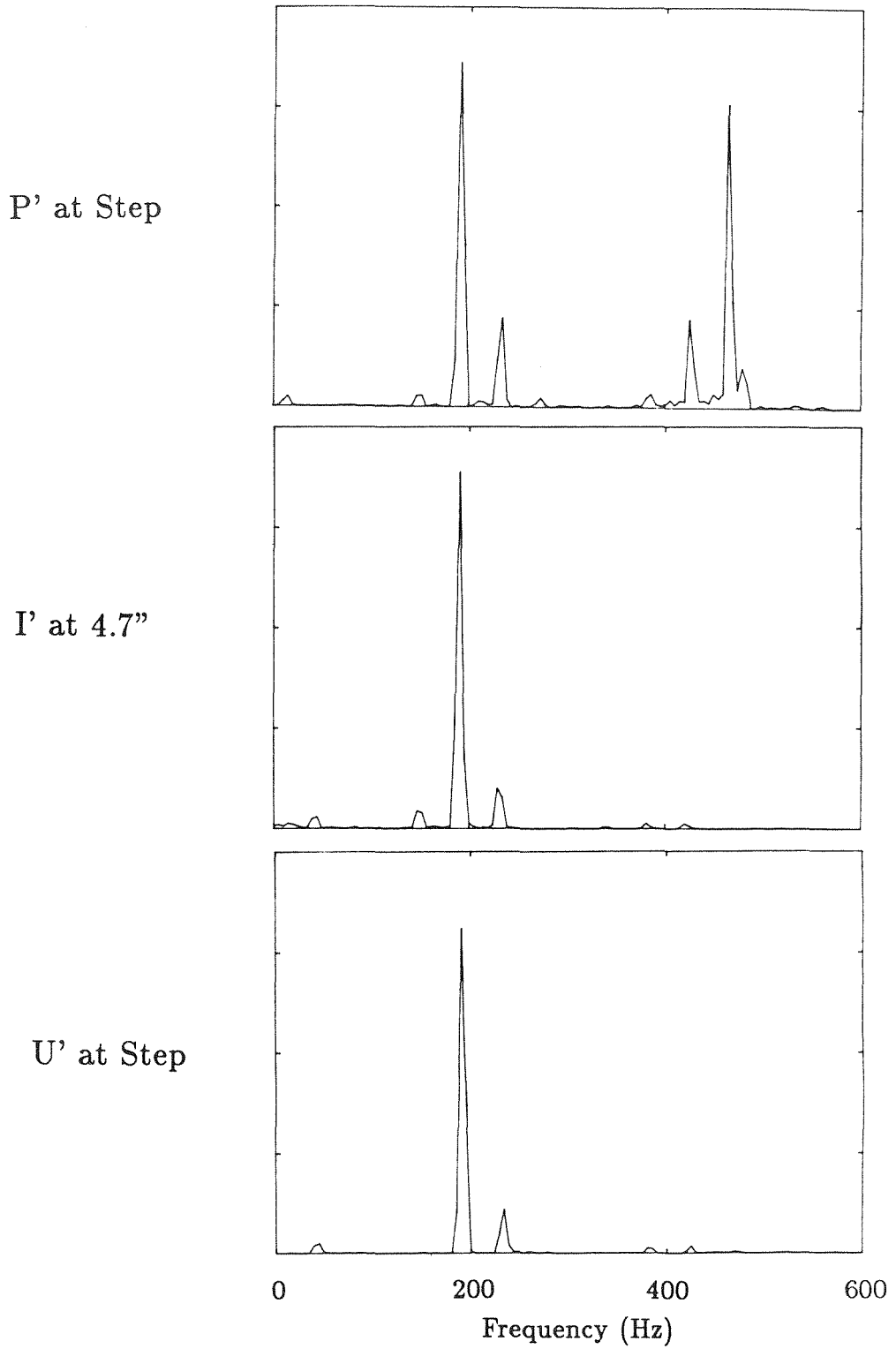


Figure 3.9: Spectra : Single Step, Methane,  $\phi = 1.0$ ,  $V_{mean} = 60 ft/sec$

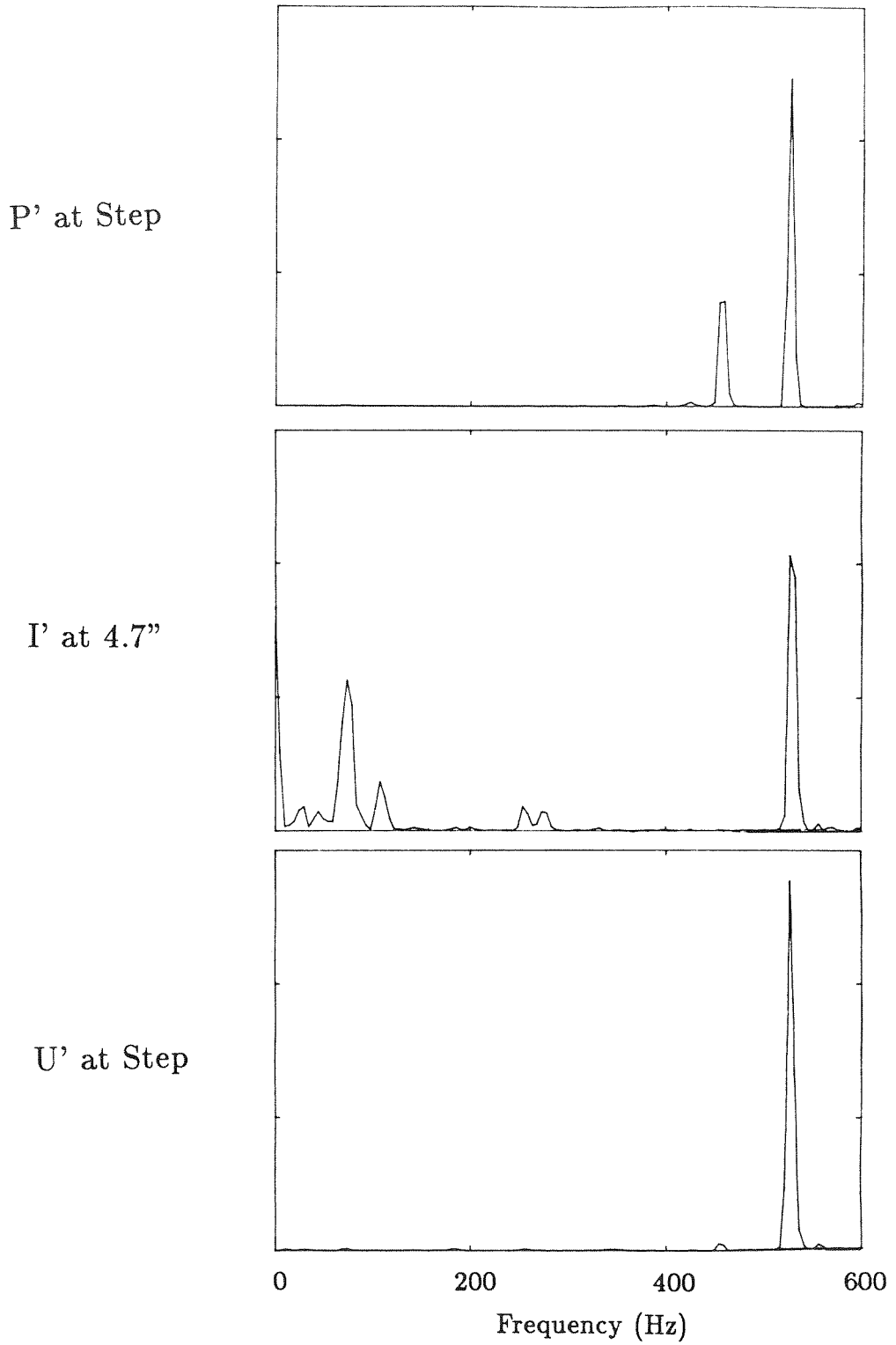


Figure 3.10: Spectra : Single Step, 15% $H_2$ –85% $CH_4$ ,  $\phi = 0.8$ ,  $V_{mean} = 150 ft/sec$

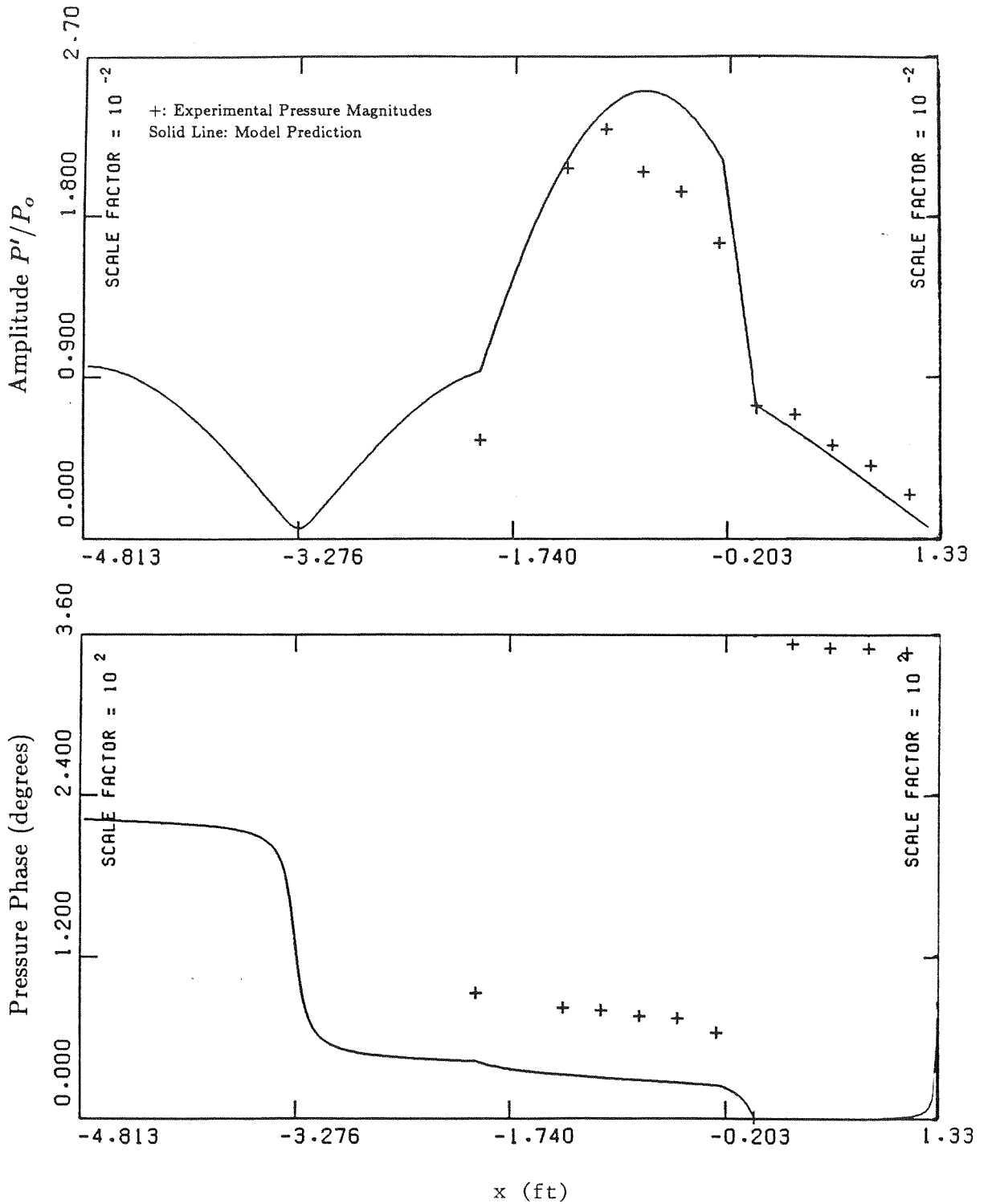


Figure 3.11: 188 Hz Mode Shape : Methane,  $\phi = 1.0$ ,  $V_{mean} = 60 \text{ ft/sec}$ ,  
 $L_{plenum} = 2.82 \text{ ft}$

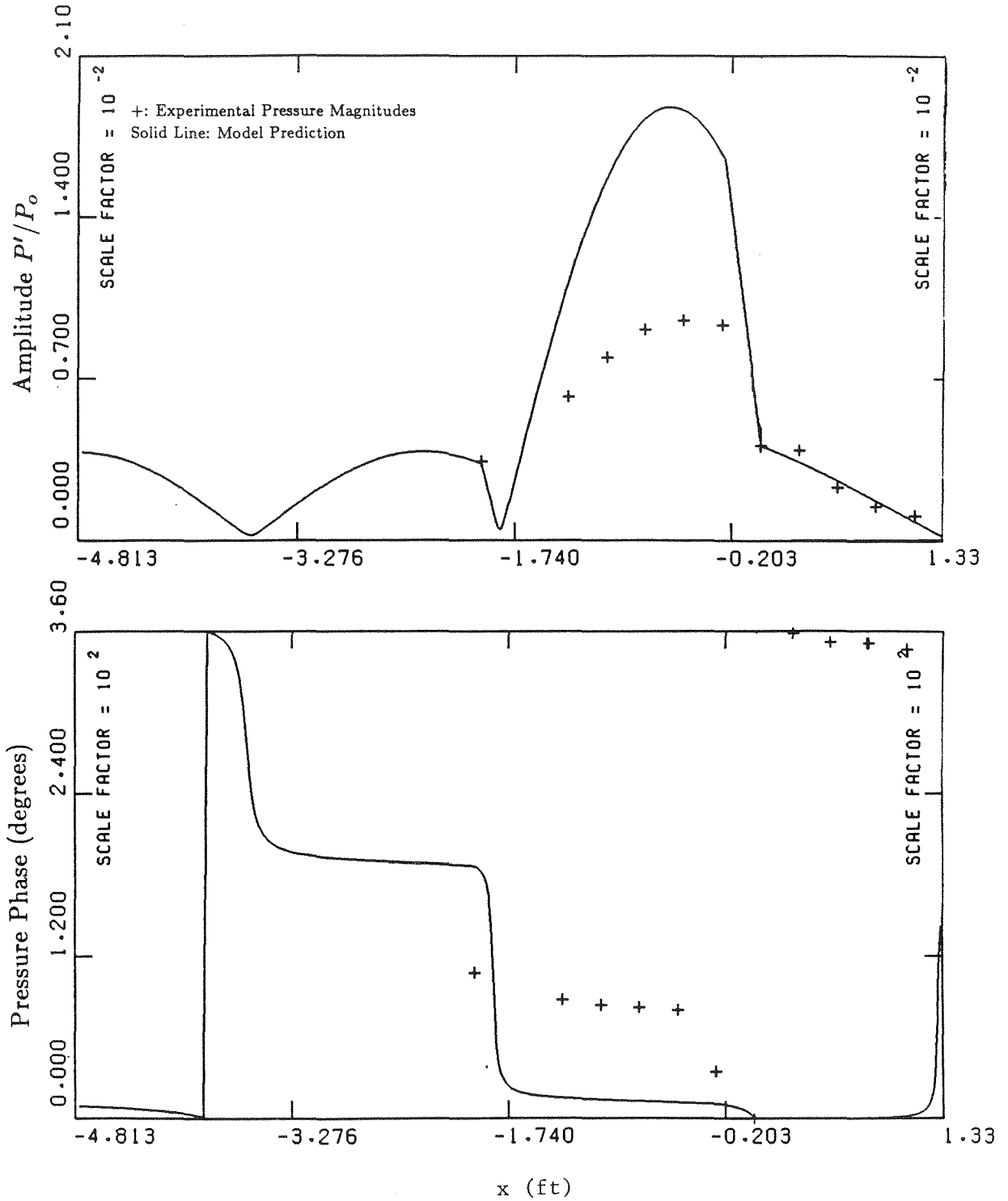


Figure 3.12: 231 Hz Mode Shape : 15% $H_2$ -85% $CH_4$ ,  $\phi = 0.86$ ,  $V_{mean} = 69 ft/sec$ ,  
 $L_{plenum} = 2.82 ft$

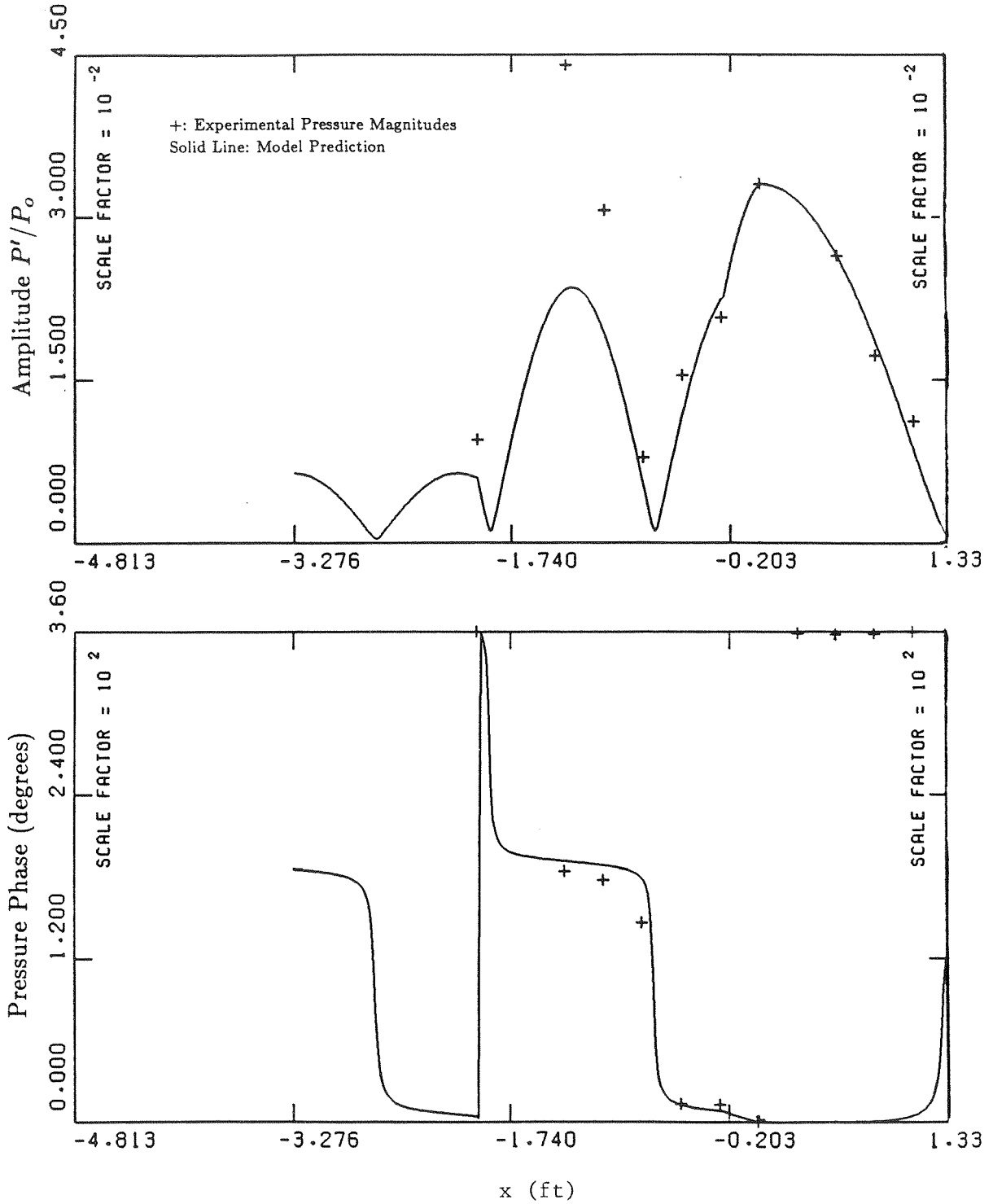


Figure 3.13: 457 Hz Mode Shape : Methane,  $\phi = 0.79$ ,  $V_{mean} = 108 \text{ ft/sec}$ ,  
 $L_{plenum} = 1.84 \text{ ft}$

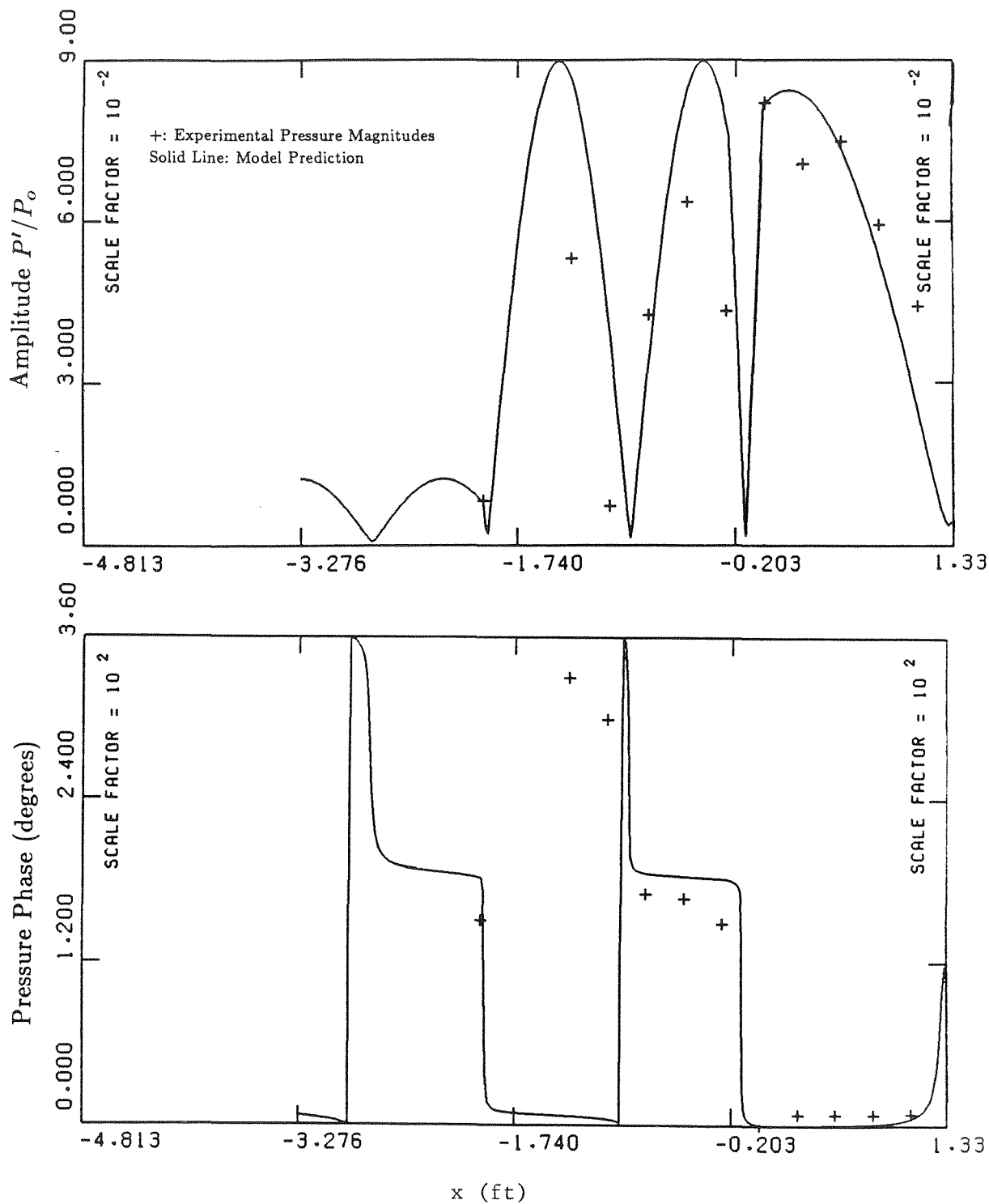


Figure 3.14: 535 Hz Mode Shape : Methane,  $\phi = 1.0$ ,  $V_{mean} = 145 \text{ ft/sec}$ ,

$$L_{plenum} = 1.84 \text{ ft}$$

# Vortex Evolution

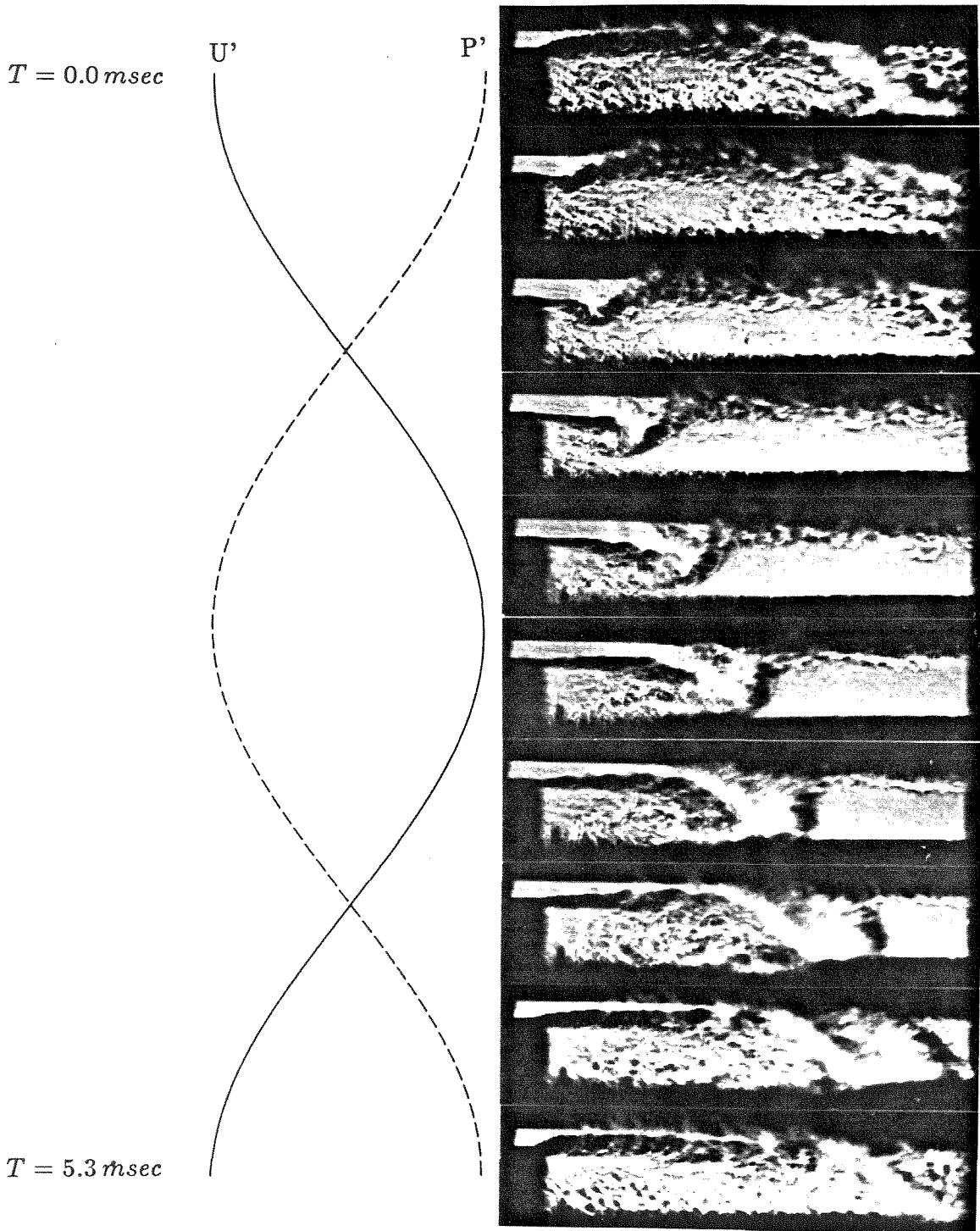


Figure 3.15: 188 Hz Shedding Movie:  $\phi = 1.0$ ,  $V_{mean} = 60 \text{ ft/sec}$ ,  $L_{plenum} = 2.82 \text{ ft}$

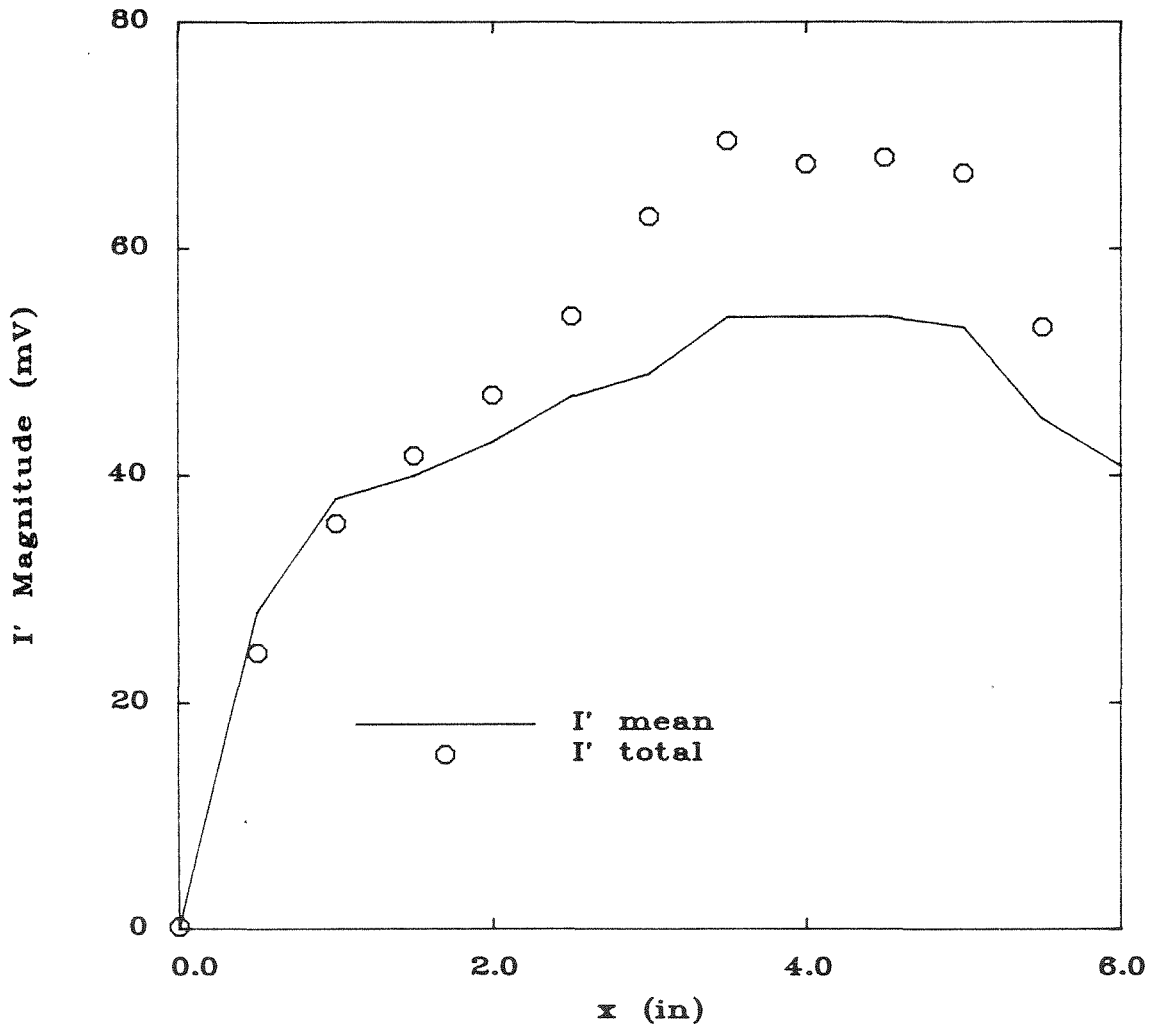
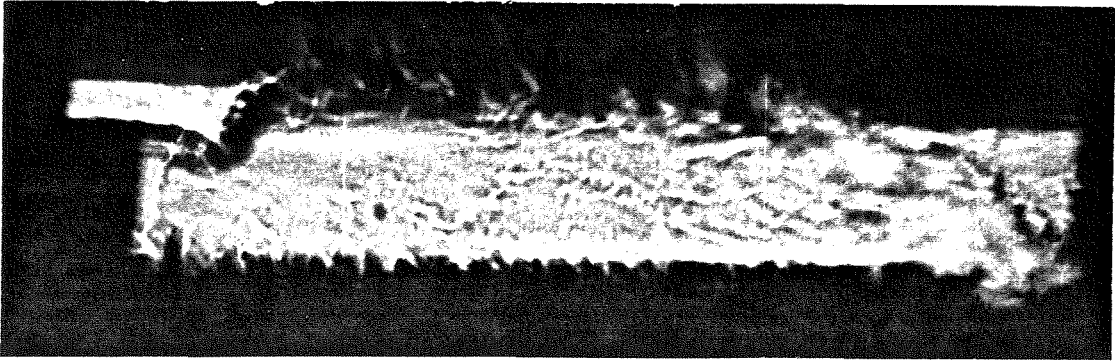


Figure 3.16: Standard Case 188 Hz Shedding :  $0^\circ$  Phase Angle

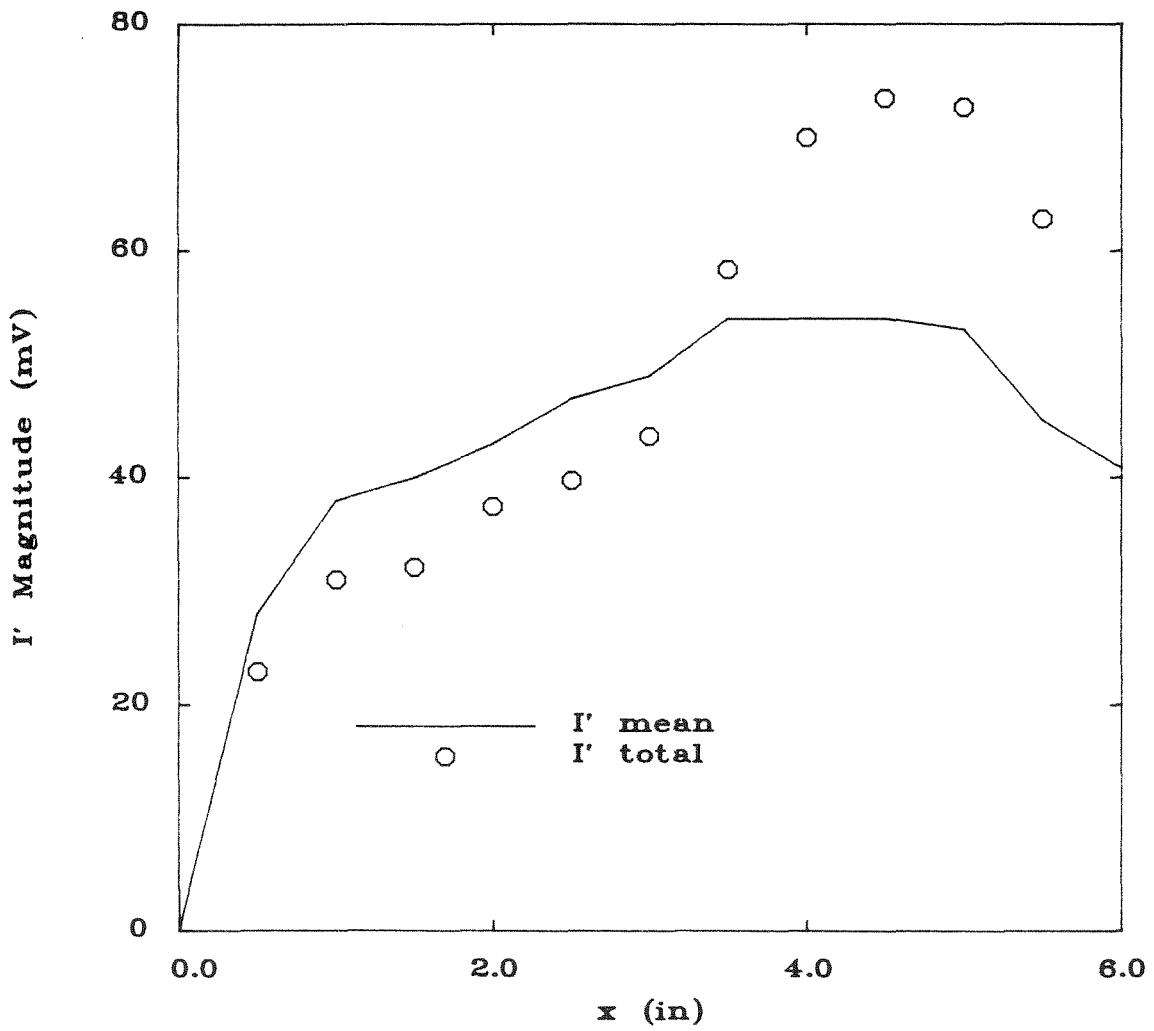
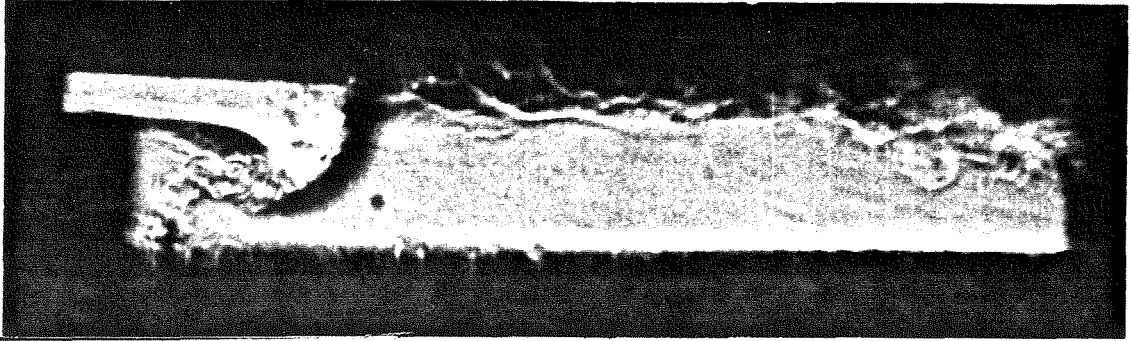


Figure 3.17: Standard Case 188 Hz Shedding : 72° Phase Angle

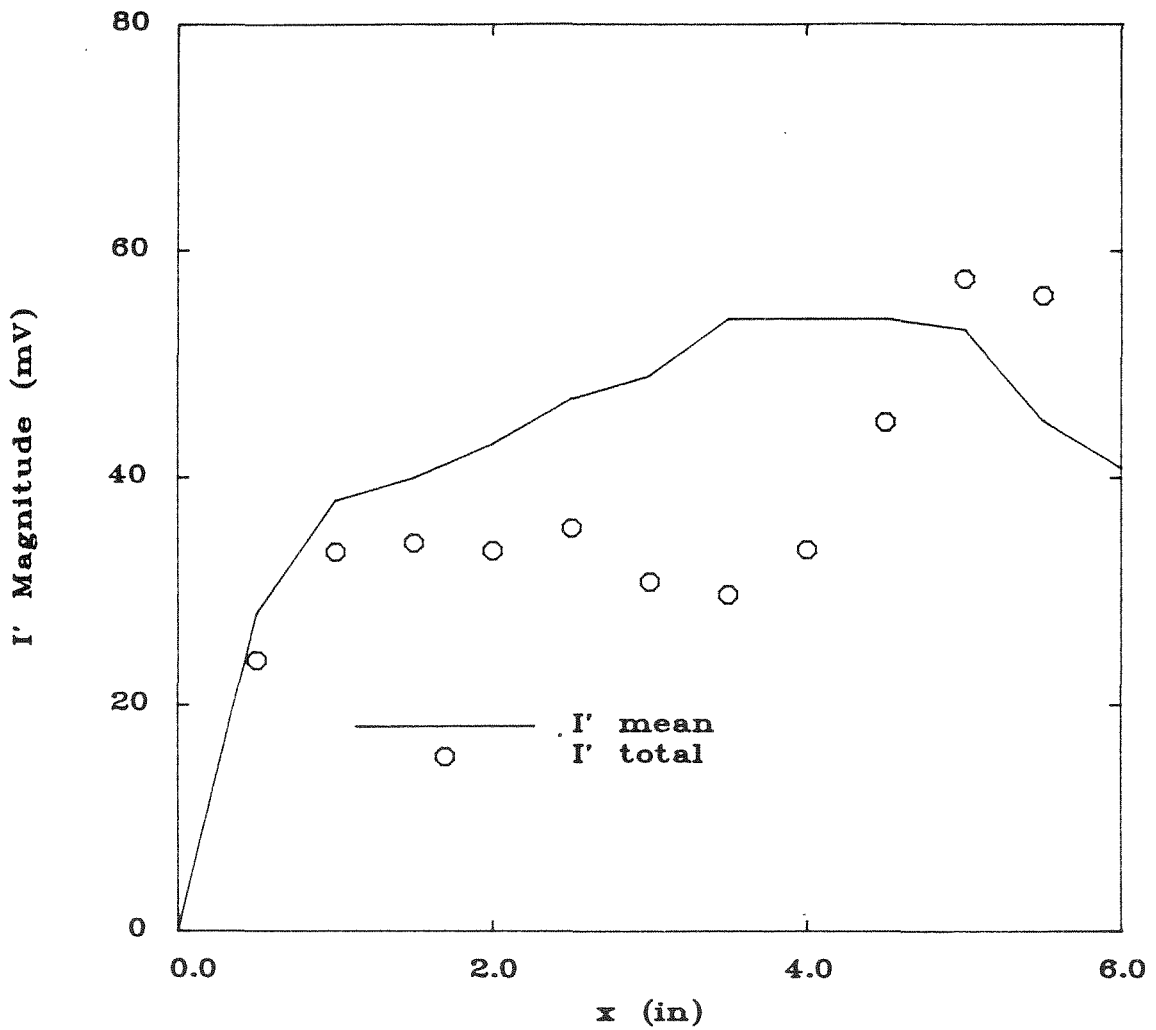
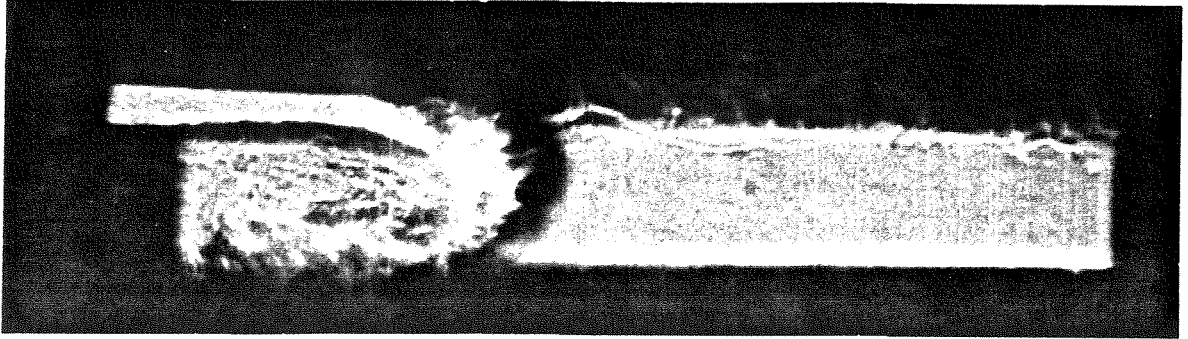


Figure 3.18: Standard Case 188 Hz Shedding : 144° Phase Angle

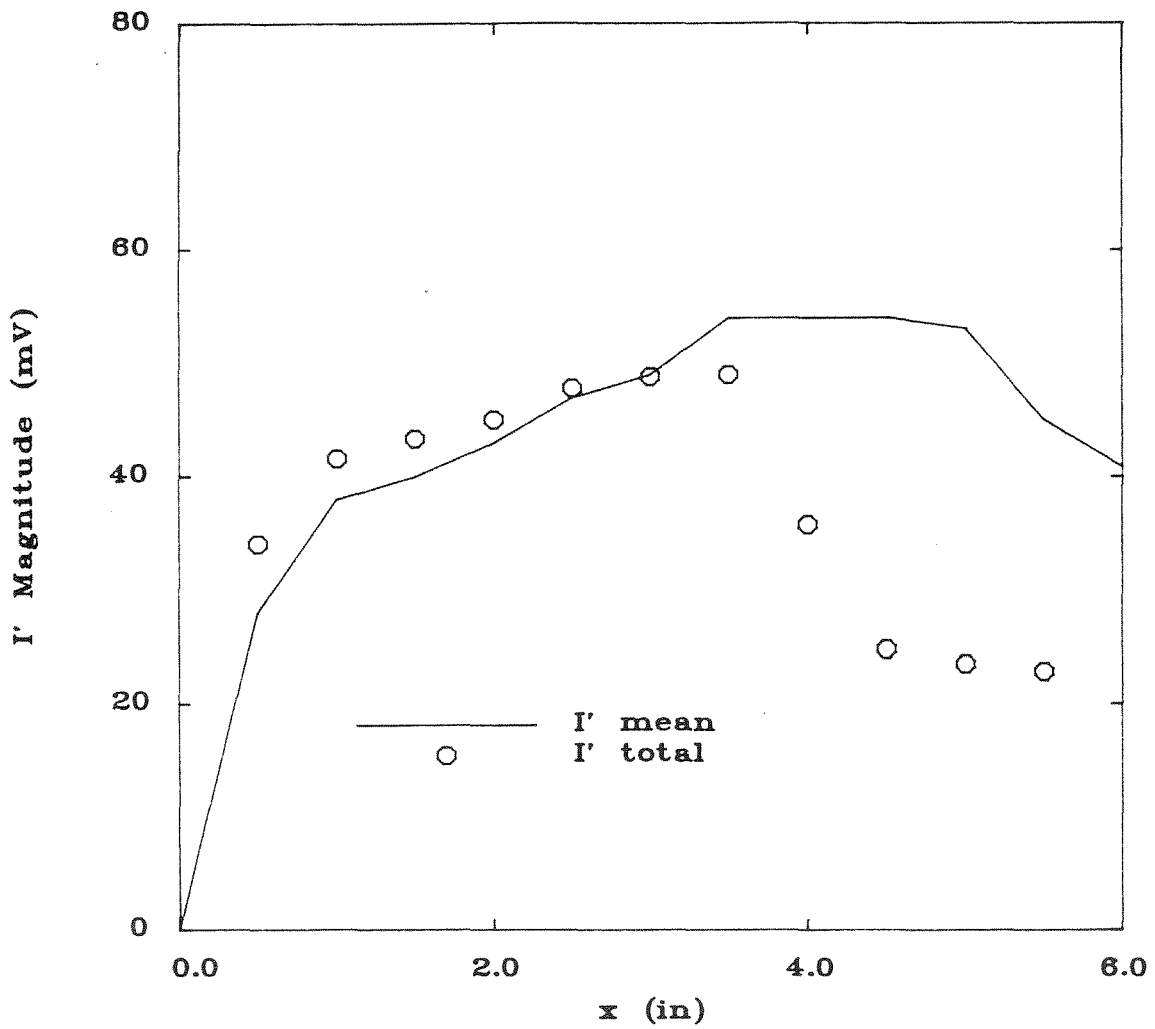


Figure 3.19: Standard Case 188 Hz Shedding :  $216^\circ$  Phase Angle

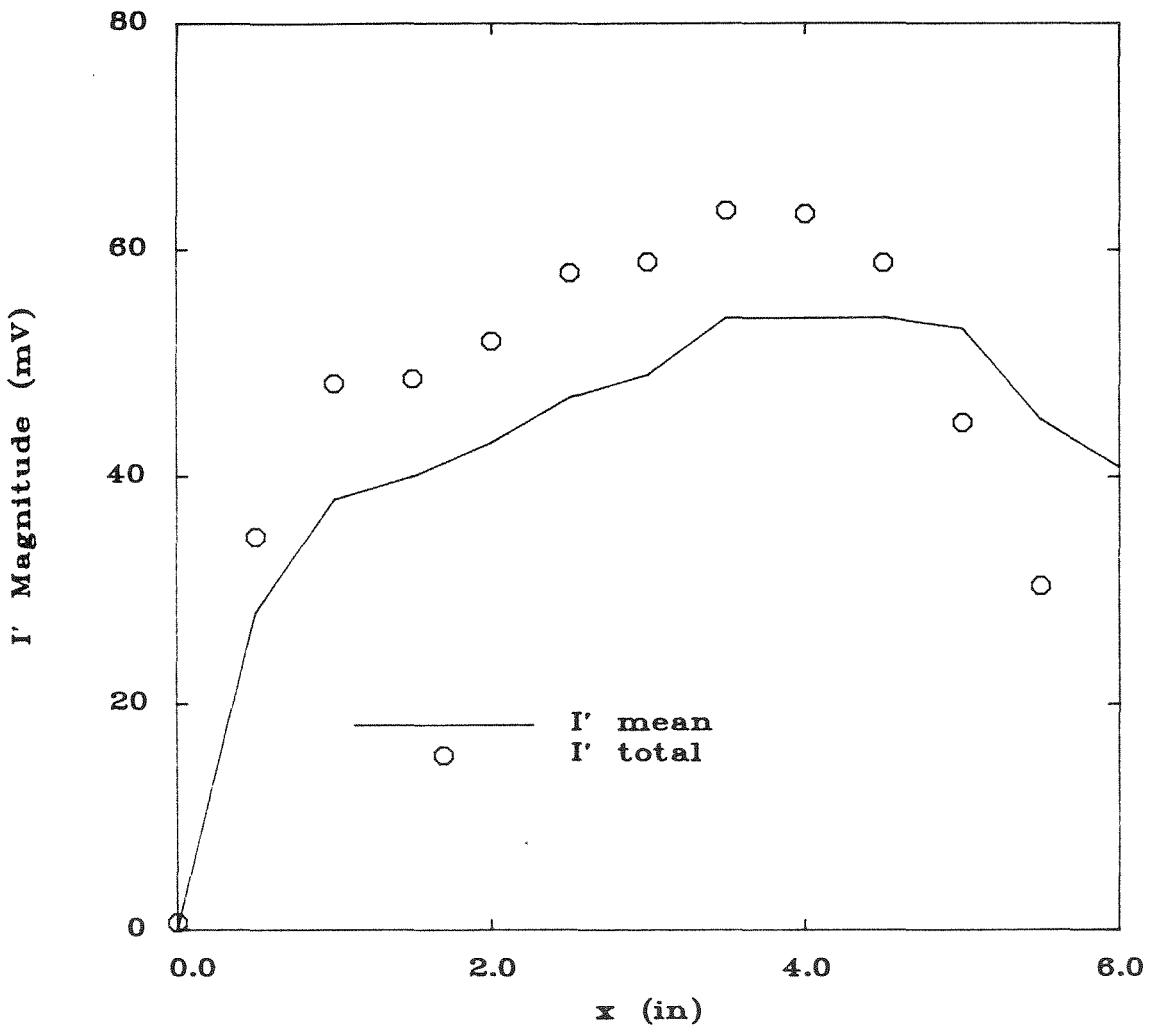
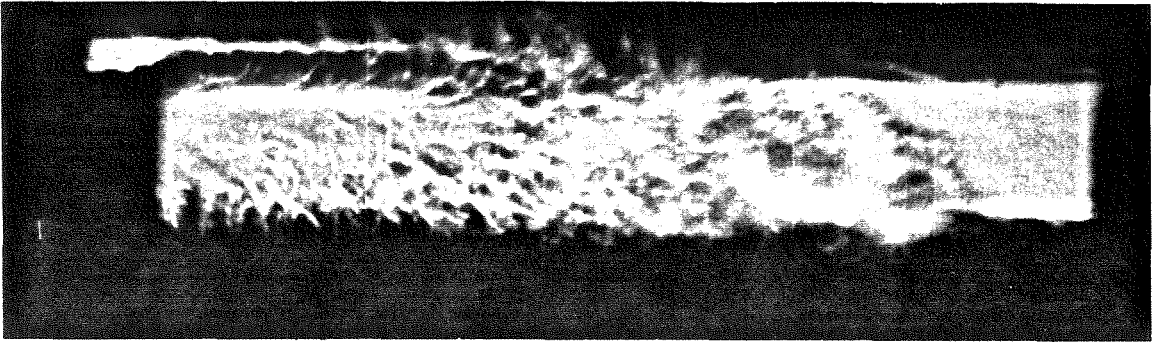


Figure 3.20: Standard Case 188 Hz Shedding : 288° Phase Angle

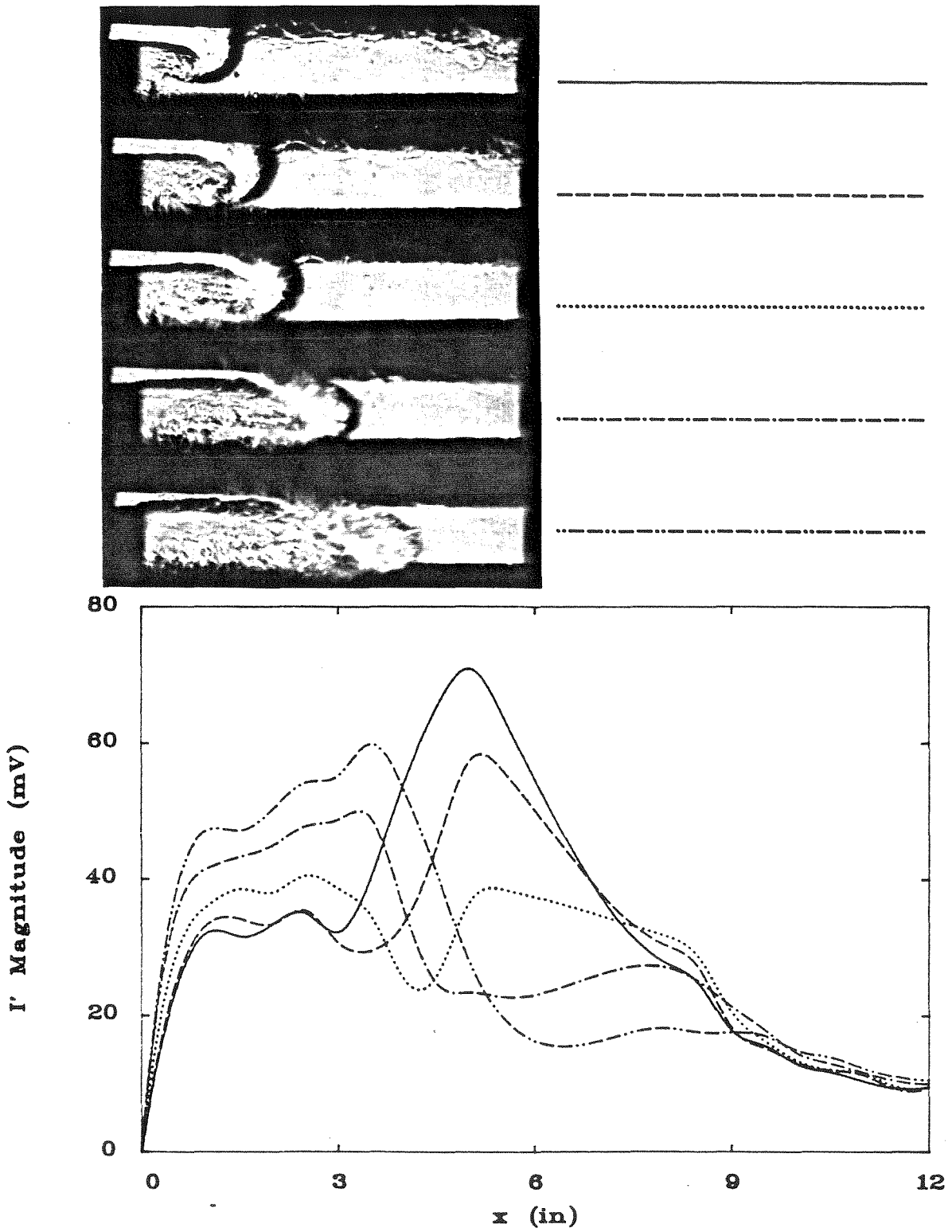


Figure 3.21: 188 Hz Shedding :  $\phi = 1.0$ ,  $V_{mean} = 60 \text{ ft/sec}$ ,  $L_{plenum} = 2.82 \text{ ft}$

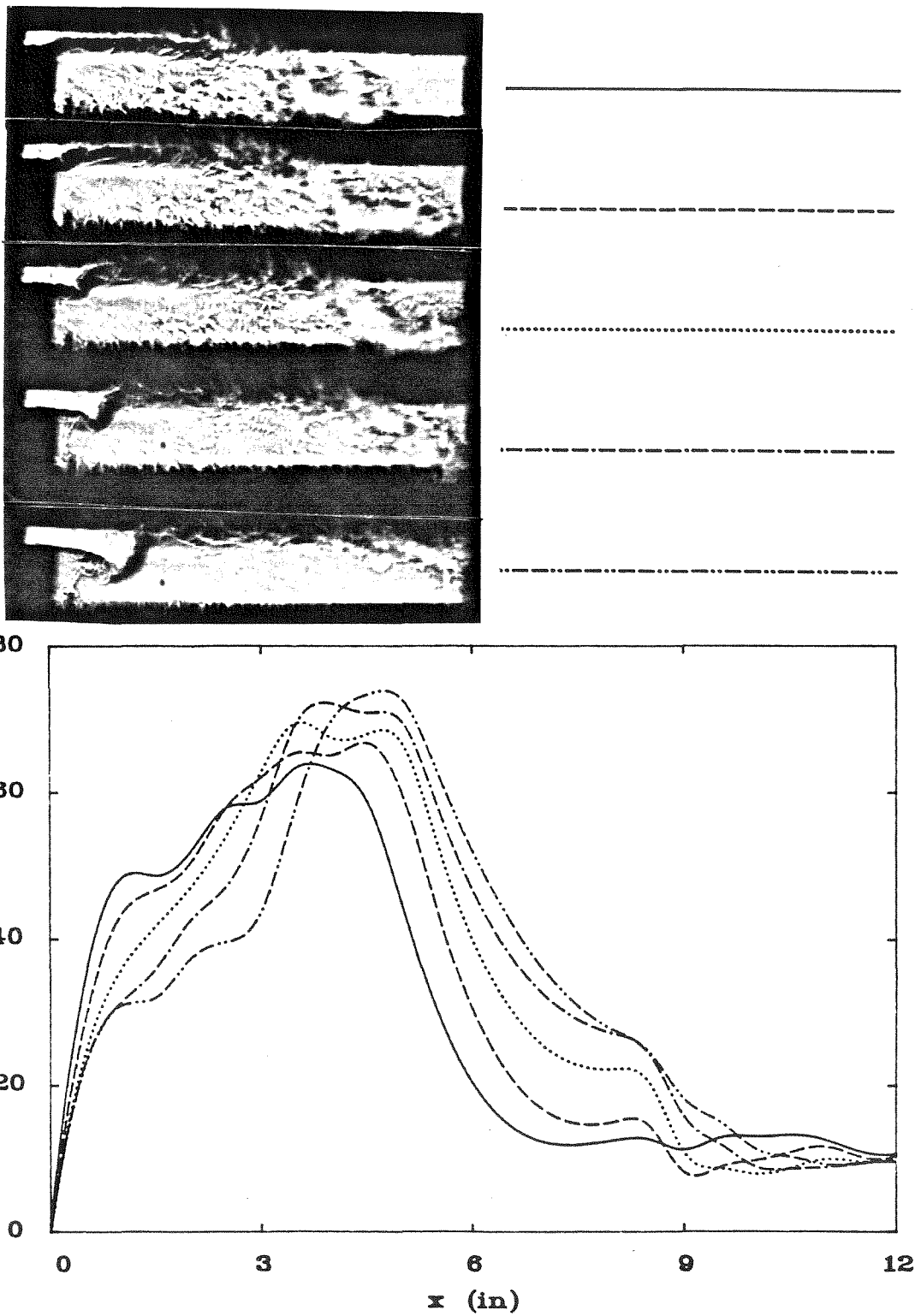


Figure 3.22: 188 Hz Shedding : 2nd Half of Cycle

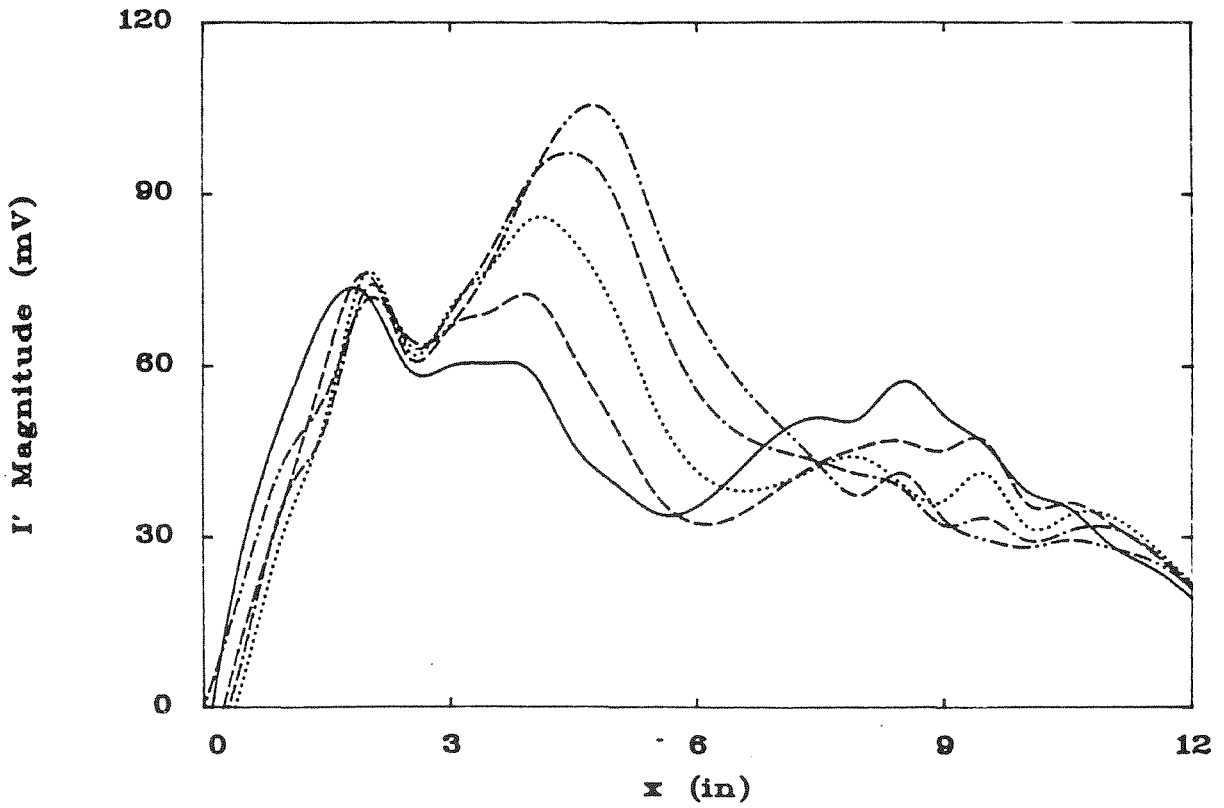
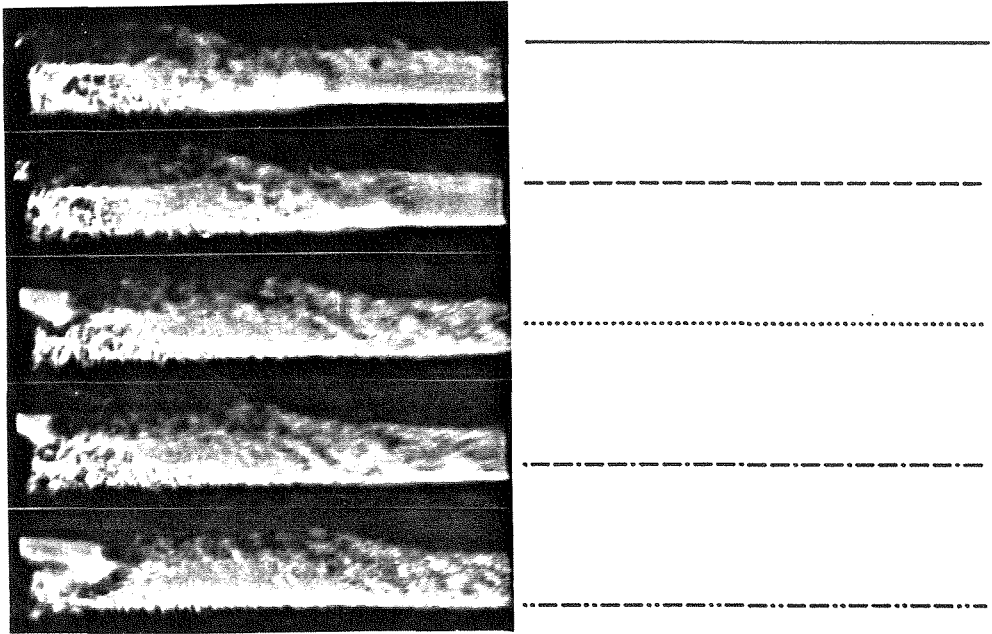


Figure 3.23: 535 Hz Shedding :  $\phi = 1.0$ ,  $V_{mean} = 145 \text{ ft/sec}$ ,  $L_{plenum} = 1.84 \text{ ft}$

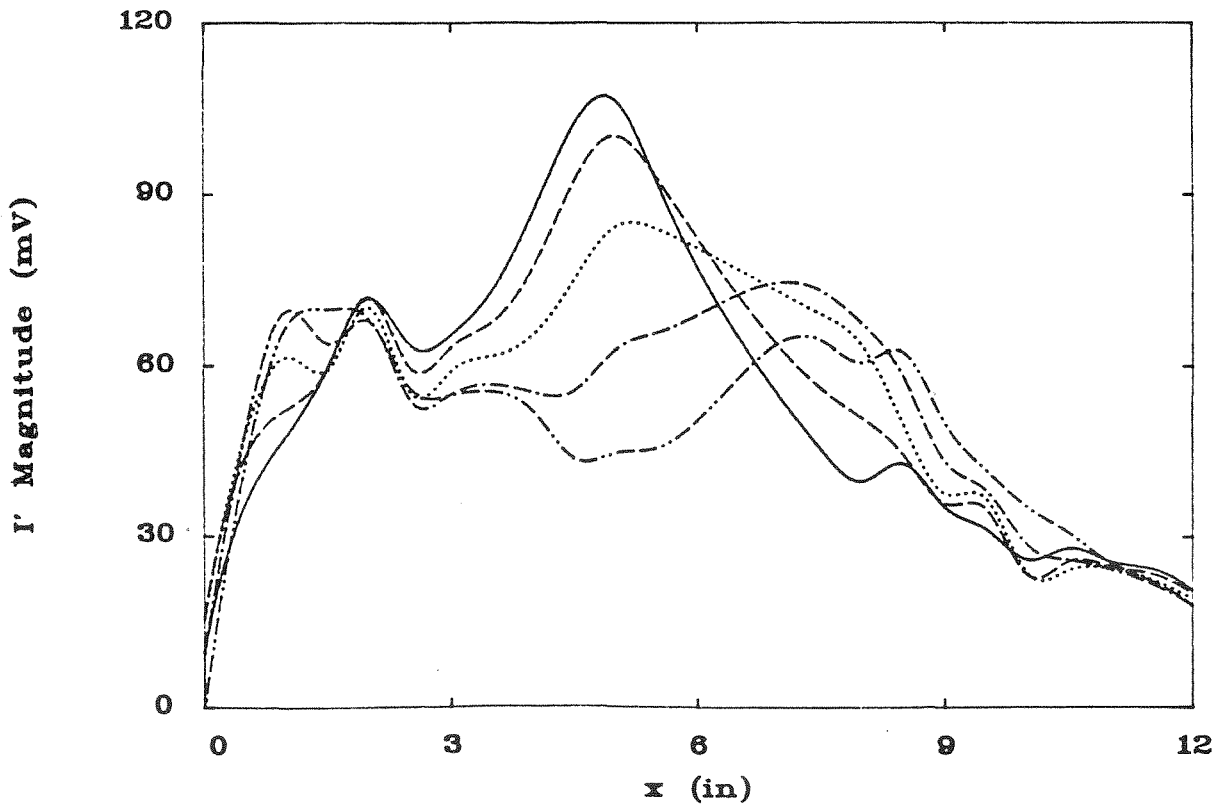
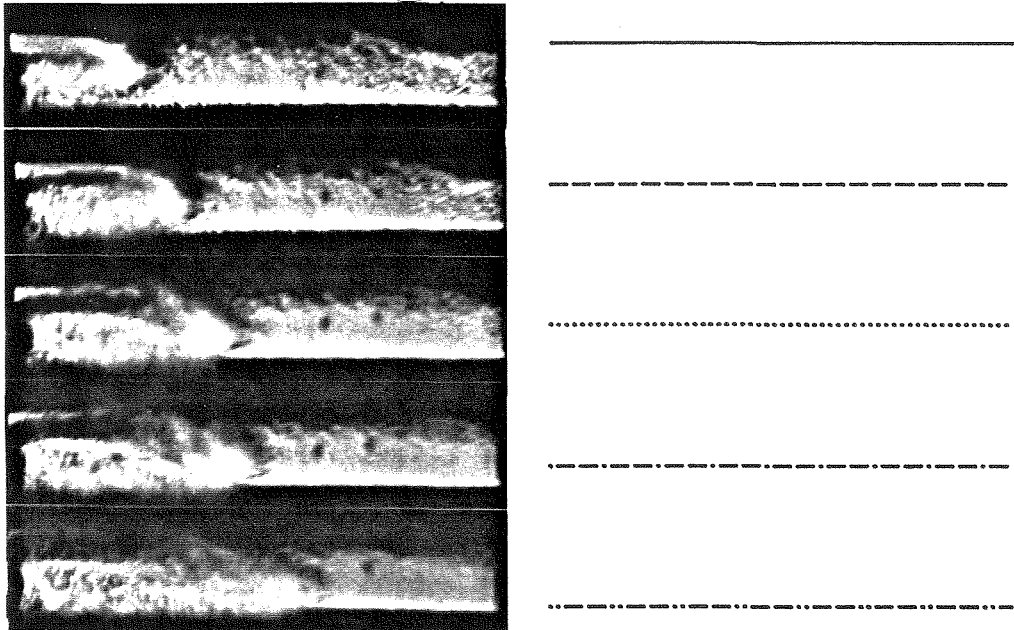


Figure 3.24: 535 Hz Shedding : 2nd Half of Cycle

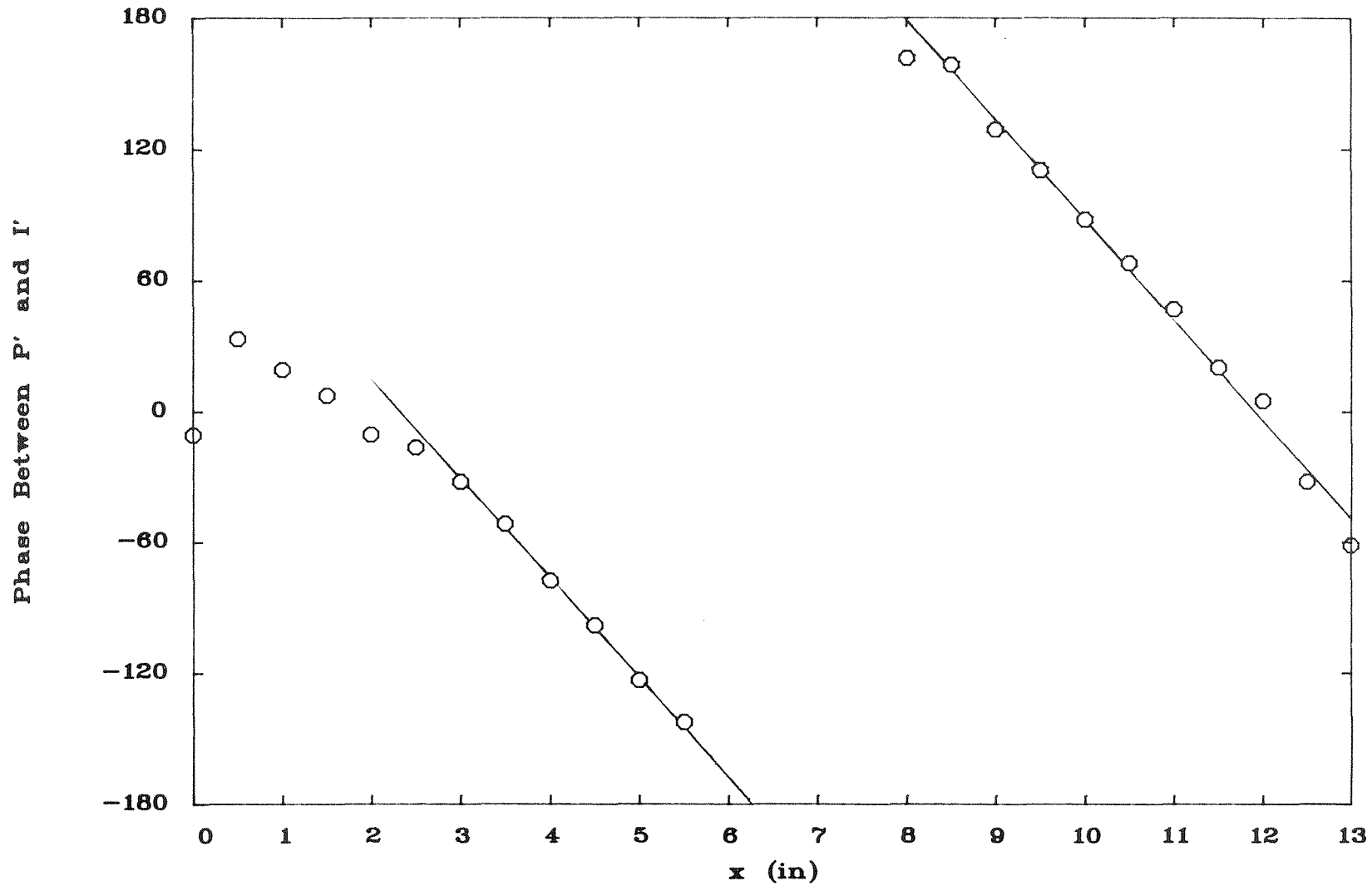


Figure 3.25: Phase Difference Between 188 Hz Components of  $p'$  and  $i'$ : Standard Case

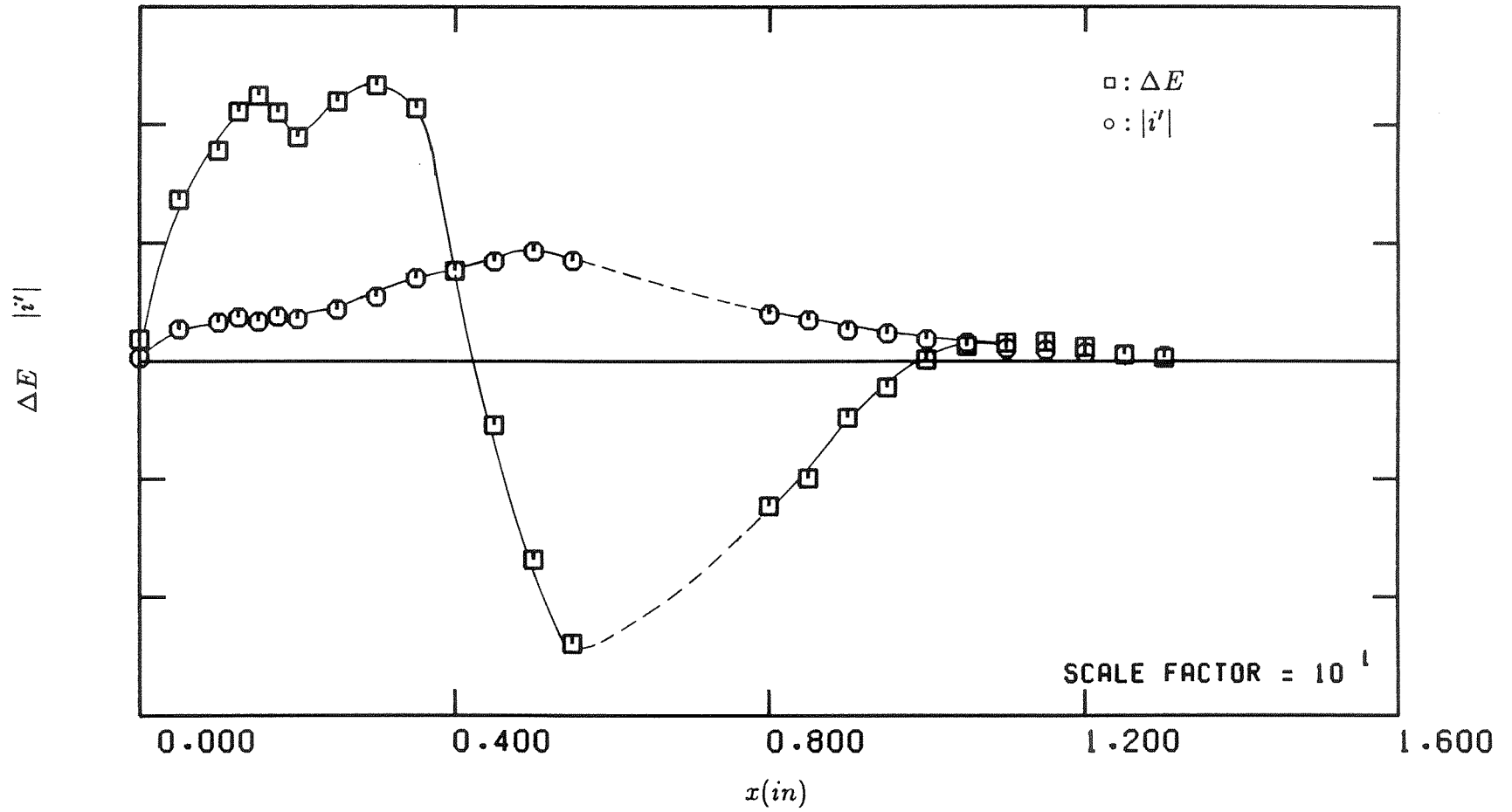


Figure 3.26: Rayleigh Criterion 188 Hz : Methane,  $\phi = 1.0$ ,  $V_{mean} = 60t/sec$ ,  $L_{plenum} = 2.82ft$

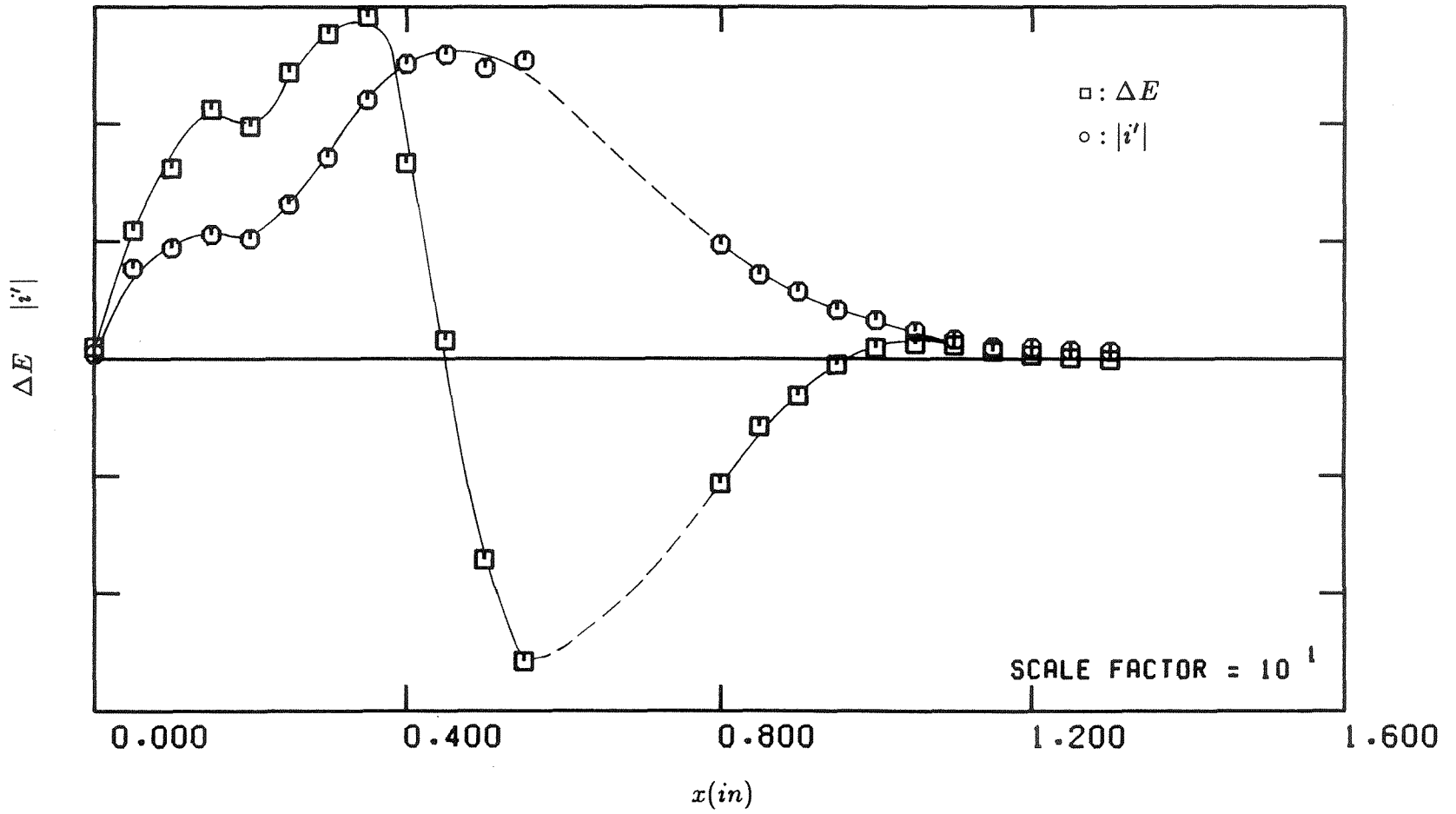


Figure 3.27: Rayleigh Criterion 188 Hz : Methane,  $\phi = 0.90$ ,  $V_{mean} = 63 \text{ ft/sec}$ ,  $L_{plenum} = 2.82 \text{ ft}$

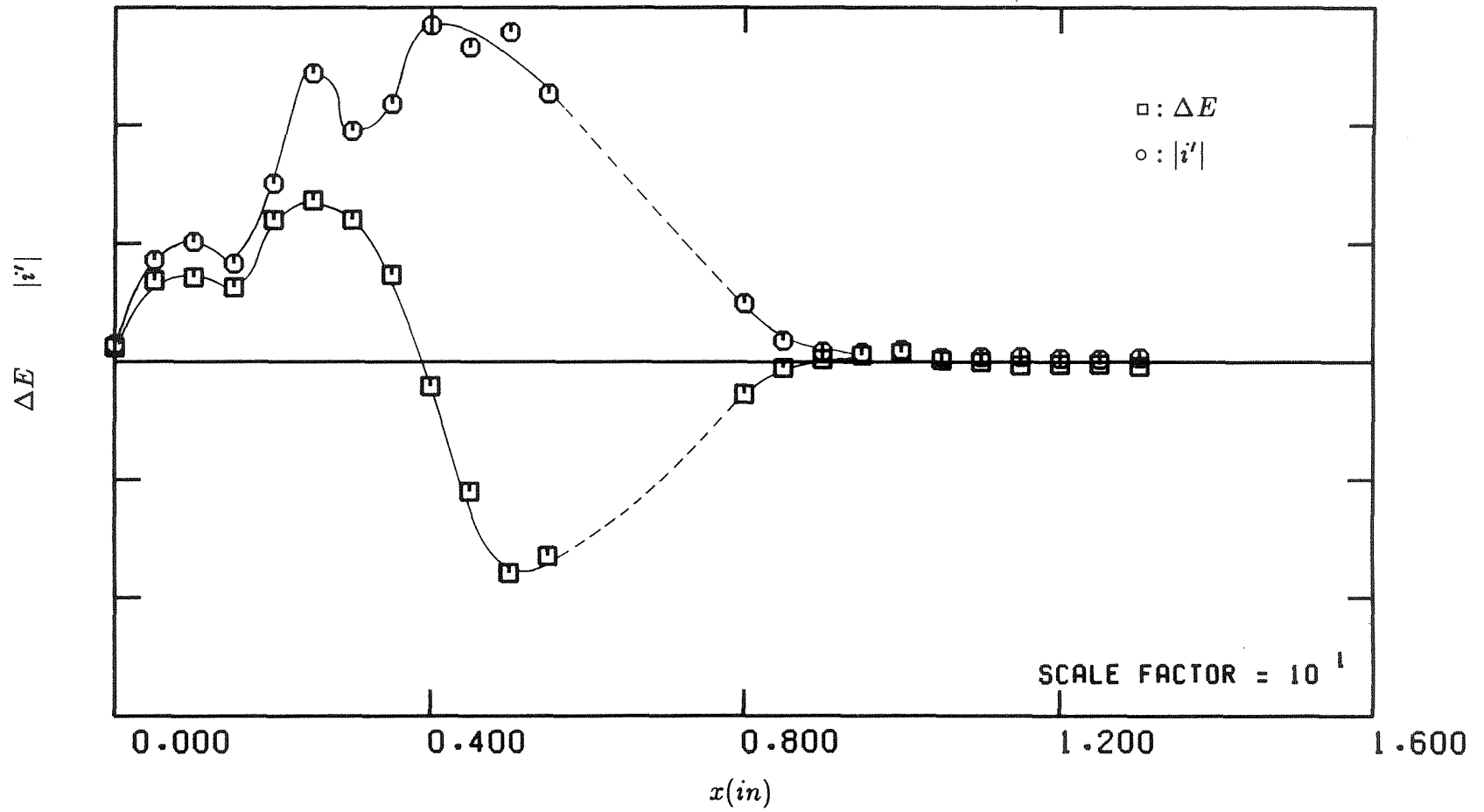


Figure 3.28: Rayleigh Criterion 231 Hz: 15% $H_2$  - 85% $CH_4$ ,  $\phi = 0.86$ ,  $V_{mean} = 69 ft/sec$ ,  $L_{plenum} = 2.82 ft$

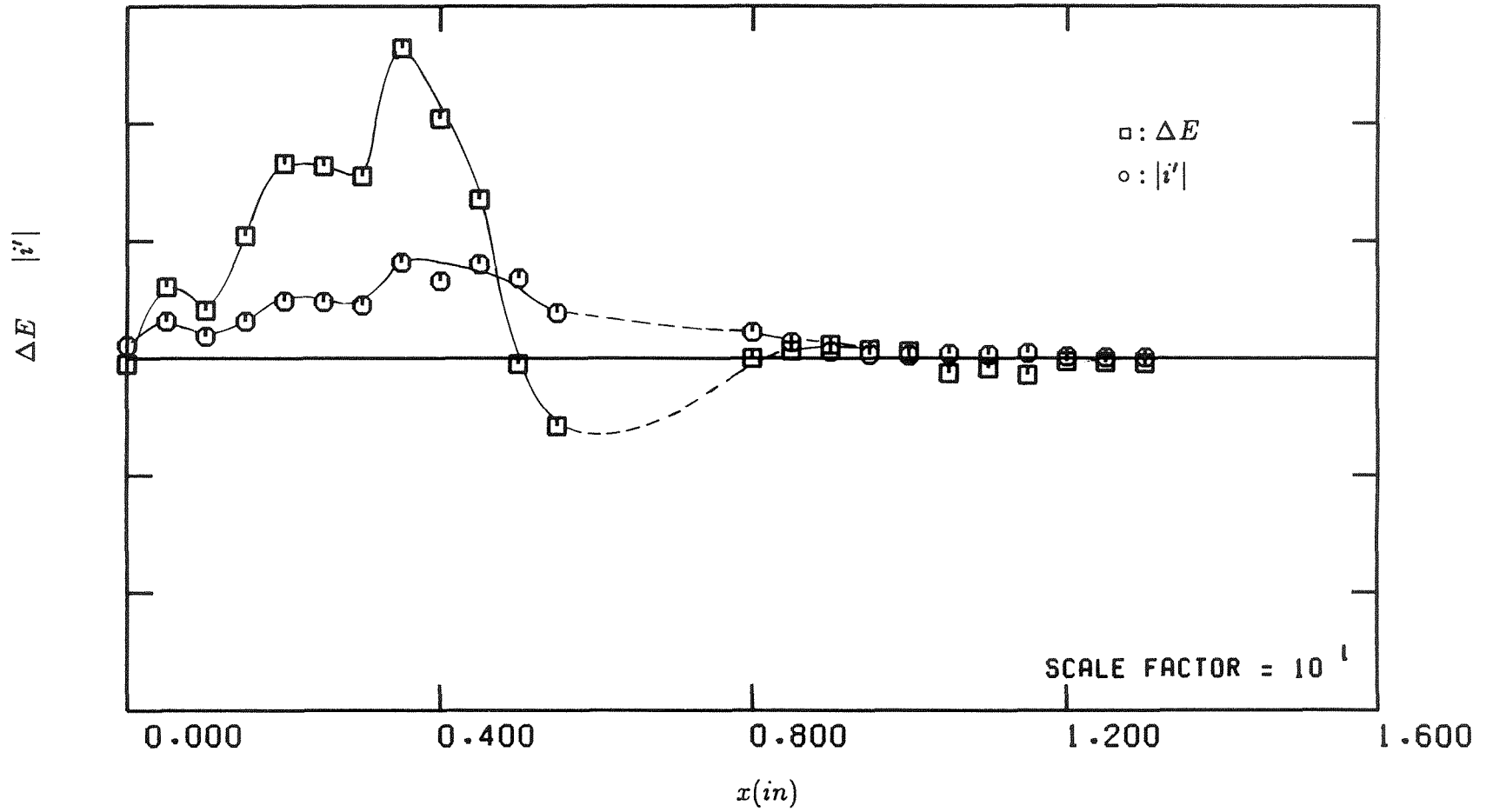


Figure 3.29: Rayleigh Criterion 457Hz : 15%  $H_2$  - 85%  $CH_4$ ,  $\phi = 0.86$ ,  $V_{mean} = 69 ft/sec$ ,  $L_{plenum} = 2.82 ft$

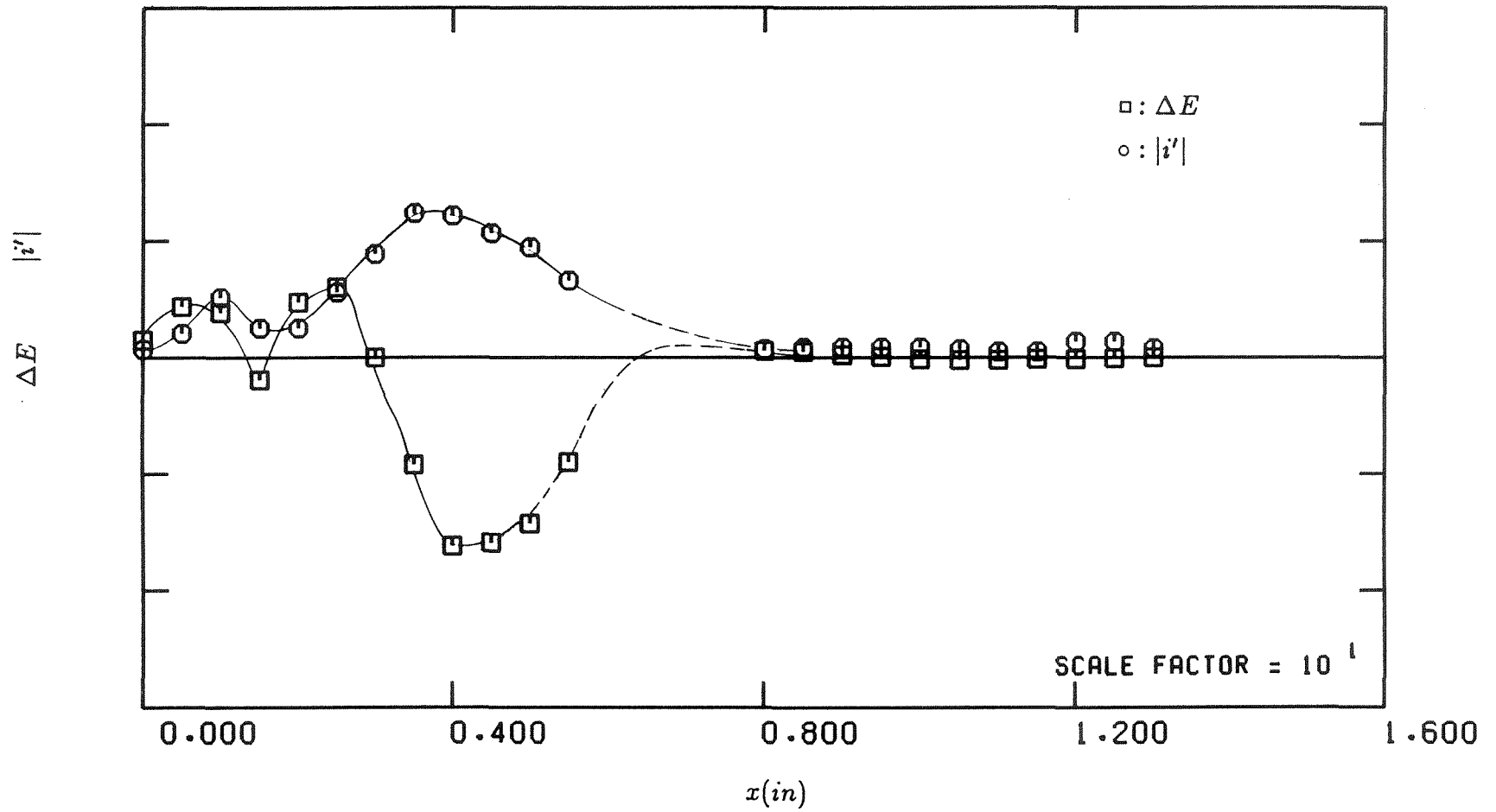


Figure 3.30: Rayleigh Criterion 267 Hz : Methane,  $\phi = 0.93$ ,  $V_{mean} = 69 ft/sec$ ,  $L_{plenum} = 2.82 ft$

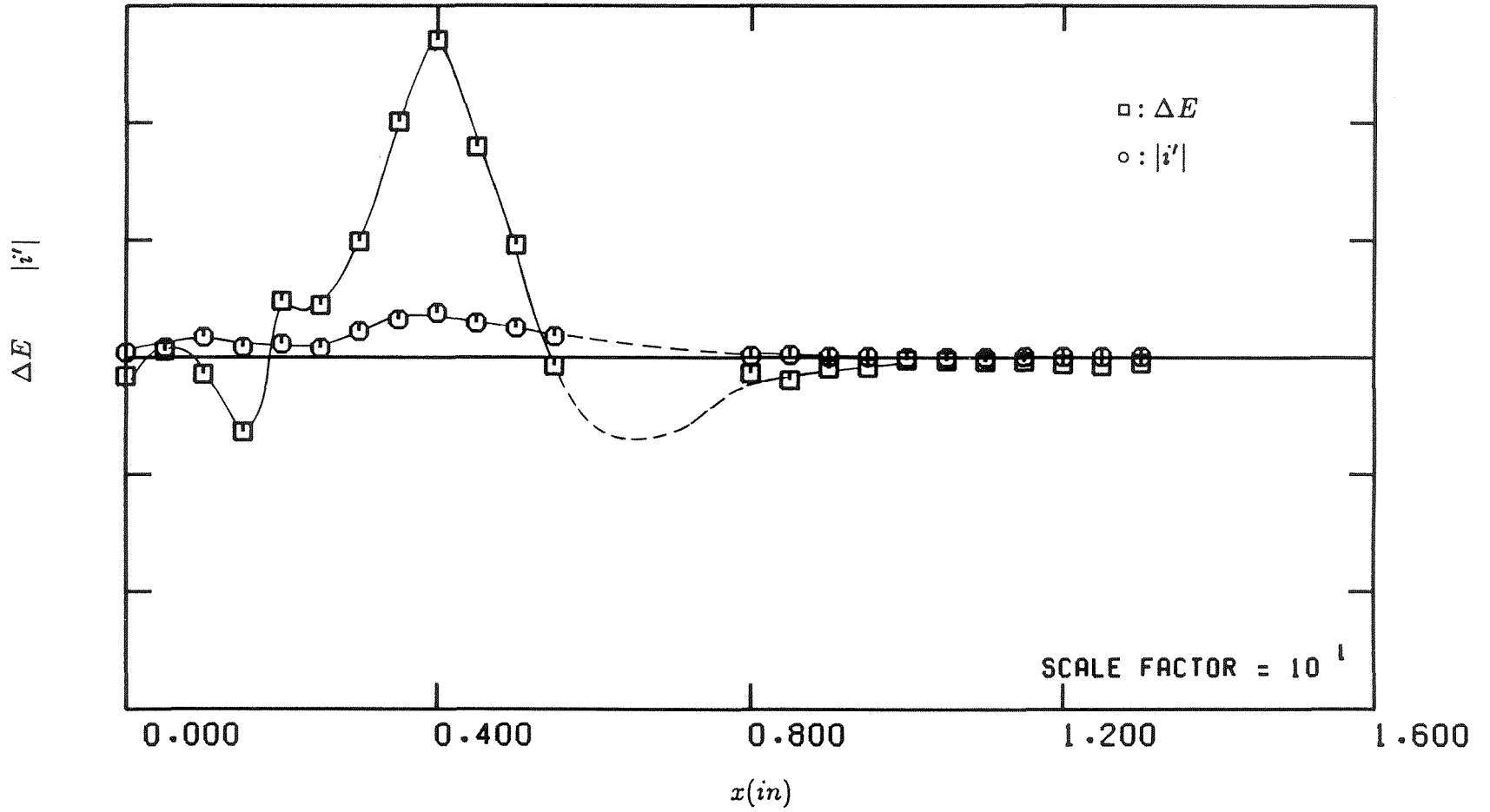


Figure 3.31: Rayleigh Criterion 535 Hz : Methane,  $\phi = 0.93$ ,  $V_{mean} = 69ft/sec$ ,  $L_{plenum} = 2.82ft$

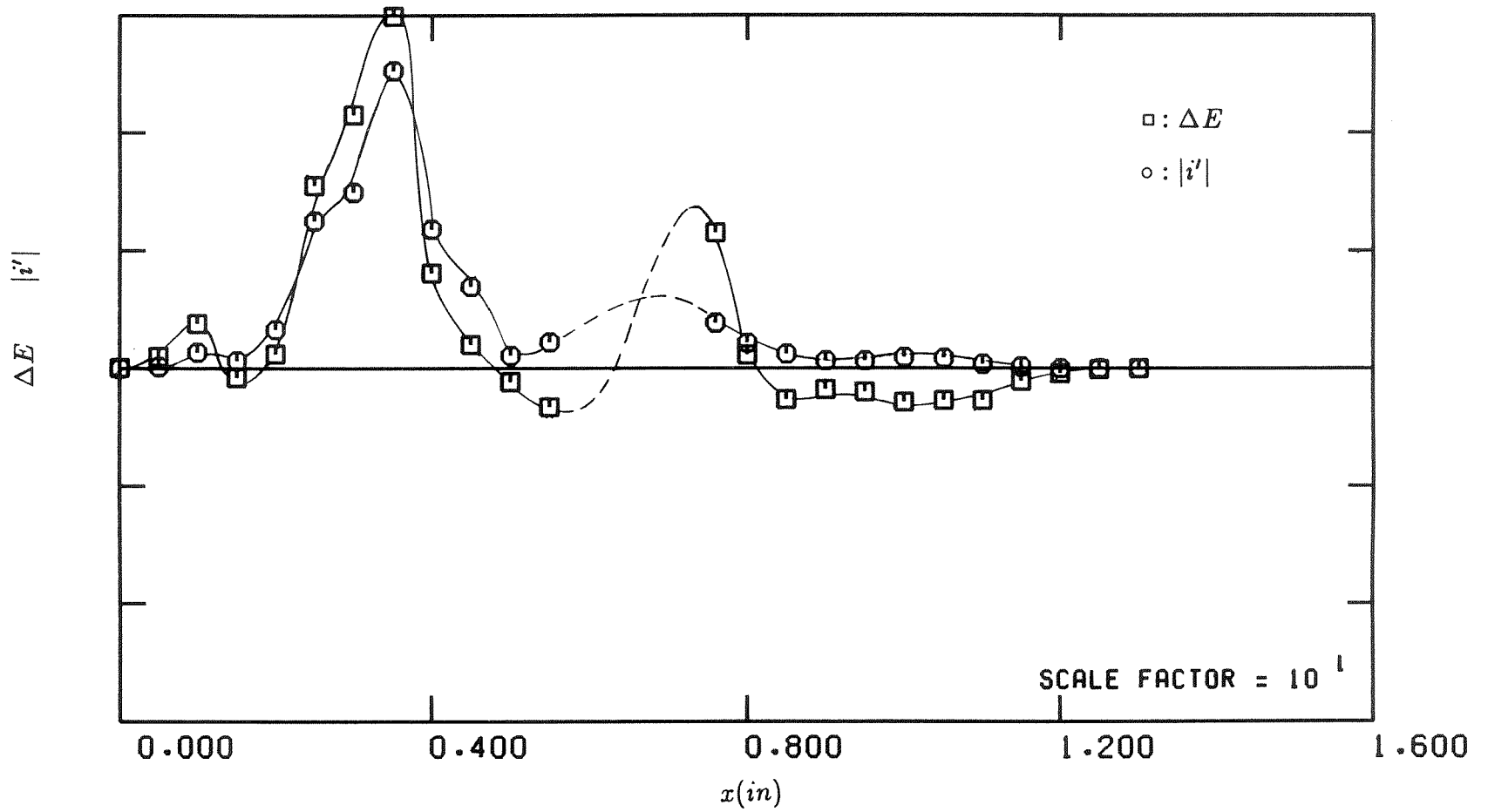


Figure 3.32: Rayleigh Criterion 457 Hz : Methane,  $\phi = 0.79$ ,  $V_{mean} = 108 ft/sec$ ,  $L_{plenum} = 1.84 ft$

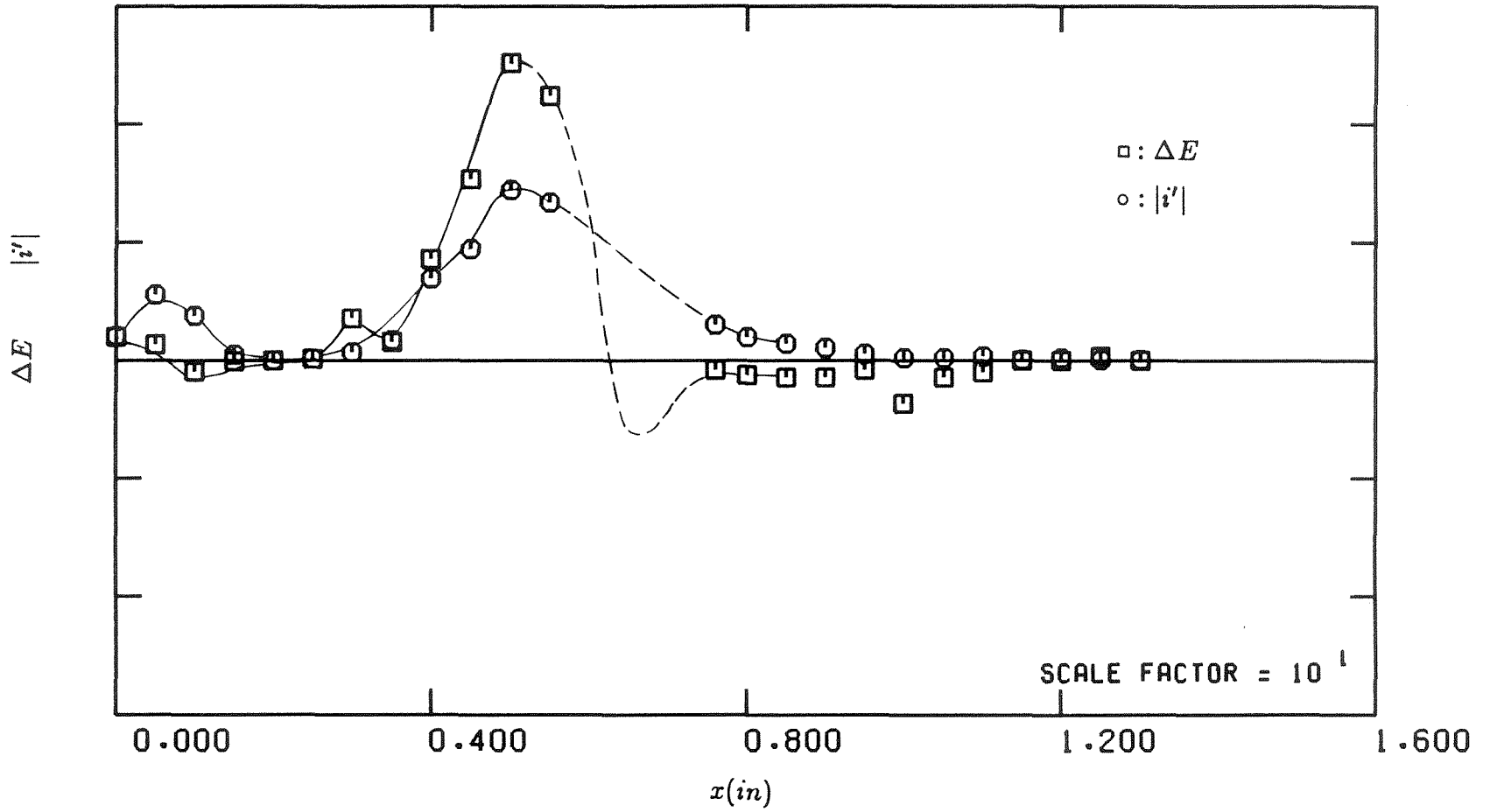


Figure 3.33: Rayleigh Criterion 535 Hz : Methane,  $\phi = 1.0$ ,  $V_{mean} = 145 ft/sec$ ,  $L_{plenum} = 1.84 ft$

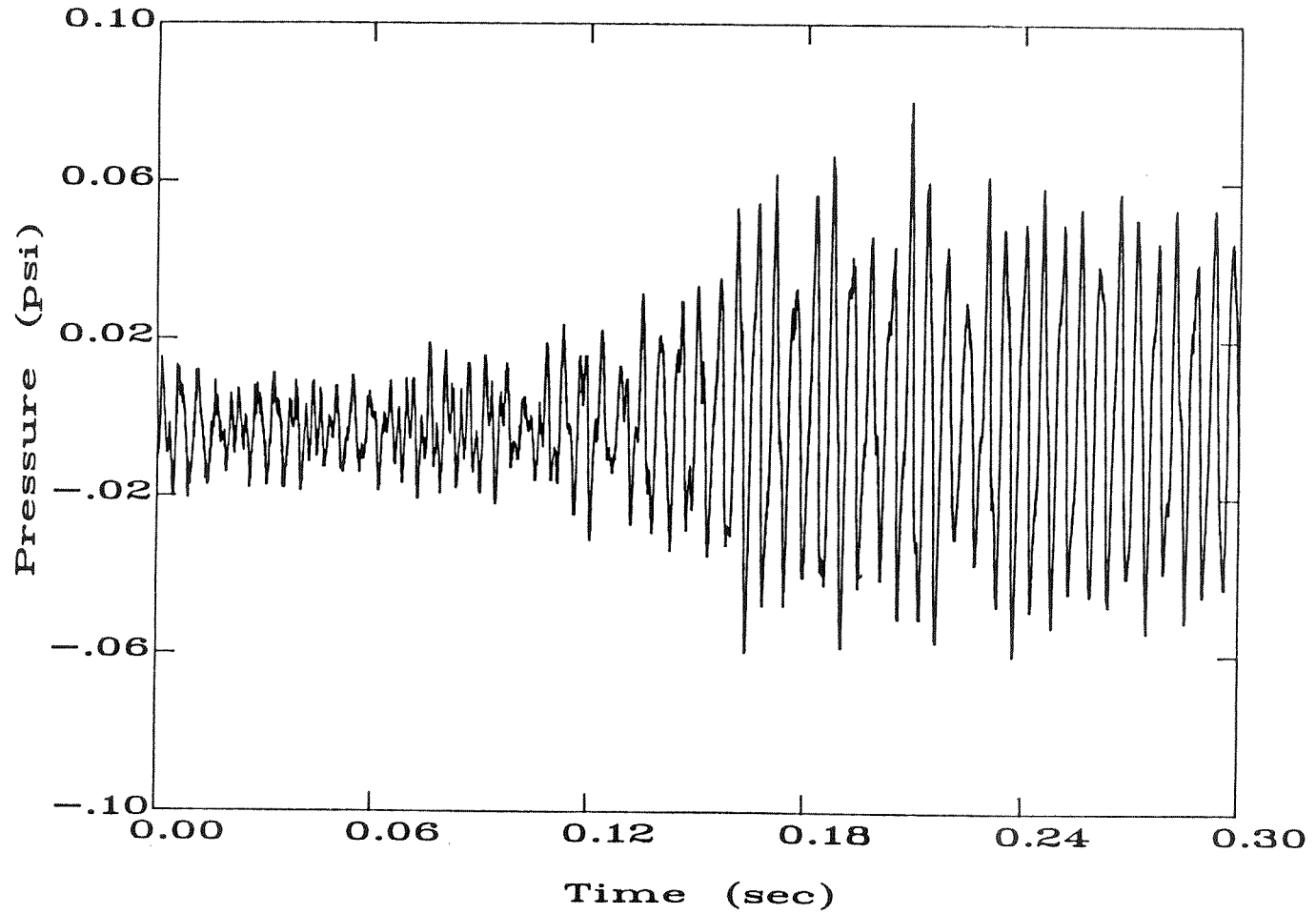


Figure 3.34: Transition: Pressure Signal at Flameholder

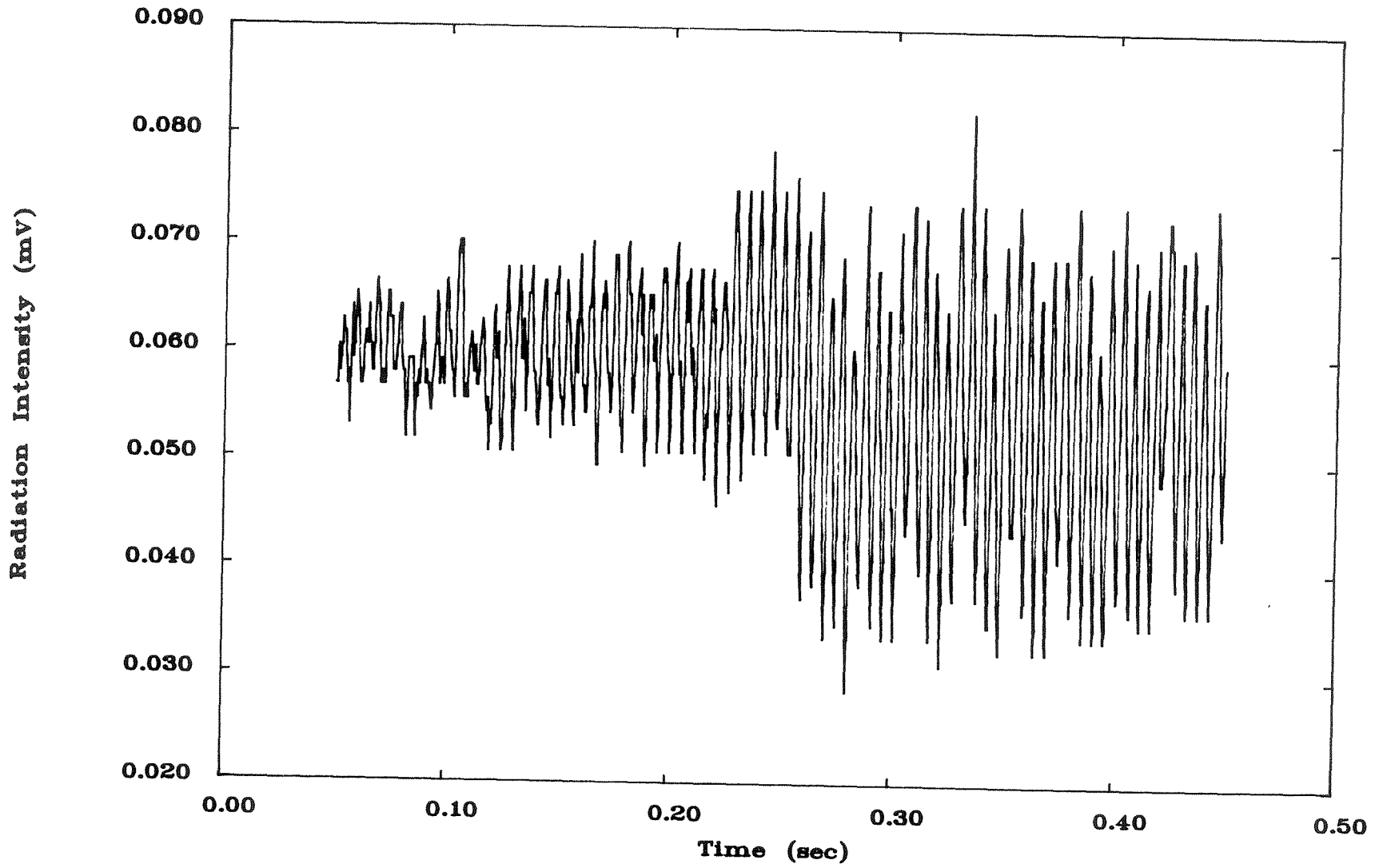


Figure 3.35: Transition: Radiation Intensity Signal at 5.0"

## Chapter 4

# Modeling of Longitudinal Mode Combustion

## Instabilities

### 4.1 Acoustic Equations with Sources

An analytical investigation of combustion instabilities is performed by using several observations of the experimental results to simplify the general equations of motion. The following procedure simplifies the general equations to equations that represent one-dimensional linearized acoustics with driving by heat or mass sources.

First, consider the inviscid non-conducting conservation equations. By neglecting body forces but including heat and mass sources, the equations can be written in the following form,

$$\frac{\partial \rho}{\partial t} + \nabla(\vec{u}\rho) = w \quad (4.1)$$

$$\rho \frac{\partial \vec{u}}{\partial t} + \rho \vec{u} \cdot \nabla \vec{u} = -\nabla p + w(\vec{u}_s - \vec{u}) \quad (4.2)$$

$$\frac{\partial p}{\partial t} + \gamma p \nabla \cdot \vec{u} + \vec{u} \cdot \nabla p = \frac{R}{C_V} \left[ q + w \left\{ h_s + \frac{(\vec{u} - \vec{u}_s)^2}{2} \right\} \right], \quad (4.3)$$

where  $\rho$ ,  $p$ ,  $\vec{u}$  are the density, pressure and velocity of the gas phase,  $q$  is the rate of heat addition, and  $w$  is the mass source that is introduced with flow speed  $\vec{u}_s$  and enthalpy  $h_s$ .

If only longitudinal modes of a system are to be studied, the gradients are taken only in the  $x$  direction and  $\bar{u}$  becomes simply  $u$ . Each of the variables is then expanded into the sum of a mean value, represented by  $(\bar{\quad})$ , and a small fluctuating value represented by  $(\quad)'$ . If the mean values are constant but the fluctuating values are functions of  $x$  and  $t$ , the equations become

$$\frac{\partial \rho'}{\partial t} + \bar{\rho} \frac{\partial u'}{\partial x} + \bar{u} \frac{\partial \rho'}{\partial x} = w' \quad (4.4)$$

$$\bar{\rho} \frac{\partial u'}{\partial t} + \bar{\rho} \bar{u} \frac{\partial u'}{\partial x} + \frac{\partial p'}{\partial x} = -\bar{w}u' + w'(u_s - \bar{u}) \quad (4.5)$$

$$\frac{\partial p'}{\partial t} + \gamma \bar{p} \frac{\partial u'}{\partial x} + \bar{u} \frac{\partial p'}{\partial x} = \frac{R}{C_V} \left[ q' + w' \left\{ h_s + \frac{(\bar{u} - \bar{u}_s)^2}{2} \right\} + \bar{w}u'(\bar{u} - u_s) \right]. \quad (4.6)$$

Now consider the case in which there exists no mean mass addition but mass is added in an oscillatory manner with the local mean flow velocity and temperature. Also, it is assumed that the square of the mean flow Mach number is much less than one. Taking the derivative of the energy equation with respect to  $t$  and subtracting the derivative of the momentum equation multiplied by  $a^2$  with respect to  $x$ , the result is

$$\frac{\partial^2 p'}{\partial t^2} - a^2 \frac{\partial^2 p'}{\partial x^2} = \frac{R}{C_V} \frac{\partial q'}{\partial t} + a^2 \frac{\partial w'}{\partial t}. \quad (4.7)$$

The result is that an oscillatory mass source has the same effect on the acoustic field as an oscillatory heat release rate. The only difference arises when boundary conditions are imposed. Since thermal conductivity has been neglected, the entropy equation is uncoupled from the energy equation and local entropy is simply convected with the mean flow (see Chu [47]). However, when the flow encounters a change in conditions, e.g., a choked nozzle, gradients in entropy may result in the generation of acoustic waves as discussed by Auerbach [22]. Effects of this type are not considered here for two reasons. First, the generation of acoustic

waves due to entropy gradients is not expected at an open exit. The laboratory combustor has an open exit, which gives the downstream boundary condition for the flow. Second, proposed instability mechanisms incorporating this mechanism predict a steady increase of the instability frequency with an increase in mean flow speed because of the reduced transport time of the convected entropy gradients. This is not observed in the experimental results.

Two analytical techniques have been applied to Equation 4.7 in an effort to understand the combustion instabilities in the laboratory combustor. In the first method, analysis assumes that the time variation of the system is periodic at some particular frequency with growth or decay of the amplitudes of the pressure and velocity fluctuations, depending on the sign of the imaginary part of the complex frequency.

Three sets of results are obtained using this approach. First, normal acoustic modes of the system are determined as eigenvalues of the acoustic system. Second, an independent forcing is applied to the system to model the combustion process. For these two cases, the imaginary part of the complex frequency is set to zero and the system response is periodic with no growth or decay of amplitudes. Finally, a linear stability calculation is carried out that includes a velocity-sensitive mass source to model the combustion rate as the feedback mechanism for instability. In this case, stability of the system depends upon the sign of the imaginary part of the complex frequency.

The second method includes assumptions about the spatial dependence of the fluctuations by using solutions represented by expansions in orthogonal acoustic modes of a general combustion chamber. The time variation can then be determined for a particular driving mechanism. The details of these methods

and documentation of the computed results follow.

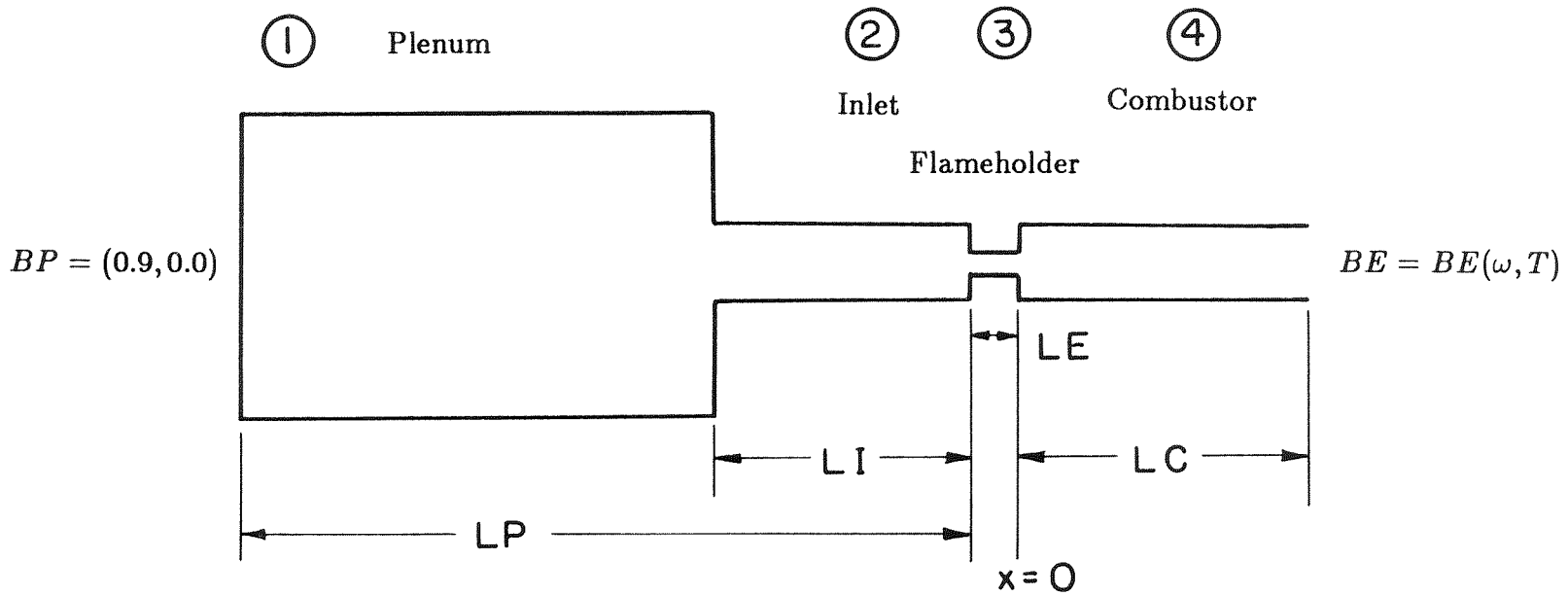
## 4.2 Solution for Quasi-Steady Behavior

If the forcing terms in Equation 4.7 are set to zero and a quasi-steady time dependence at a complex frequency  $\omega$  is assumed, then the acoustic wave equation is separable and ordinary differential equations are obtained for the spatial dependence of the fluctuating quantities. For this case, the effect of the mean flow Mach number can be retained and included in Equation 4.7. The solution for  $p'$  and  $u'$  can then be written in terms of upstream and downstream travelling acoustic waves as follows,

$$\frac{p'}{\gamma \bar{p}} = P^+ \exp\left\{i\omega\left(\frac{x}{a(M+1)} - t\right)\right\} + P^- \exp\left\{i\omega\left(\frac{x}{a(M-1)} - t\right)\right\} \quad (4.8)$$

$$\frac{u'}{a} = P^+ \exp\left\{i\omega\left(\frac{x}{a(M+1)} - t\right)\right\} - P^- \exp\left\{i\omega\left(\frac{x}{a(M-1)} - t\right)\right\}. \quad (4.9)$$

These equations can be used in an acoustic model to investigate the behavior of the laboratory combustion instabilities after a stable limit cycle has been obtained by setting the imaginary part of  $\omega$  to zero. The modeling of the apparatus shown in Figure 2.2 consists of four constant area segments joined with abrupt area changes as shown in Figure 4.1. The assumption of abrupt area changes is valid when the actual length of area change is small compared to the acoustic wavelength under consideration. Also, the heat addition process in the combustion chamber is modeled as an abrupt jump in the temperature, mean flow velocity, and sound speed .



Matching:  $p'$  continuous,  $u'$  satisfies continuity except at flameholder where:

$$a_4 A_4 u'_4 = a_3 A_3 u'_3 + F \exp(-i\omega t)$$

$$T = T_{room} \text{ for } x < 0 \text{ and } T = T_{comb} \text{ for } x > 0$$

Figure 4.1: Quasi-Steady Acoustic Model

### 4.2.1 Natural Modes

The above equations are used as solutions in each segment with matching conditions applied at the interfaces and ideal reflection coefficients applied at the ends. The matching conditions require continuity of pressure and mass flow at the interfaces. This results in a set of eight equations for the eight unknown complex constants  $P$ . The eigenvalues of the coefficient matrix can be solved to give the natural acoustic modes of the system, and the eigenvectors can be used to form the acoustic mode shapes of the natural frequencies,  $\omega_n$ . Smith [10] performed this analysis and compared the frequencies of the resulting natural modes to the frequencies of peaks obtained in some experimental spectra. The results are shown in the following table.

<u>Computed <math>\omega_n</math></u>	<u>Measured Peaks</u>
180Hz	188Hz
229	231
385	377
470	457
533	535

### 4.2.2 Forcing with Mass Source

To model the effect of the heat addition process on the acoustic field, an oscillatory mass source is input at the dump plane to represent the fluctuating heat release rate that is present during the instability. This term changes only the matching condition at the dump plane to require that  $u'_4 a_4 A_4 = u'_3 a_3 A_3 + F \exp\{-i\omega t\}$ , where  $F$  is the amplitude of the mass source that is introduced at frequency  $\omega$ ,  $a$  represents the sound speed of each section, and  $A$  is the cross-sectional area.

The matching condition requiring continuity of the pressure at the dump plane is retained. For a given frequency and amplitude of forcing,  $p'(x, t)$  and  $u'(x, t)$  can be determined.

Various reflection coefficients can be used, and non-ideal values are responsible for the damping in the system. In this study, the upstream reflection coefficient is determined by the ratio of the areas of the inlet pipe and the plenum section. For the downstream exit, experimental values of the exit impedance of a circular duct exhausting a hot gas are used. The experimental correlations of Mahan, Cline, and Jones [49] are used. This impedance is dependent upon the temperature of the gas, the acoustic frequency, and radius of the exit, which is taken to be the hydraulic radius of the rectangular cross section.

### Mode Shapes

The amplitude of the response as a function of the location in the system can be determined for a particular frequency and forcing amplitude. This spatial variation of amplitude is very similar to the modes obtained using the eigenvectors for the system with no forcing. The theoretical pressure mode shapes shown in Figures 3.11– 3.14 are obtained by setting the frequency of forcing equal to the frequency of the experimental spectral peak, and the amplitude is selected to match the experimental value at the dump plane.

### System Response to Forcing

The responses of the fluctuating pressure and velocity are determined for 1Hz increments of frequency from zero to 600 Hz for an arbitrary fixed forcing amplitude. The amplitude and phase of the oscillatory pressure at the dump plane are shown in Figure 4.2 as a function of the frequency of the unit forcing. The solid line represents the amplitude of the response, and the dotted line represents

the phase difference between the response immediately downstream of the step and the forcing. The response of the fluctuating velocity at the dump plane is shown in Figure 4.3.

The results reveal peaks in the amplitude response curves very near the the natural modes that are determined without forcing. The height and width of each peak are determined by the boundary conditions that are responsible for the damping in the system. Larger damping values give lower and broader peaks in the response curves. The frequencies of the peaks generally correspond to the lengths of the separate chambers used in the model. A shorter length of the plenum chamber results in a higher frequency for the peaks below 300 Hz. Similarly, a shorter length of the combustion chamber results in a higher frequency for the peaks above 300 Hz.

The response curves for the pressure amplitude at the dump plane reveal that the system is most sensitive to forcing close to 470 Hz or 530 Hz. However, the amplitude response of the velocity at the dump plane is most sensitive at the lower frequencies around 180 Hz and 230 Hz and is also sensitive to forcing near 530 Hz.

The peak near 460 Hz is substantially lower. This demonstrates that the sensitivity of the system and the damping are not the only factors determining the magnitude of response. Also, the location at which the response is monitored is important. This can be seen by considering the combustion chamber to be an ideal “organ pipe” of the same length as the actual combustor. In this case the natural mode is also close to 460 Hz. The closed end is at an antinode in the pressure mode shape; therefore, the pressure response at that location is large. However, the closed end is near a node in the velocity mode shape and no

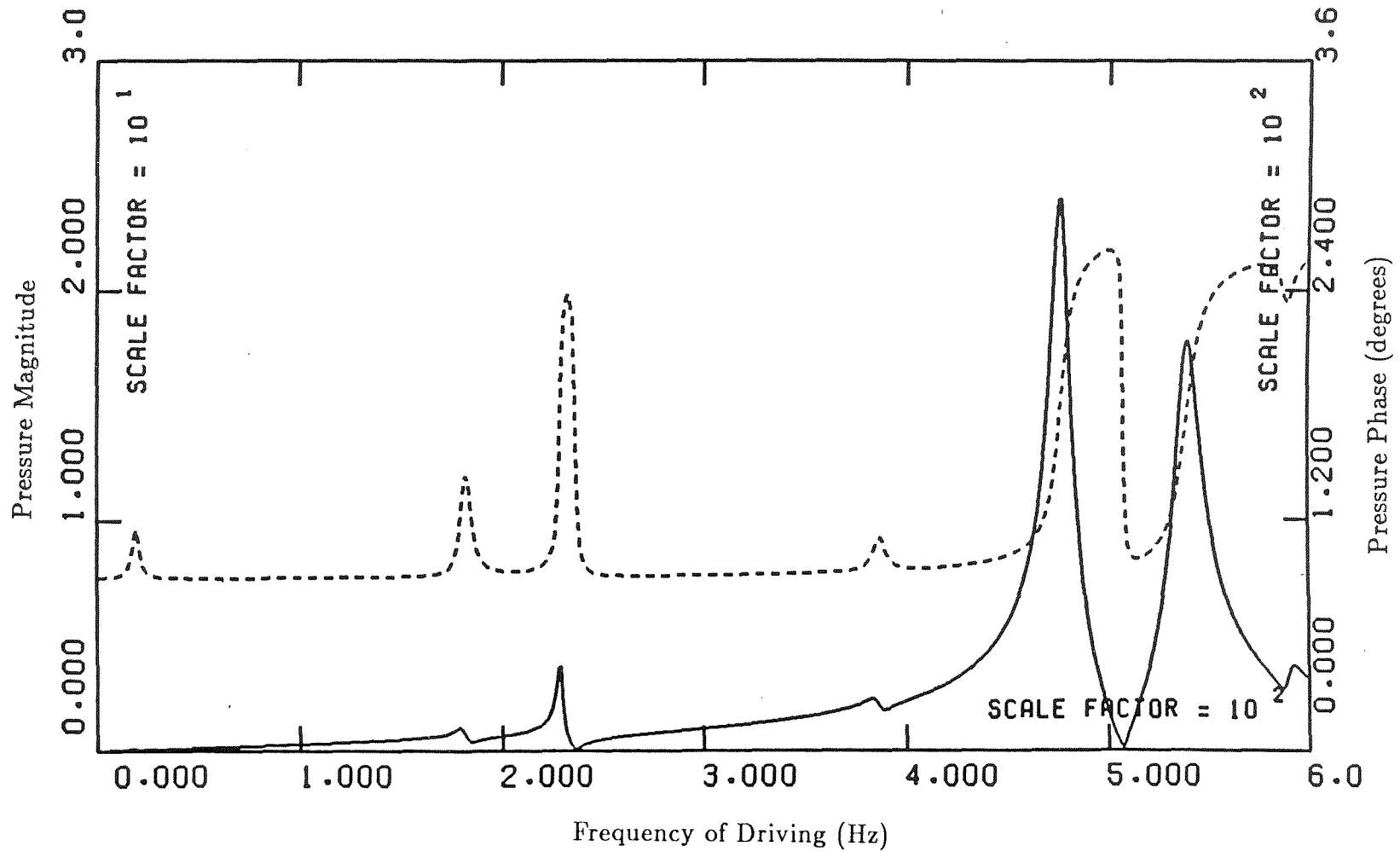


Figure 4.2: Pressure Response to Unit Driving

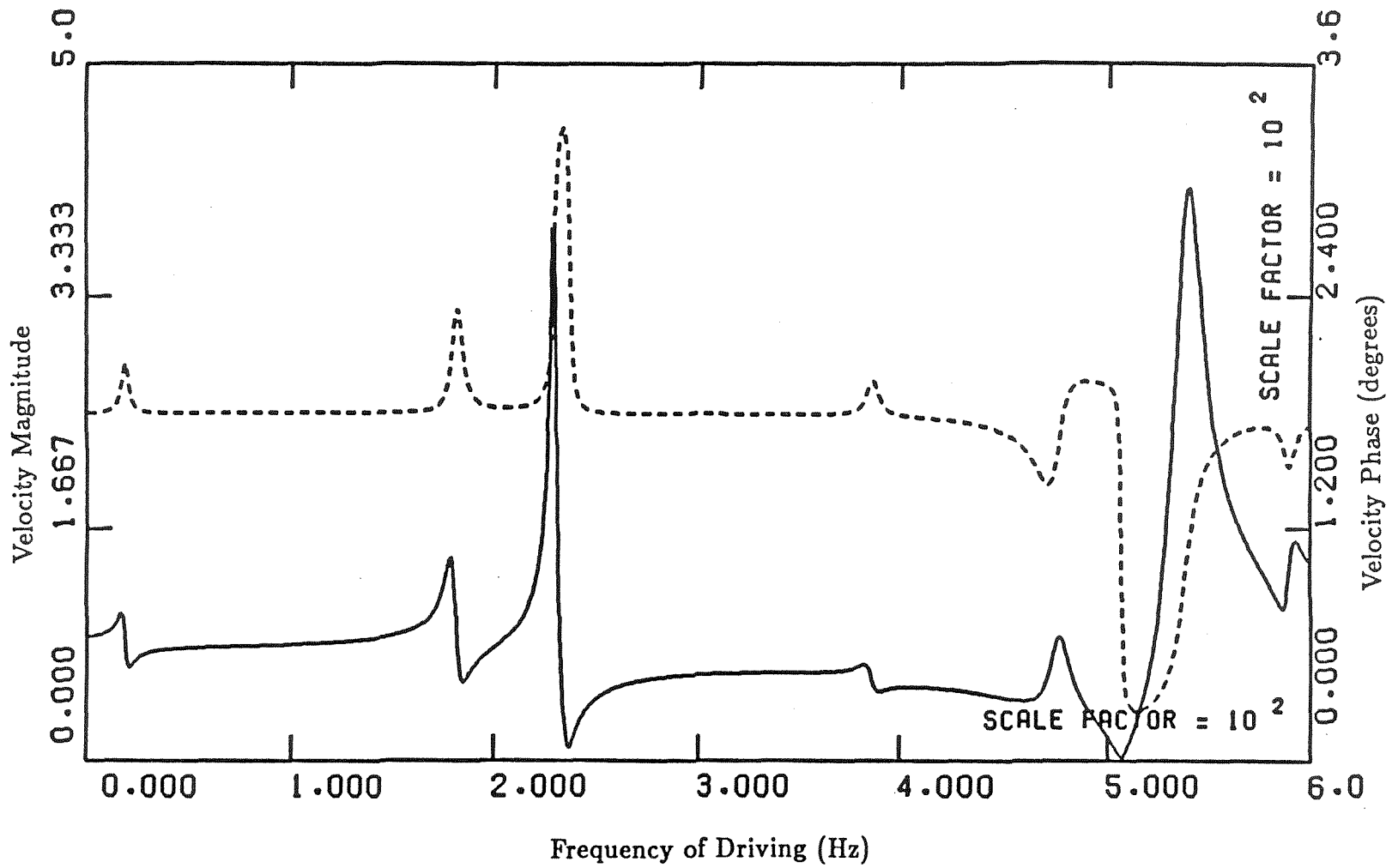


Figure 4.3: Velocity Response to Unit Driving

amplitude response occurs at that location. The model used is more complicated than an ideal organ pipe analysis, but this simplification demonstrates the effect that the location can have on the response shown in the curves.

The results are shown for the monitoring location at the dump plane because, in the laboratory combustor, velocity fluctuations at this location result in vortex shedding that yields oscillatory heat release rates. Thus, a feedback mechanism is postulated which, with the modeling of the relationship between  $u'$  and  $q'$  in Chapter 4, can be used to predict amplitudes of the quasi-steady pressures and velocities.

Since in the laboratory combustor the oscillatory combustion is associated with vortex shedding phenomena, the heat release rate is coupled to the velocity fluctuations. However, according to Rayleigh's criterion, the phase difference between the heat release rate and the oscillatory pressure is the important quantity concerning the stability of the system. Therefore, the phase difference between the  $p'$  and  $u'$  may be very important in the determination of system stability. By using the phase differences that are similar to the dotted lines in Figures 4.2–4.3 but monitored over the step instead of downstream, the phase difference between  $p'$  and  $u'$  is determined as a function of frequency. These results are presented in Figure 4.4.

The figure reveals that  $p'$  and  $u'$  are generally one-quarter of a cycle out of phase, but large changes occur near resonant frequencies. In particular, the phase difference passes through  $180^\circ$  near frequencies that correspond to the 188, 231, and 535 Hz modes. These phase differences have important implications for the stability of the system and further discussion is included in the next section.

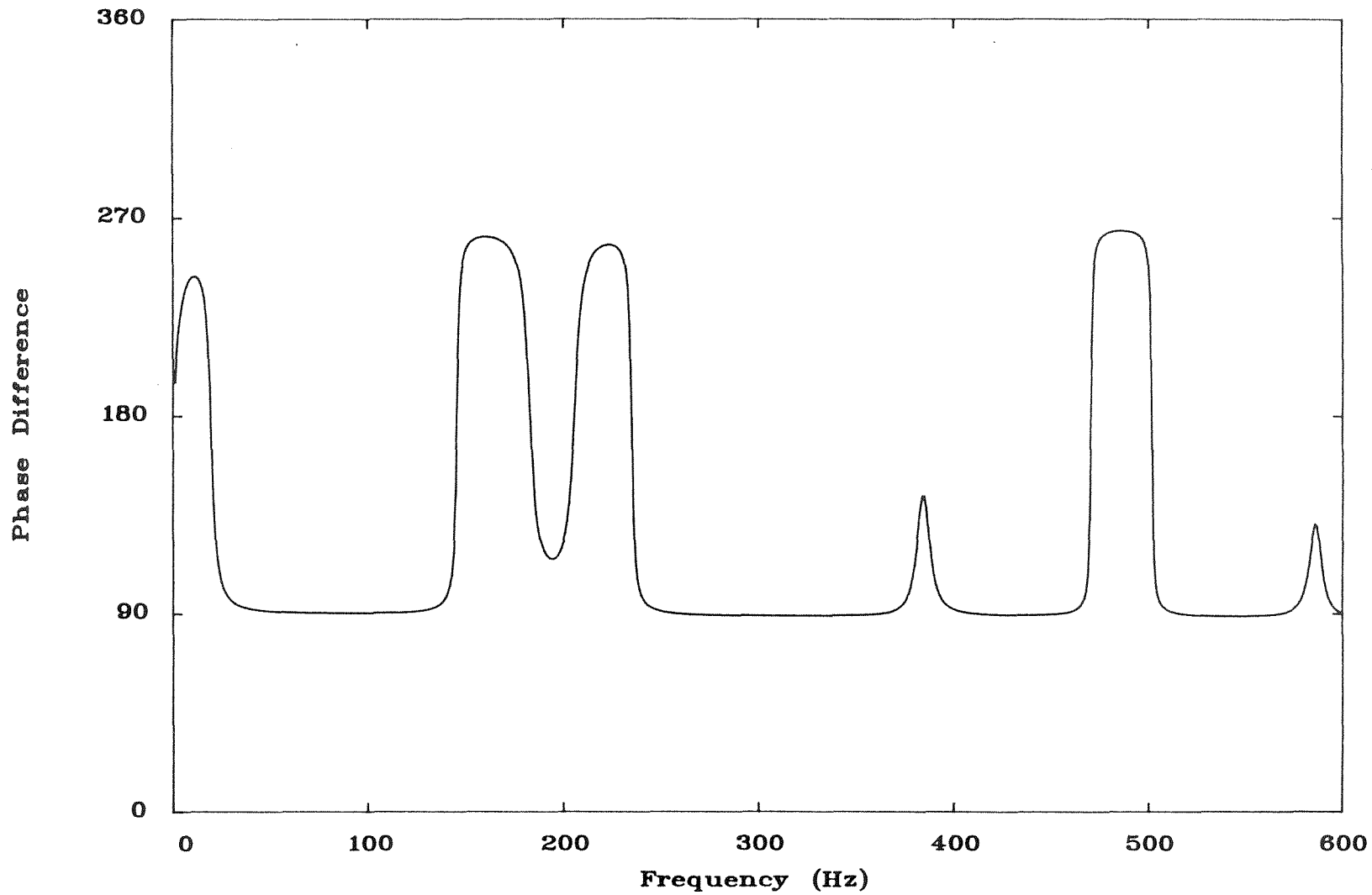


Figure 4.4: Phase Difference Between  $p'$  and  $u'$  Above Flameholder

### 4.2.3 Linear Stability Using Velocity-Sensitive Mass Source

To consider a feedback mechanism associated with vortex shedding, the forcing of the volume flow at the flameholder that is proportional to the velocity over the flameholder is used. However, a phase lag corresponding to the fluid mechanical and chemical induction time is included as well so that the matching condition at the flameholder becomes  $u'_4 a_4 A_4 = u'_3 a_3 A_3 + F u'_3 \exp \{-i\omega(t - \tau)\}$ . The constant  $F$  is the proportionality constant between the velocity and the amplitude of the volume source.

Using this formulation, a single, complex algebraic equation is obtained with four unknowns:  $\omega_r$ ,  $\omega_i$ ,  $F$ , and  $\tau$ , where the first two parameters correspond to the real and imaginary parts of the complex  $\omega$ , respectively. Thus, eigenvalues can be obtained by specifying any two of these parameters. By choosing  $\omega_i$  to be zero, the neutral stability boundary can be found for any value of one of the remaining parameters.

Considering the neutral stability curve when  $\omega_r$  is chosen, then values of both  $\tau$  and  $F$  are determined. When this calculation is performed for values of  $\omega_r$  between zero and 600 Hz, the results plotted in Figures 4.5 and 4.6 are obtained. In the first figure, it is seen that near natural frequencies of the system, the forcing amplitude required for instability is very small. This amplitude is the proportionality constant between the velocity over the flameholder and the volume source. Thus, the forcing amplitude,  $F$ , is basically an interaction index and must not be confused with the actual magnitude of the volume source. If ideal reflection coefficients are used, this amplitude is zero at frequencies corresponding to natural modes of the system.

In Figure 4.6, the neutral stability boundaries for the time delay param-

eter,  $\tau$ , are shown. The cross-hatched regions represent damped behavior, and the other regions represent cases in which  $\omega_i$  is positive and instability is predicted. The general trend of a shorter reaction delay at higher frequencies of oscillation is seen in the figure. For a given frequency of oscillation, the neutral stability boundaries satisfy Rayleigh's criterion. In other words, the phase difference between the pressure oscillations and the volume source takes the form,  $n 180^\circ + 90^\circ$ , where  $n$  is an integer. This can be seen by subtracting the phase difference between  $p'$  and  $u'$  shown in Figure 4.4 from the curves in Figure 4.6 normalized by  $\omega_\tau$ .

For frequencies corresponding to normal modes of the system, the slope of the curve is very steep, so that  $\tau$  changes rapidly for small changes in frequency. By plotting  $\tau$  as a function of the forcing amplitude required for neutral stability for frequencies between 175 and 185 Hz, the first curve in Figure 4.7 results. The largest value of  $\tau$  corresponds to 175 Hz and the smallest to 185 Hz. The curves at higher values of the forcing amplitude represent unstable growth corresponding to higher values of  $\omega_i$ . Thus, for an increase of only 10 Hz in the oscillation frequency,  $\tau$  decreases by about 40% for the neutral stability curve.

This linear stability theory provides a framework in which growth or decay of the pressure oscillations can be predicted for a given time delay and interaction index. The actual combustion process involves heat release at various locations in the system with different corresponding time delays. Thus, some regions of combustion may result in driving of the oscillation, while other regions damp the acoustic field. Also, this theory determines the stability characteristics but says nothing about the evolution towards a neutral stability boundary, i.e., limit cycle behavior. For an understanding of this evolution, a mechanism that brings more

information about the relationship between the parameters must be invoked.

Possible mechanisms leading to limit cycle behavior are discussed in the final section of this chapter, and the physical processes implied for each mechanism are discussed. Finally, the experimental results of the transition to instability for one case are compared to the proposed model to help determine the actual mechanism resulting in limit cycle behavior.

The following section provides a different method of analysis that is used to investigate the evolution of general instability phenomena.

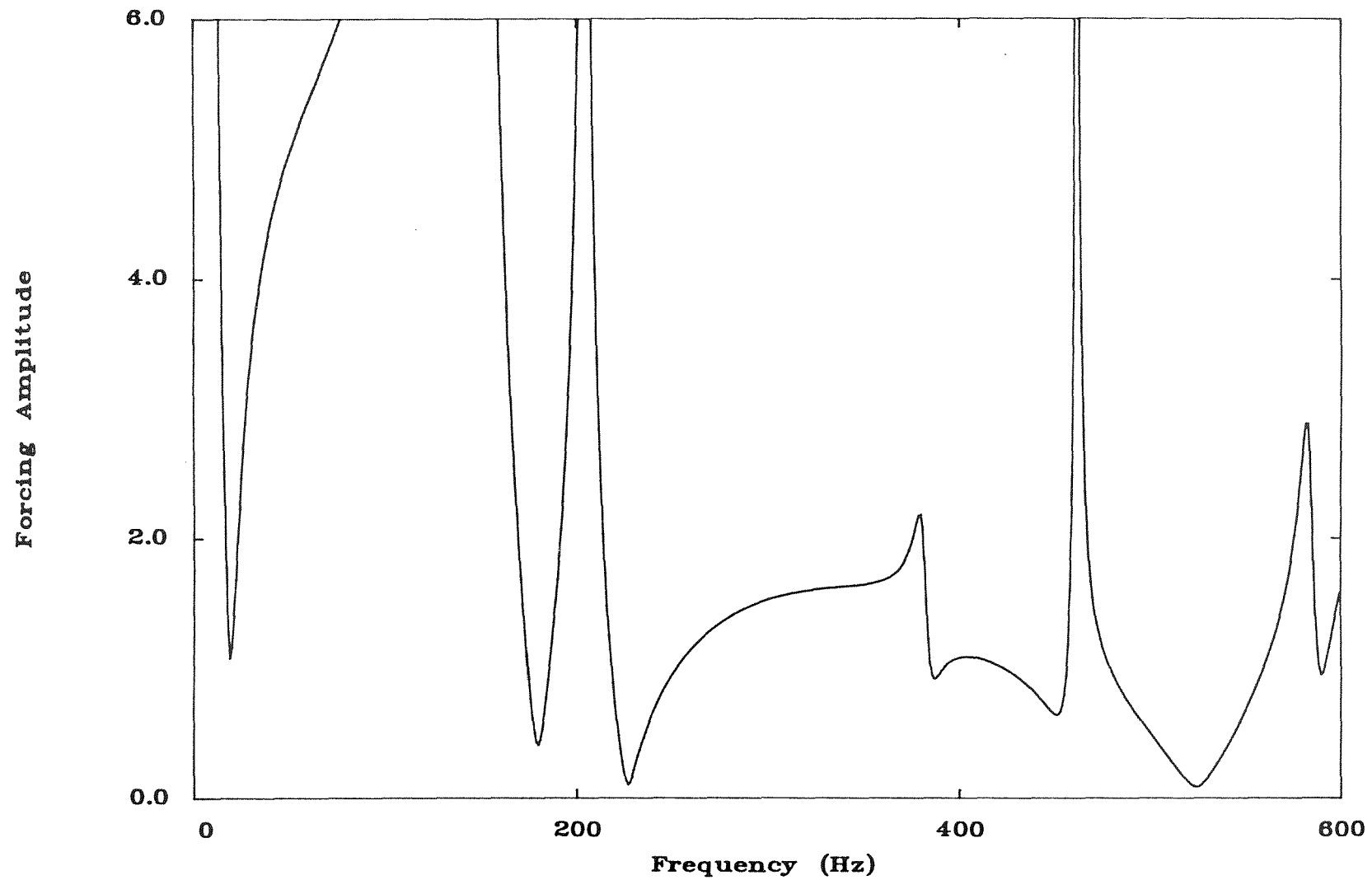


Figure 4.5: Interaction Index for Neutral Stability

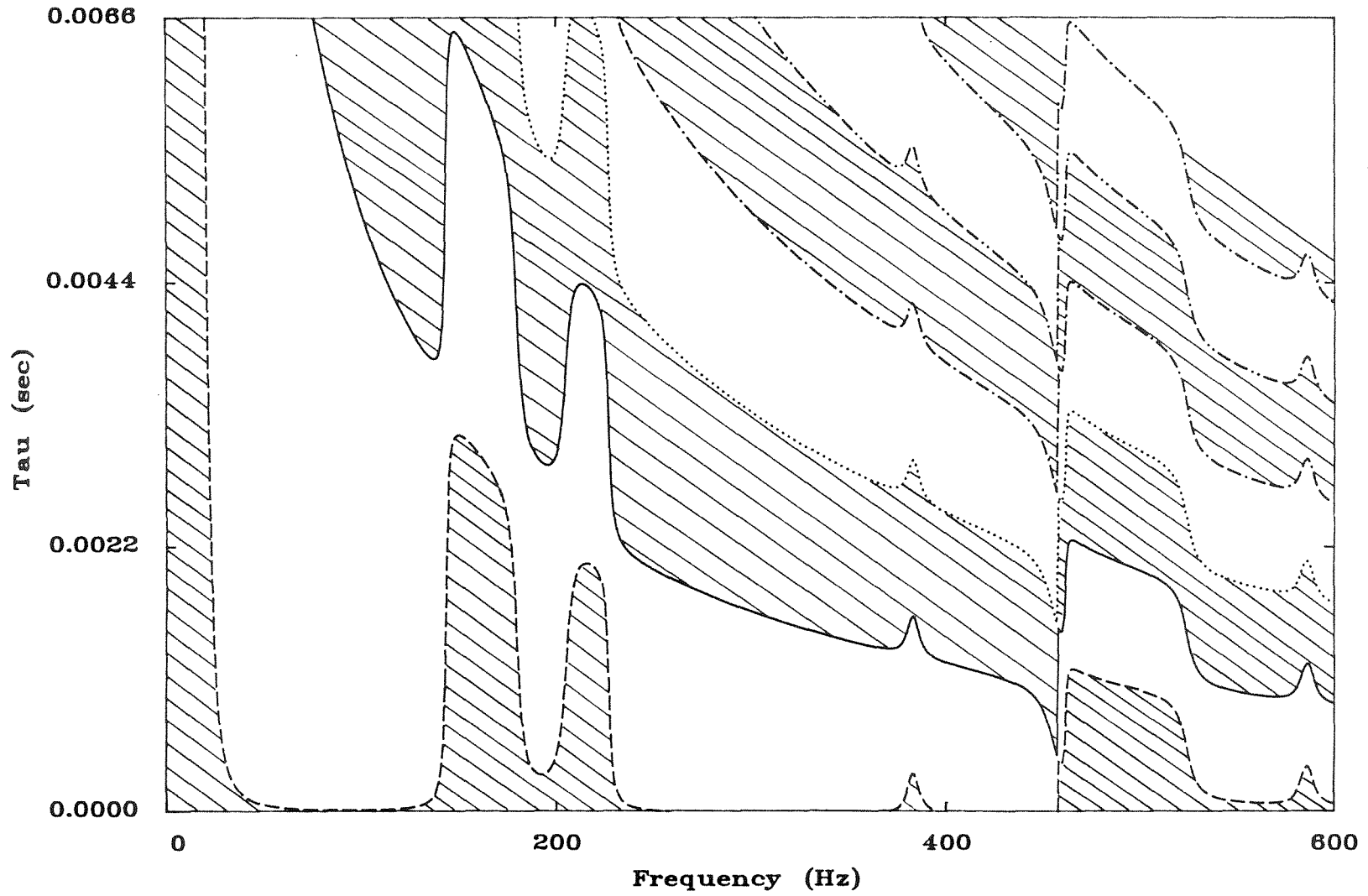


Figure 4.6: Time Delays for Neutral Stability

### 4.3 Solution for Time Development of Normal Modes

To investigate the evolution of the oscillatory character of a particular chamber for various driving mechanisms, a form of the method of weighted residuals can be used to solve Equation 4.7 for given boundary conditions,

$$\hat{n} \cdot \frac{\partial p'}{\partial x} = -f, \quad (4.10)$$

where  $\hat{n}$  is the outward normal at the ends of the chamber.

An approach described in detail by Culick [20] can be used to solve Equations 4.7 and 4.10 and is described briefly here. A solution for the oscillatory pressure can be expanded in the orthogonal acoustic modes of the system,  $\psi_n$ , which are defined by the equations,

$$\frac{\partial^2 \psi_n}{\partial x^2} + \left(\frac{\omega_n}{a}\right)^2 \psi_n = 0 \quad (4.11)$$

$$\hat{n} \cdot \frac{\partial \psi_n}{\partial x} = 0, \quad (4.12)$$

where  $\omega_n$  is the frequency for the  $n^{\text{th}}$  mode. The orthogonality of the modes defined in this way allows use of the relations,

$$\int \psi_m \psi_n dx = \delta_{mn} E_n^2, \quad (4.13)$$

where

$$E_n^2 = \int \psi_n^2 dx \quad (4.14)$$

and the integrals are performed over the length of the chamber.

The fluctuating pressure is then expanded in these normal modes with a time-varying coefficient for each mode.

$$p' = \bar{p} \sum \eta_n(t) \psi_n(x) \quad (4.15)$$

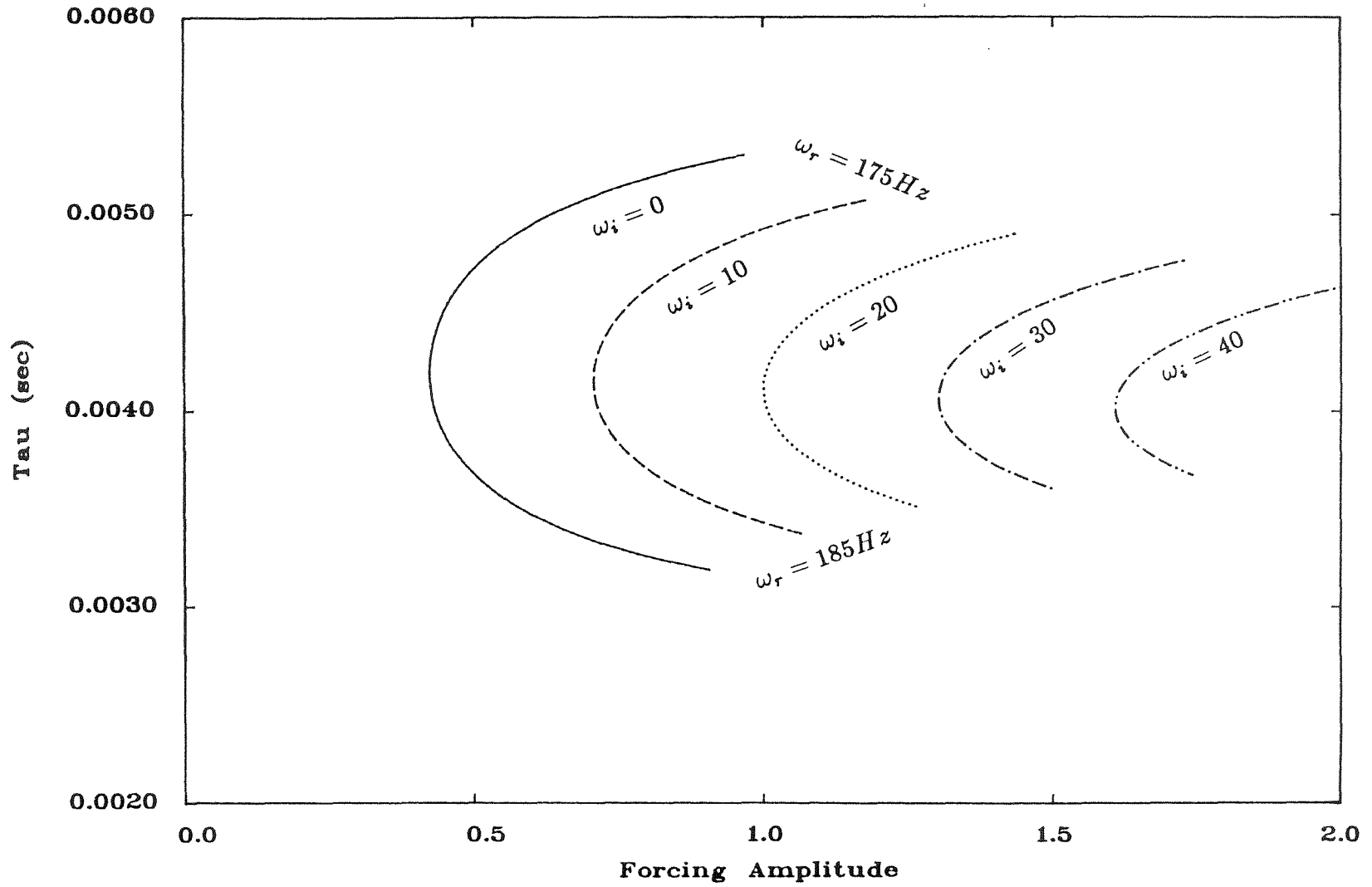


Figure 4.7: Stability Characteristics Near 188 Hz Mode

This is substituted in Equation 4.7, neglecting mass sources, and Equation 4.11 is multiplied by this expansion. Equation 4.7 is then multiplied by  $\psi_n$  and the two equations are then subtracted and integrated over the length of the chamber. By using the orthogonality relations 4.13 and 4.14, Green's theorem, and the boundary conditions 4.10 and 4.12, a set of ordinary differential equations for the modal coefficients is produced such that

$$\frac{d^2 \eta_n}{dt^2} + \omega_n^2 \eta_n = \frac{R}{C_v \bar{p} E_n^2} \int \psi_n \frac{\partial q'}{\partial t} dx - \left\{ \frac{a^2 \psi_n f}{\bar{p} E_n^2} \right\}_{ends}, \quad (4.16)$$

where the first term on the right side represents the driving by heat addition and the second term represents driving by non-ideal boundary conditions. If the ends are assumed to reflect acoustic waves perfectly, then  $f = 0$  and only the heat addition term is retained.

Equation 4.16 represents the time evolution of the amplitude of the fluctuating pressure in a chamber with heat release. One-dimensional small disturbances are considered while neglecting body forces, viscous forces, thermal conduction, and mass addition. The potential for energy addition to these small pressure disturbances by heat release is much larger than other mechanisms of energy addition. In Appendix A it is shown that if the fluctuating heat release rate is in phase with the pressure, energy is added to the small disturbances. This can also be shown by solving Equation 4.16 for a particular form of the heat release rate. This analysis provides a different derivation of Rayleigh's Criterion and is presented in Appendix B.

This solution method provides valuable insight into the time development of the pressure oscillations associated with normal acoustic modes of a combustor. However, when combustion of the reactants results in a fairly abrupt expansion of the gases, a phase change of the velocity fluctuations is expected as modeled

in the quasi-steady analysis. This results in changes in the phase difference between  $p'$  and  $u'$  at different locations in the system and for different frequencies of oscillation as shown in Figure 4.4. Representation of these phase changes by normal modes of the system may require many terms in the expansion. Thus, modeling of the entire acoustic system by this method is not attempted.

#### 4.4 Nonlinear Development of Combustion Instability

The limit cycle behavior that is observed experimentally cannot be described by the linear stability analysis that assumes a constant time delay parameter, i.e.,  $\tau$  used above and  $\xi$  in Appendix B. Some physical relationship between the parameters in the stability problem must be included in the analysis to distinguish stable equilibrium from unstable equilibrium points along the neutral stability boundaries. If this relationship results in variations of the parameters that occur over a time scale that is long compared to the period of oscillation, then the linear stability theory may adequately simulate the nonlinear growth.

If the phase difference between the heat release rate and the pressure oscillations is in some way dependent upon the amplitude of the oscillations, then both the linear stability analysis for the entire acoustic system and Equation 4.16 for a general combustor provide the mathematical framework in which self-excited, nonlinear growth can occur in a general combustion chamber. However, the phase difference between  $p'$  and  $u'$  is important and is included only in the velocity-sensitive mass source analysis. Therefore, discussion will focus on this analysis.

The nonlinearity is contained completely in the variation of the oscillation frequency,  $\omega_r$ , the time delay parameter,  $\tau$ , and the interaction index,  $F$ , with the amplitude of the velocity over the flameholder. No gasdynamic nonlinearities are

assumed. The mechanism of self-excitation resulting in limit cycle behavior can be idealized as occurring via one of three paths. These are shown in Figure 4.8 for frequencies near the 188 Hz mode. The curves are identical to those in Figure 4.7 except that values of  $\omega_r$  sweep over the broader range from 170 Hz to 190 Hz.

#### 4.4.1 Path 1: Saturation of Forcing Amplitude

Path 1 represents the case in which oscillations at a fixed frequency near a natural frequency of the system grow and reach a finite-limiting amplitude. This path would result if the interaction index,  $F$ , between the velocity oscillations and magnitude of the oscillatory heat release rate was a sensitive function of the amplitude of the oscillation. If the amplitude of the fluctuating heat release rate becomes saturated as the velocity fluctuations grow in magnitude, Path 1 is the result and the final point is a stable equilibrium point.

As seen in Figure 4.4, the phase difference between  $p'$  and  $u'$  changes only with changes of  $\omega_r$ . Thus, the normal mode analysis can provide useful insight for this path of nonlinear growth. For the pressure-sensitive time lag results in Appendix B,  $\xi$  is the time-delay parameter and  $Q_n$  is the corresponding interaction index. From Equation B.10 it is observed that for a fixed oscillation frequency to occur as the amplitude of the pressure oscillations changes, the interaction index,  $Q_n$  must vary in a particular manner with the time delay parameter. Keeping the oscillation frequency constant may be a somewhat artificial requirement that restricts the other parameters in the problem. Indeed, in Figure 4.8  $\tau$  is seen to increase slightly as the growth occurs at a fixed frequency of oscillation.

However, if the actual combustion process results in a broadening of the  $q'$  distribution as the strength of the large vortex increases, the mean heat release

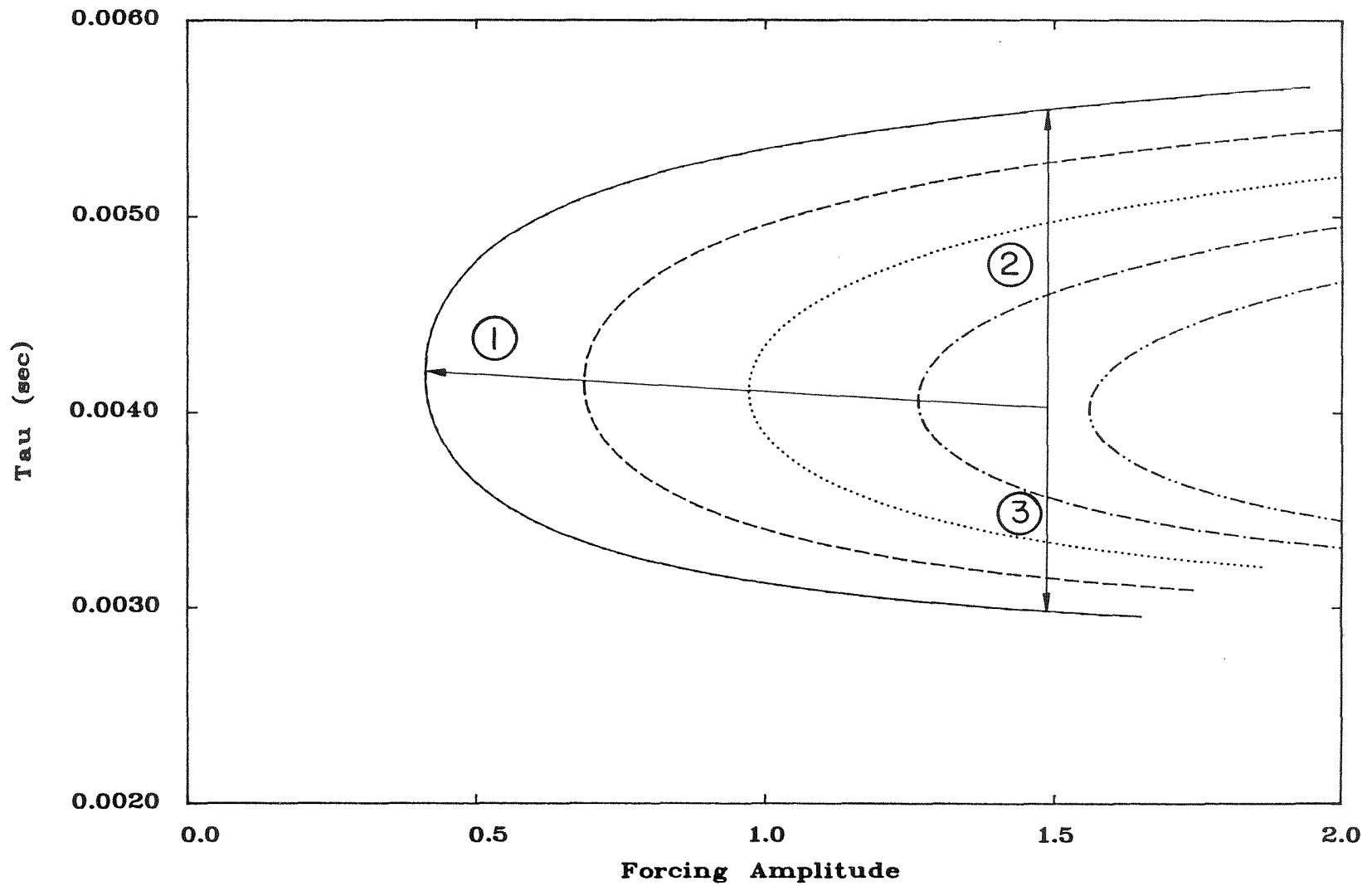


Figure 4.8: Idealized Mechanisms Leading to Limit-Cycle Behavior

rate may increase but the fluctuating component may saturate. Thus, some saturation of the interaction index may occur and contribute to the nonlinear behavior of the system.

For this path,  $u'$  lags  $p'$  by about  $180^\circ$  and  $\tau$  is about  $270^\circ$  degrees. This results in a situation where  $q'$  lags  $p'$  by  $90^\circ$  so that Rayleigh's Criterion is satisfied.

#### 4.4.2 Path 2: Increases in the Time Delay with Amplitude Growth

Path 2 represents the case in which increases in the time delay  $\tau$  occur as the amplitude of the velocity fluctuations increases for a constant interaction index,  $F$ . The path can be thought of as representing a physical mechanism in which the kinetics alone determine the time delay as suggested by Westbrook [18] in his analysis of pulsed combustors.

The combustion process is considered to be occurring in a well-stirred reactor with periodic additions of a fuel and air mixture. As the oscillation amplitude grows, a larger amount of cold reactants is brought into the combustor. For each cycle, this gas mixes with a fixed amount of products to give an initial temperature that is lowered for larger mixture ratios of cold reactants. Chemical kinetics then gives the result that a longer chemical induction time occurs for larger oscillation amplitudes (see Figure 2.5).

For this path, if the heat is released in phase with the pressure at small amplitudes of oscillation, the growth of the amplitude will yield successively longer time delays and a lowering of the oscillation frequency until a stable equilibrium point is reached.

This model predicts that for higher frequency modes of the system to be excited, the prompt combustion required for feedback would require low ampli-

tudes of oscillation to give the low mixture fractions of cold reactants required for a short chemical delay time. Experimentally, the opposite trend generally holds in which higher frequency modes usually exhibit higher amplitudes of oscillation.

The limit cycle behavior observed occurs when driving and damping of the acoustic field are of equal magnitude. The results used to obtain Figure 4.4 show that  $p'$  leads  $u'$  by about  $90^\circ$ , and the resulting limit cycle is achieved for  $\tau$  near  $360^\circ$  to provide a quarter of a cycle delay in the heat release rate from the pressure oscillations.

#### 4.4.3 Path 3: Decreases in the Time Delay with Amplitude Growth

The final model represents the case in which increases in the velocity amplitude yield decreases in the time delay parameter  $\tau$ . A physical mechanism resulting in this behavior was investigated by Hendricks [34] for combustion instabilities in a rearward-facing step combustor. This study was discussed in Chapter 3. Hendricks determined that as the amplitude of the velocity fluctuation is increased, the time from vortex shedding to vortex impingement on the lower wall below the step is decreased. Thus, the mixing process of fresh reactants with hot products is enhanced for larger velocity amplitudes and a shorter reaction time results. This study suggests a mechanism by which larger pressure and velocity amplitudes may yield shorter reaction delay times.

For this model, if  $q'$  and  $p'$  are initially in phase, the amplitudes will increase and the vortex mixing time delay will decrease accordingly, and an increase in the frequency of oscillation will occur which results in a more rapid change in the phase difference between  $p'$  and  $u'$ . Thus, as growth in the amplitude of the velocity fluctuation occurs,  $\tau$  decreases and  $\omega_r$  increases for constant  $F$  and a

limiting amplitude is reached as the phase lag of the heat release rate from the pressure oscillations approaches one-quarter of a cycle of oscillation.

For amplification of higher frequency modes of the system, this model predicts larger amplitudes resulting in enhanced mixing to give the shorter time delays required for feedback. This trend is observed experimentally.

When the stable equilibrium point is reached,  $p'$  lags  $u'$  by about  $90^\circ$  and  $\tau$  is near  $180^\circ$ , so that no driving or damping of the acoustic field occurs.

#### 4.4.4 Conclusions

Three simple idealized models that yield nonlinear behavior for pressure oscillations in combustion chambers are presented. In general, some physical mechanism relating  $F$ ,  $\tau$ , and  $\omega_r$  can result in nonlinear behavior. All three models result in  $p'$  leading  $q'$  by one-quarter of a cycle of oscillation. Path 1 represents an idealized path that can occur only for particular variations of  $\tau$  and  $F$ ; however, the saturation mechanism of  $F$  may play a role in the nonlinear behavior. Path 2 implies that higher frequency modes would correspond to lower amplitudes of oscillation, which is not observed experimentally. However, Path 3 correctly predicts the behavior that higher frequency modes correspond to higher amplitudes of oscillation.

The spectrum analysis results discussed in Chapter 3 consistently reveal vortex shedding frequencies that are slightly higher than the predicted natural frequencies. Along with the observation that higher frequency modes have higher amplitudes of oscillation, this suggests that Path 3 is a plausible physical model for nonlinear growth. However, the measured phase difference between  $p'$  and  $u'$  is nearly  $180^\circ$  for the 188 Hz mode, and the measured delay from vortex shedding to

the time at which the bulk of the heat is released is nearly  $270^\circ$ . This corresponds to the predictions of Path 1. Thus, some other path that incorporates effects of both Path 1 and Path 3 is most likely to occur.

## Chapter 5

### Summary and Conclusions

An investigation of the mechanism leading to growth and sustenance of large pressure oscillations at frequencies associated with longitudinal acoustic modes of a laboratory combustor has been performed. The acoustic modes are determined by the longitudinal geometry of the entire system including the supply chambers and the combustor itself. As in actual propulsion systems, the turbulent flame is stabilized in a recirculation zone. The flow speeds are high enough to produce a mixing layer that contains the reacting gases.

Flow visualization results during combustion instability reveal that large vortex structures are shed at a frequency corresponding to either an acoustic mode of the system or at a subharmonic of a mode. A one-dimensional acoustic analysis of the system is used to determine the natural frequencies and the corresponding mode shapes. These are compared to the experimental frequencies of oscillation and the experimental pressure mode shapes when operating conditions yield large pressure oscillations. The frequencies agree quite well with the experiment and the theory predicts the location of modal nodes and the mode shapes fairly accurately.

The frequency of oscillation depends upon the geometry of the flameholder, the mean flow speed, the fuel type, and the equivalence ratio. A parametric study was performed to investigate the dependence of the vortex shedding frequency

upon variations in the mean flow speed and equivalence ratio for a fixed geometry and fuel type. The results reveal that small changes in equivalence ratio can lead to excitation of acoustic modes of greatly varying frequency. Thus, the chemical induction time was determined to be important in even very low frequency instabilities. The chemical time dependence is consistent. High-frequency modes can be excited for equivalence ratios near stoichiometric but not for lean or rich mixtures, and fuels including high fractions of hydrogen generally result in instabilities of high-frequency modes. Reduction of the step height results in the excitation of higher-frequency modes as well. This shows that the influence of mixing as the vortex structure impinges on the lower wall of the combustor is important for most instabilities observed. Finally, higher frequency modes are observed at higher mean flow speeds. This is not well understood but may be caused by decreases in the mixture fraction of cold reactants at high speeds resulting in a shorter chemical reaction time.

Comparison of frames from shadowgraph movies with instantaneous distributions of the radiation intensity in the combustion chamber during combustion instability reveals that combustion levels in the regions near the flameholder continue to rise long after the large vortex structure passes. However, at downstream locations, the amplitude of the fluctuating radiation intensity signal is larger and the peak in reaction occurs only shortly after the vortex passes. Thus, an apparent combustion wave results and is measured to move at a nearly constant velocity that is about twice the mean flow speed for standard operating conditions. The accelerating vortex structure, on the other hand, is measured to move at about half the mean flow speed over the flameholder.

The importance of Rayleigh's Criterion is discussed in some detail as

the predominant driving and damping mechanism for instabilities of combustion chambers. Energy considerations show that the potential for the addition of energy to the acoustic field as a result of coupling of pressure fluctuations and heat release rate fluctuations is about two orders of magnitude greater than other energy transfer mechanisms in the laboratory system. Therefore, the phase difference between the fluctuating pressure and the oscillatory radiation intensity signal were measured at locations throughout the combustion chamber for several example operating conditions. The results indicate that regions of strong damping generally occur immediately upstream of the location at which the amplitude of the radiation intensity is a peak. Similarly, regions of strong damping of the acoustic energy usually occur just downstream of this location. Thus, the location of the largest heat release generally occurs at a time during the pressure oscillation that results in no driving or damping of the acoustic field after a finite limiting amplitude has been reached.

Modeling of the feedback mechanism to determine the phase difference between the pressure and the heat release oscillations traditionally uses a pressure-sensitive time delay to predict linear stability characteristics of a particular system. This has given considerable success for liquid-propellant and solid-propellant systems. However, in combustion systems in which the flame is stabilized in a recirculation zone, the feedback mechanism associated with vortex shedding phenomena is sensitive to the velocity fluctuations at the flameholder.

A linear stability model based on a velocity-sensitive mass source is used for the geometry of the laboratory combustor. The combustion is modeled by a volumetric source downstream of the flameholder whose amplitude is related to the amplitude of the velocity fluctuations over the flameholder and whose phase

lags the same velocity by some time delay. The solution method requires that particular values of the time delay and the interaction index determine the amplification rate and frequency of the oscillation. For feedback within one cycle of oscillation, the time delay required for instability is generally shorter for higher frequencies. Large changes in the phase difference between the pressure fluctuation and the velocity fluctuations occur near natural frequencies of the system. This has a strong influence on the stability boundaries predicted for the system.

Finally, possible mechanisms of nonlinear growth are described within the framework of the velocity-sensitive mass source, linear stability theory. Experimental results for particular operating conditions reveal that a combination of the idealized mechanisms that are discussed may be responsible for limit cycle behavior. Experimental results show that the amplitudes of high frequency modes are generally larger than the amplitudes of low frequency modes, and the frequency of oscillation is usually higher than predicted frequencies. These results suggest a nonlinear evolution that involves an increase in the frequency of oscillation and a decrease in the time delay parameter as the amplitude of the oscillation increases and reaches a finite-limiting amplitude.

## References

- [1] Rogers, D. E. and Marble, F., "A Mechanism for High-Frequency Oscillations in Ramjet Combustors and Afterburners," *Jet Propulsion*, vol. 26, p. 456, 1956.
- [2] Lawn, C. J., "Criteria for Acoustic Pressure Oscillations to be by a Diffusion Flame," in *Nineteenth Symposium (International) on Combustion*, pp. 374–386, The Combustion Institute, 1982.
- [3] Mugridge, B. D., "Combustion Driven Oscillations," *Journal of Sound and Vibration*, vol. 70, pp. 437–452, 1980.
- [4] Hegde, U. G., Reuter, D., Daniel, B. R., and Zinn, B. T., "Flame Driving of Longitudinal Instabilities in Dump Type Ramjet Combustors," in *AIAA 24th Aerospace Sciences Meeting*, January 1986. AIAA-86-0371.
- [5] Byrne, R. W., "Longitudinal Pressure Oscillations in Ramjet Combustors," in *AIAA/SAE/ASME 19th Joint Propulsion Conference*, June 1983. AIAA-83-2018.
- [6] Shonerd, D. E., "Studies of Flame-Front Oscillations," Report No. 3-18, Jet Propulsion Laboratory, 1952.
- [7] Gangi, A. and Sawyer, R., "Turbulence, Combustion, Pollutant and Stability Characterization of a Premixed, Step Combustor," Contract Report No.

- 3230, NASA, 1982.
- [8] Keller, J., Vaneveld, L., Korschelt, D., Hubbard, G., Ghoniem, A. F., Daily, J., and Oppenheim, A., "Mechanism of Instabilities in Turbulent Combustion Leading to Flashback," *AIAA Journal*, vol. 29, pp. 454–462, 1982.
- [9] Vaneveld, L., Hom, K., and Oppenheim, A. K., "Secondary Effects in Combustion Instabilities Leading to Flashback," *AIAA Journal*, vol. 22, pp. 81–83, 1984.
- [10] Smith, D. A., *An Experimental Study of Acoustically Excited, Vortex Driven, Combustion Instability Within a Rearward Facing Step Combustor*. PhD thesis, California Institute of Technology, Pasadena, California, 1985.
- [11] Smith, D. A. and Zukoski, E. E., "Combustion Instability Sustained by Unsteady Vortex Combustion," in *AIAA/SAE/ASME/ASEE 21st Joint Propulsion Conference*, 1984. AIAA-85-1248.
- [12] Aaron, K. M., *Edgetones and Acoustic Resonances in a Duct*. PhD thesis, California Institute of Technology, Pasadena, California, 1985.
- [13] Lord Rayleigh, *The Theory of Sound*, p. 227. Vol. II, Dover Publications, 1945.
- [14] Putnam, A. and Faulkner, L., "An Overview of Combustion Noise," in *AIAA/ASME 3rd Joint Thermophysics, Fluids, Plasma and Heat Transfer Conference*, June 1982. AIAA-82-0927.
- [15] Crocco, L. and Cheng, S., *Theory of Combustion Instability in Liquid Propellant Rocket Motors*. Butterworths Scientific Publications, 1956.

- [16] Merk, H. J., "An Analysis of Unstable Combustion of Premixed Gases," in *Sixth Symposium (International) on Combustion*, pp. 500–512, The Combustion Institute, 1956.
- [17] Yang, V., *Pressure Oscillations in Liquid-Fueled Ramjet Engines*. PhD thesis, California Institute of Technology, Pasadena, California, 1984.
- [18] Westbrook, C. K., "Successive Reignition of Fuel-Air Mixtures and Pulse Combustion," in *Fall Meeting of the Western States Section of the Combustion Institute*, 1985.
- [19] Ponizy and Wojcicki, "On Modelling of Pulse Combustors," in *Twentieth Symposium (International) on Combustion*, pp. 2019–2024, The Combustion Institute, 1984.
- [20] Culick, F. E. C., "Nonlinear Behavior of Acoustic Waves in Combustion Chambers," Tech. Rep., California Institute of Technology, Pasadena, California, April 1975.
- [21] Sterling, J. D. and Zukoski, E. E., "Longitudinal Mode Combustion Instabilities in a Dump Combustor," in *AIAA 25th Aerospace Sciences Meeting*, January 1987. AIAA-87-0220.
- [22] Auerbach, J. M., *Experimental Studies of the Noise Produced in a Supersonic Nozzle By Upstream Acoustic and Thermal Disturbances*. PhD thesis, California Institute of Technology, Pasadena, California, 1975.
- [23] Abouseif, G., Keklak, J. A., and Toong, T., "Ramjet Rumble: The Low Frequency Instability Mechanism in Coaxial Dump Combustors," *Combustion Science and Technology*, vol. 36, pp. 83–108, 1984.

- [24] Humphrey III, J. W., *Linear and Nonlinear Acoustics with Nonuniform Entropy in Combustion Chambers*. PhD thesis, California Institute of Technology, Pasadena, California, 1986.
- [25] Chomiak, J., "Application of Chemiluminescence Measurement to the Study of Turbulent Flame Structure," *Combustion and Flame*, vol. 18, pp. 429–433, 1972.
- [26] Hurle, I. R., Price, R. B., Sugden, T. M., and Thomas, A., *Sound Emission from Open Turbulent Premixed Flames*, pp. 409–427. Vol. 303, Proc. Roy. Soc., 1968.
- [27] Diederichsen, J. and Gould, R., "Combustion Instability: Radiation from Premixed Flames of Variable Burning Velocity," *Combustion and Flame*, vol. 9, pp. 25–31, 1965.
- [28] Huot, J., Frost, D., and Lim, C., "Radiation from Flames," Ae 104 Report, California Institute of Technology, Pasadena, California, 1951.
- [29] Clark, T. P. and Bittker, D. A., "A Study of the Radiation from Laminar and Turbulent Open Propane-Air Flames as a Function of Flame Area, Equivalence Ratio, and Fuel Flow Rate," NACA RM, Lewis Flight Propulsion Laboratory, Cleveland, Ohio, 1954.
- [30] John, R. R. and Summerfield, M., "Effect of Turbulence on Radiation Intensity From Propane-Air Flames," *Jet Propulsion*, vol. 27, p. 169, 1957.
- [31] Sobota, T. H., *An Experimental and Numerical Investigation of Swirling Flows in a Rectangular Nozzle*. PhD thesis, California Institute of Technology, Pasadena, California, 1987.

- [32] Carrier, G., Fendell, F., and Marble, F., "The Effect of Strain Rate on Diffusion Flames," *SIAM Journal of Applied Mathematics*, vol. 28, p. 463, 1975.
- [33] Karagozian, A., *An Analytical Study of Diffusion Flames in Vortex Structures*. PhD thesis, California Institute of Technology, Pasadena, California, 1982.
- [34] Hendricks, G. J., *Two Mechanisms of Vorticity Generation in Combusting Flow Fields*. PhD thesis, California Institute of Technology, Pasadena, California, 1986.
- [35] Marble, F. and T.C. Adamson, J., "Ignition and Combustion in a Laminar Mixing Zone," *Jet Propulsion*, vol. 24, p. 85, 1954.
- [36] Dooley, D., *Combustion in Laminar Mixing Regions and Boundary Layers*. PhD thesis, California Institute of Technology, Pasadena, California, 1956.
- [37] Bush, W. B. and Fendell, F. E., "Asymptotic Analysis of Laminar Flame Propagation for General Lewis Numbers," *Combustion Science and Technology*, vol. 1, pp. 421–428, 1970.
- [38] Coffee, T. P., "Kinetic Mechanisms for Premixed, Laminar, Steady State Methane/Air Flames," *Combustion and Flame*, vol. 55, pp. 161–170, 1984.
- [39] Andrews, G. and Bradley, D., "The Burning Velocity of Methane-Air Mixtures," *Combustion and Flame*, vol. 19, pp. 275–288, 1972.
- [40] Yu, G., Law, C., and Wu, D., "Laminar flame Speeds of Hydrocarbon + Air Mixtures with Hydrogen Addition," *Combustion and Flame*, vol. 63, pp. 339–347, 1986.

- [41] Damkohler, G., "The Effect of Turbulence on the Flame Velocity in Gas Mixtures," Technical Memorandum, NACA, Washington D.C., 1940.
- [42] Broadwell, J. and Breidenthal, R., "A Simple Model of Mixing and Chemical Reaction in a Turbulent Shear Layer," *Journal of Fluid Mechanics*, vol. 125, pp. 397–410, 1982.
- [43] Broadwell, J. and Dimotakis, P., "Implications of Recent Experimental results for Modelling Reactions in Turbulent Flows," in *AIAA 22nd Aerospace Sciences Meeting*, January 1984. AIAA-84-0545.
- [44] Spalding, D. B., "The ESCIMO Theory of Turbulent Combustion," No. 71TS/76/13, Imperial College, London, 1976.
- [45] Zukoski, E. E. and Marble, F. E., "Experiments Concerning the Mechanism of Flame Blowoff from Bluff Bodies," in *Proceedings of Gas Dynamics Symposium on Aerothermochemistry*, pp. 205–210, Northwest University Press, 1956.
- [46] Oates, G. C., "The Aerothermodynamics of Aircraft Gas Turbine Engines," No. TR 78-52, Air Force Aero-Propulsion Laboratory, 1978.
- [47] Chu, B. T., "On the Energy Transfer to Small Disturbances in a Viscous Compressible Heat Conductive Medium," AFOSR contractor report, The Johns Hopkins University, 1956.
- [48] Culick, F. E., "A Note on Rayleigh's Criterion," to be published, California Institute of Technology, Pasadena, California, 1987.
- [49] Mahan, J., Cline, J., and Jones, J., "A Temperature Correlation for the

Radiation Resistance of a Thick-Walled Circular Duct Exhausting a Hot Gas," *J. Acoust. Soc. Am.*, vol. 75, pp. 63-71, 1984.

## Appendix A

### Derivation of Rayleigh's Criterion

The one-dimensional perturbation equations for the momentum and energy , Equations 4.5–4.6, are multiplied by  $u'$  and  $\frac{p'}{\gamma\bar{p}}$ , respectively. These are added with no mass sources to obtain

$$\begin{aligned} \left(\frac{\partial}{\partial t} + \bar{u}\frac{\partial}{\partial x}\right)\left(\frac{\bar{\rho}u'^2}{2} + \frac{p'^2}{2\gamma\bar{p}}\right) &= \frac{\gamma-1}{\gamma\bar{p}}q'p' - \frac{\partial}{\partial x}(u'p') - \frac{u'p'}{\gamma\bar{p}}\frac{\partial\bar{p}}{\partial x} \\ &\quad - \left(\rho'u'\bar{u} + \bar{\rho}u'^2 + \frac{p'^2}{\bar{p}}\right)\frac{\partial\bar{u}}{\partial x}, \end{aligned} \quad (\text{A.1})$$

where the left side of this equation represents the variation of the energy associated with the acoustic field.

At this point an estimation of the potential order of magnitude of the terms on the right side of the above equation is performed using amplitudes common to the laboratory combustor. This reveals that  $\frac{\gamma-1}{\gamma\bar{p}}|q'||p'|$  is approximately two orders of magnitude greater than the other terms that could transfer energy from the mean flow to the acoustic field. Thus, considering a combustor in which  $\bar{u}$  is small, only the  $p'q'$  coupling term remains and the above equation becomes,

$$\frac{\partial e}{\partial t} = \frac{\gamma-1}{\gamma\bar{p}}q'p', \quad (\text{A.2})$$

where the energy associated with the acoustic field is

$$e = \frac{\bar{\rho}u'^2}{2} + \frac{p'^2}{2\gamma\bar{p}}. \quad (\text{A.3})$$

Finally, if we consider a combustion chamber with ideal boundary conditions that relate  $p'$  and  $u'$  at the inlet and exit of the chamber, we can integrate the above equation to get Rayleigh's Criterion,

$$\Delta E = \frac{A(\gamma - 1)}{\gamma \bar{p}} \int dx \int_t^{t+\tau} p' q' dt, \quad (A.4)$$

where  $A$  is the cross-sectional area of the combustor and  $\Delta E$  is the increment of energy added to the acoustic field during the time  $\tau$ .

## Appendix B

### Rayleigh's Criterion by Normal Mode Solution

Equation 4.16 represents the time evolution of the amplitude of the normal modes of a chamber due to heat release and is written,

$$\frac{d^2\eta_n}{dt^2} + \omega_n^2\eta_n = \frac{R}{C_v\bar{p}E_n^2} \int \psi_n \frac{\partial q'}{\partial t} dx \equiv F_n. \quad (B.1)$$

By considering the energy in an oscillator, Culick [48] showed that if the heat release rate has some component in phase with the oscillatory pressure, energy will be added to the oscillator. This can also be shown as follows.

A solution for  $\eta_n$  is assumed of the form,

$$\eta_n(t) = A(t) \sin(\omega_n t) + B(t) \cos(\omega_n t), \quad (B.2)$$

where the coefficients are slowly varying functions of time. Derivatives are taken and substituted into the above equation, and because of  $A$  and  $B$  are slowly varying, their second derivatives are assumed to be small compared to their first derivatives. By multiplying by  $\cos(\omega_n t)$  and integrating over one cycle, orthogonality implies that,

$$\frac{dA_n}{dt} = \frac{1}{2\pi\omega_n} \int_0^{2\pi} F_n \cos \psi_n d\psi_n. \quad (B.3)$$

Similarly, by multiplying by  $\sin(\omega_n t)$  and integrating,

$$\frac{dB_n}{dt} = \frac{-1}{2\pi\omega_n} \int_0^{2\pi} F_n \sin \psi_n d\psi_n. \quad (B.4)$$

If the oscillatory heat release is separable into a spatial varying component and a time-varying component that is proportional to the time varying portion of the pressure amplitude with some time delay, it can be written

$$q' = q_n(x)\eta_n(t - \xi), \quad (B.5)$$

where  $\xi$  is the time delay. By using this,

$$F_n = 2 Q_n \omega_n \left\{ A(t) \cos \{ \omega_n(t - \xi) \} - B(t) \sin \{ \omega_n(t - \xi) \} \right\}, \quad (B.6)$$

where the terms with the derivatives of the coefficients are neglected, and

$$Q_n \equiv \frac{\gamma - 1}{2 \bar{p} E_n^2} \int \psi_n(x) q_n(x) dx. \quad (B.7)$$

After expanding the integrals in the equations for the coefficients, the equations become

$$\frac{dA}{dt} = Q_n \{ A \cos \omega_n \xi + B \sin \omega_n \xi \} \quad (B.8)$$

$$\frac{dB}{dt} = Q_n \{ -A \sin \omega_n \xi + B \cos \omega_n \xi \}. \quad (B.9)$$

The solution to these equations is

$$\eta_n(t) = \exp \{ Q_n \cos(\omega_n \xi) t \} \sin \{ t(\omega_n - Q_n \sin \omega_n \xi) + \phi_n \}, \quad (B.10)$$

where  $\phi_n$  are the phases of the normal modes.

This solution shows that if  $\cos \omega_n \xi$  is positive for  $Q_n$  positive, the oscillatory pressure will grow exponentially. Thus, if the heat release rate is in phase with the oscillatory pressure, instability results. It is interesting to note that  $F_n$  in Equation B.1 contains  $\frac{\partial q'}{\partial t}$  but the resulting energy addition depends only on the phase of  $q'$  itself. Another important result is that if  $\xi$  changes, then the frequency of oscillation changes as well.